

STUDIES ON SOME ASPECTS OF ELECTROCHEMICAL GRINDING

Thesis submitted for the award of the degree
of

DOCTOR OF PHILOSOPHY
IN
ENGINEERING

by

TARAPADA BHOWMICK

Under the supervision of

Prof. P.K. MISHRA



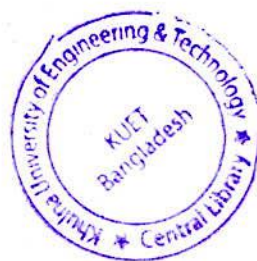
DEPARTMENT OF MECHANICAL ENGINEERING

INDIAN INSTITUTE OF TECHNOLOGY

KHARAGPUR-721302, INDIA

AUGUST, 1999.

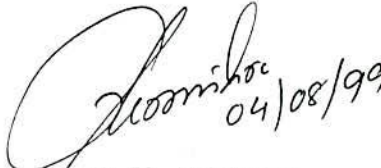
Dedicated to my Beloved Mother
and
In memory of my Beloved Father



CERTIFICATE

This is to certify that the thesis entitled, "**Studies on Some Aspects of Electrochemical Grinding**", submitted to the Indian Institute of Technology, Kharagpur by **Tarapada Bhowmick** for the award of the degree of **Doctor of Philosophy in Engineering** is a record of bonafide research work carried out by him under my supervision and guidance. The results embodied in this thesis have not been submitted to any other Institute or University for the award of any degree or diploma.

In my opinion, the thesis is worthy of consideration for the award of the degree of **Doctor of Philosophy in Engineering** in accordance with the regulations of the Institute.


(Dr. P. K. Mishra)

Professor

Department of Mechanical Engineering

Indian Institute of Technology

Kharagpur, India

ACKNOWLEDGEMENTS

With deep sincerity and respect, the author acknowledges his profound gratefulness and indebtedness to **Dr. P.K. Mishra**, Professor of Mechanical Engineering Department, IIT, Kharagpur for suggesting the problem, unfailing guidance, encouragement, advice imparted in execution and completion of the work throughout the period of the investigation.

I would like to express my sense of gratitude to **Prof. G.L. Dutta**, Ph. D. course coordinator and **Prof. P.K. Nag**, Head of the Mechanical Engineering Department for their help and encouragement.

The advice and help received from **Prof. A.B. Chottapadhyaya**, Ex-Head of the Mechanical Engineering Department is gratefully acknowledged.

The author gratefully acknowledges the special committee members directing the doctoral work for their valuable advice, discussion, and support.

I also wish to express my heartiest thanks to all the faculty members, especially to **Prof. A.K. Chottapadhyaya**, **Prof. S.K. Roy Choudhury**, **Prof. S. Pal** and **Prof. A. Roy Choudhury** of Mechanical Engineering Department for their encouragement and valuable help.

It is my duty to express my indebtedness to **Indian Council for Cultural Relations (ICCR)** for providing me the scholarship during the period of this investigation.

I am also grateful to **Prof. M.A. Hannan**, Ex-Director of Bangladesh Institute of Technology (BIT), Khulna for giving me deputation to do Ph.D. at IIT, Kharagpur, India.

I wish to express my sincere sentiments to **Mrs. P.K. Mishra** for her affection and blessings.

I like to present my sincere thanks to research scholar **Mr. Mihir Ranjan Halder** for his help during the preparation of text of the thesis. Thanks are also due to research scholars **Mr. Joydev Rana** and **Mr. Nikhil Ranjan Dhar** for their help.

I would like to record my appreciation to **Mr. Sudhir Chandra Dutta** of training shop, **Mr. G.N. Paria** and **Mr. D.K. Chakraborty** of EPP Laboratory for their help during fabrication works of the experimental set up.

I am thankful to the staff of Mechanical Engineering Department for their sincere co-operation and help. Thanks are also due to **Mr. Ashoke Das** for taking the pain of typing part of the thesis.

I am indebted to all those who have been associated with me during the course of my work and for all those who prayed for me.

I would also like to express my sincere appreciation to my very affectionate nephew **Titu**, and loving **Mani** for their good service and active co-operation rendered throughout my study.

Lastly, I express my heartfelt gratitude to my mother, brothers and other family members for their blessings and moral support.

Kharagpur: August, 1999



T.P. Bhowmick
4/8/99
(T.P. Bhowmick)

BIO - DATA

Tarapada Bhowmick, S/O Late Ramesh Chandra Bhowmick and Smt. Chapala Bhowmick was born on 3rd December 1951 in Brahmanbaria, Bangladesh. He did his schooling from Nabinagar High School and passed Higher Secondary Certificate Examination from Comilla Victoria Government College in 1969. Shri Bhowmick studied at the University of Chittagong, Bangladesh and completed Bachelor of Science in Engineering (Mechanical) in 1976. In 1984, he gained his Master of Science in Engineering (IP) from Bangladesh University of Engineering & Technology, Dhaka. Currently he is attached to the Department of Mechanical Engineering, IIT, Kharagpur, since 1992 India for Ph.D. programme under the Government of India Scholarship.

He has gathered three years (1976-1979) of industrial experience, one year from Bangladesh Power Development Board, and two years from Bangladesh Machine Tools Factory Ltd. Ghazipur, Dhaka. He joined Bangladesh Institute of Technology (BIT), Chittagong (Erstwhile Engineering College, Chittagong) in 1980 as a faculty member and since then he has been teaching at different BIT's Bangladesh till today.

Presently he is working in Bangladesh Institute of Technology (BIT), Khulna as an Assistant Professor (Mechanical). His areas of interest include non-conventional manufacturing, machine tools engineering, and production engineering.

His permanent address is:

Village - Sreerampur
Post - Sreerampur
P.S. - Nabinagar
Dist. - Brahmanbaria
Bangladesh



Signature

ABSTRACT

Electrochemical grinding (ECG) has become more and more important for its industrial use, in machining problems associated with grinding hard and wear resisting and even very soft electrically conductive materials. In a survey on ECG process, little attempts on theoretical analysis of the process rather more experimental investigations have been made.

The main objective of the present work was to develop theoretical models to explain joint phenomena, mechanism and electrochemistry i.e. (i) to determine metal removal rate due to mechanical and that of electrochemical action individually, (ii) to find out the feed force required in ECG process, and (iii) to corroborate the models with experimental results. For this, an industrial model for the electrochemical grinding machine with hydraulic feed control system has been developed retrofitting an existing obsolete manual feed surface grinder. Different stages of grinding action are thoroughly analyzed and corresponding force components are established in terms of chip thickness, stress and loading coefficients. An octagonal extended ring type grinding dynamometer of stainless steel has been designed, constructed and calibrated. A high gain operational amplifier has been built to record force components.

Electrochemical grinding geometry and kinematics are analyzed, and electrochemical and mechanical aspects of the process have been extensively studied. Investigation on the different process parameters and their inter-relations are also made.

Experiments have been conducted on stainless steel and tungsten carbide (GT 20) to examine the validity of the theoretical works and other experimental investigations. Theoretical analyses have been carried out on the determination of MRR and feed force. Different stages of grinding actions viz. sliding, ploughing, cutting, rubbing, viscous drag due to electrolyte pool are considered in feed force analysis. The depth of cut is used for combined mechanical and electrochemical

actions. They are experimentally verified and found within the closure range of acceptance for industrial exploitation. The results indicate that material removal rate due to electrochemical action can be achieved up to 90% of the total material removed, and as a result, the feed force in ECG is found very less compared to conventional grinding.

Key words: electrochemical grinding, material removal rate, feed force, dynamometer, calibration, electrochemistry, electrolytic action.

LIST OF FIGURES

| Fig. No | Description | Page No. |
|---------|---|----------|
| 1.1 | Surface Roughness and Tolerances Produced by Non-conventional Machining Processes | 7 |
| 1.2 | Summary of the General Effects of Electrochemical Grinding | 9 |
| 1.2 | Basic Scheme of ECG Process | 11 |
| 2.1 | The Chart for Surface ECG to Determine Contact Length and Feed Rates | 27 |
| 3.1 | Electrolytic Cell Showing Movement of Ions | . |
| 3.2 | Potential Profile in the Machining Gap | 47 |
| 3.3 | Potential Distribution in the Machining Gap | 50 |
| 3.4 | Effects of Electrochemistry in ECG | 51 |
| 3.5 | Passivity Film Characterization | 56 |
| 4.1 | Scheme for Straight Surface Grinding | 61 |
| 4.2 | Electrochemical Grinding Scheme | 62 |
| 4.3 | Grinding Geometry | 64 |
| 4.4 | Undeformed Chip Geometry for Straight Surface Grinding | 67 |
| 4.5 | Undeformed Chip Shapes for Maximum Chip Thickness | 69 |
| 4.6 | Inter-relationship amongst ECG Process Parameters | 73 |
| 4.7 | Illustration of Ploughing Followed by Transition to Chip Formation | 75 |
| 4.8 | Effect of Metal Removal Rate on the Ploughing Contribution | 76 |
| 4.9 | Schematic of Surface Grinding Operation Showing Individual Chip in Insert | 77 |
| 4.10 | Grinding Operation Showing Sliding Action | 78 |
| 4.11 | Enlarged View of Sliding Angle | 79 |
| 4.12 | Electrochemical Action of the Grinding Wheel | 88 |
| 4.13 | Simulated Position of the Grinding Wheel in Mechanical Action | 92 |
| 4.14 | Vector Representation of Forces | 92 |
| 5.1 | Schematic Layout of Electrochemical Grinding Machine | 102 |
| 5.2 | Schematic Diagram of the Experimental Set-up for ECG | 104 |

| | | |
|------|--|-----|
| 5.3 | Hydraulic Circuit for Feed Control | 105 |
| 5.4 | Drawing of Hydraulic Cylinder and Piston | 107 |
| 5.5 | Linear Operational Amplifier | 110 |
| 5.6 | Circuit Diagram of the Amplifier | 111 |
| 5.7 | Designed Dimension of the Dynamometer | 114 |
| 5.8 | Grinding Dynamometer Showing the Position of Strain Gauges | 115 |
| 5.9 | Bridge Connections | 116 |
| 5.10 | Strain Gauge Connections | 116 |
| 5.11 | Calibration Curves of Dynamometer for Horizontal load | 118 |
| 5.12 | Calibration Curves of Dynamometer for Vertical load | 118 |
| 5.13 | Represents the Fabricated Parts and the Connections Tapped for DC Source | 120 |
| 5.14 | Orthographic Views of Elements Attached to Work Table | 121 |
| 5.15 | Experimental Set-up | 122 |
| 6.1 | Effect of Voltage on Current Density for Different Depths of Cut | 138 |
| 6.2 | Effect of Voltage of Current Density for Different Electrolytes | 138 |
| 6.3 | Effect of Voltage of Current Density for Different Electrolyte Concentrations | 139 |
| 6.4 | Effect of Current Density on MRR for Stainless Steel | 140 |
| 6.5 | Effect of Current Density on MRR for Tungsten Carbide, GT20 | 141 |
| 6.6 | Effect of Voltage on Surface Finish for Different Feed Forces | 142 |
| 6.7 | Effect of Current on Surface Roughness for Different Depths of Cut | 142 |
| 6.8 | Surface Texture of Tungsten Carbide | 144 |
| 6.9 | Surface Texture of Stainless Steel | 145 |
| 6.10 | Effect of Voltage on Spindle Load for Different Feed Rates | 146 |
| 6.11 | Effect of Electrolyte Flow on Current Density | 147 |
| 6.12 | Effect of Current Density on Feed Force | 148 |
| 6.13 | Effect of Current Density on Radial and Feed Force | 149 |
| 6.14 | Effect of Depth of Cut on Material Removal Rate | 149 |
| 6.15 | Effect of Current Density on Process Efficiency | 150 |
| 6.16 | Effect of Feed Force on Process Efficiency | 151 |

| | | |
|------|--|-----|
| 6.17 | Effect of Feed on Radial and Feed Force | 152 |
| 6.18 | Relationship between Feed force and Current in ECG | 153 |
| 6.19 | Theoretical and Experimental Results of MRR | 154 |
| A5.1 | Rotational Sensitivity and Stiffness of an Extended Octagonal Ring | 183 |
| A5.2 | Relation Between t/r and Strain Output for Different Rings | 185 |
| A5.3 | Geometry of Dynamometer | 186 |

LIST OF TABLES

| Table No. | Description | Page No. |
|-----------|--|----------|
| 1.1 | Non-Conventional Material Removal Processes | 3 |
| 1.2 | Classification of Nonconventional Machining Processes | 4 |
| 1.3 | Process Economy for Nonconventional Machining | 5 |
| 1.4 | Process Capabilities for Nonconventional Machining | 5 |
| 1.5 | Physical Parameters of Nonconventional Machining Processes | 6 |
| 1.6 | Comparison of ECG to Precision Conventional Milling and Grinding | 10 |
| 3.1 | The Common Electrolytes Used in ECG Operation | 45 |
| 4.1 | Metal Removal Rates for Various Metals | 96 |
| 6.1 | The Composition of Stainless Steel | 128 |
| 6.2 | The Composition of Tungsten Carbide, GT20 | 128 |
| 6.3 | Calculation Steps for ECE Weight (Stainless steel) | 129 |
| 6.4 | Calculation Steps for ECE Weight (Tungsten Carbide) | 130 |
| 6.5 | Comparison of Theoretically and Experimentally Obtained MRR | 155 |
| A5.1 | Data for Calibration of Dynamometer (Horizontal Load) | 188 |
| A5.2 | Data for Calibration of Dynamometer (Vertical Load) | 189 |
| A6.1 | Some Properties of WC-Co Materials | 190 |
| A 6.2 | Values of Different Parameters for Feed Force | 191 |
| A 6.3 | Grinding Conditions for Feed Force | 192 |

KEY NOTES

Abbreviation

Following standard and nonstandard abbreviations have been used in the text and illustrations of the dissertation.

| | |
|---------|----------------------------|
| GF | gauge factor |
| ID | internal diameter |
| ECM | electrochemical machining |
| MRR | material removal rate |
| DC | direct current |
| ECG | electrochemical grinding |
| AC | alternate current |
| V | voltage |
| KVA | kilovolt ampere |
| ECE | electrochemical equivalent |
| WC | tungsten carbide |
| LCD | liquid crystal display |
| DVM | digital voltmeter |
| OP Amp | operational amplifier |
| G-ratio | grinding ratio |
| SS | stainless steel |
| DNC | direct numeric control |
| CNC | computer numeric control |
| PVC | polyvinyl chloride |
| CBN | cubic boron nitride |

Symbols

Bold face with \wedge as superscript symbols indicate unit vectors. All headings in the main text are numbered using two and three digits, with decimal point *between* two digits. Two digits number indicates a section with first number as the number of chapter and second as the number of the section. In three digits number last number indicates subsection.

Figures, Tables and equations in the main text number with two digits - first one indicates the chapter and second as the actual number. Appendices are numbers as follows:

A 1.2 - means Appendix 2 related to Chapter 1 etc. Figures, tables and equations in Appendices are numbered by using the actual number after number of Appendix. For example, Fig. A.1.2.1 means the Fig. 1 in Appendix A.1.2. Number in between [] in the text indicates the serial number of the list of references.

Subscripts

| | |
|------|---------------------------------------|
| E | electrochemical |
| M | mechanical |
| T | total |
| TH | total horizontal |
| e | property of electrolyte |
| m | property of metal |
| n | normal |
| r | radial |
| t | tangential |
| +, - | property of +ve, -ve electrolyte ions |

(Other subscripts are defined in the text)

NOMENCLATURE

Followings are the principal notations. Some nomenclatures are described in the illustration (refer also the keynotes).

English Symbol

| | |
|---------------------------------|--|
| A | projected area of the abrasive grain, mm ² |
| A _p | wheel peripheral contact area perpendicular to current flow direction, mm ² |
| A _{pl} | area of cylinder on piston side, mm ² |
| A _{pr} | area of cylinder on piston rod side, mm ² |
| A _s | area of side contact, mm ² |
| C | abrasive grit protrusion distance from wheel bond, mm |
| D | diameter of wheel, mm |
| E | electrochemical equivalent of the workpiece, coulomb |
| E _{cell} | total emf of an electrolytic cell, volt |
| E _{red} | single electrolyte potential of the electrode forming reduction, volt |
| E _{ox} | single electrode potential of the electrode forming oxidation reaction, volt |
| F | Faraday constant equal to 96500C Mol ⁻¹ |
| F _c | cutting force, N |
| F _N | normal force, N |
| F _p | ploughing force, N |
| F _r | radial force, N |
| F _f | feed force, N |
| F _s | sliding force, N |
| F _T | tangential force, N |
| (F _p) _{TH} | total feed force due to ploughing, N |
| (F _r) _{TH} | total feed force due to rubbing, N |
| (F _c) _T | total feed force due to electrolyte pool, N |
| (F _s) _{TH} | total feed force due to sliding, N |
| (F _c) _{TH} | total feed force due to cutting, N |
| H | electrolyte film thickness at maximum pressure, mm |

| | |
|-----------|---|
| I | current allowed to flow, ampere |
| K | electrolyte conductivity, $\Omega^{-1} \text{ mm}^{-1}$ |
| K_i | coefficient fraction of weight for element i in the alloy % |
| L | distance between abrasive cutting points, mm |
| N_w | wheel speed, rpm |
| P | pressure intensity, N/mm^2 |
| P_P | pressure required of the fluid on piston side, N/mm^2 |
| P_{pr} | pressure required of the fluid on piston rod side, N/mm^2 |
| Q | total volumetric removal rate, mm^3/sec |
| Q_E | electrochemical volumetric metal removal rate, mm^3/s |
| Q_M | mechanical volumetric metal removal rate, mm^3/sec |
| R | linear rate of dissolution perpendicular to the workpiece, mm/sec |
| \bar{R} | resultant displacement vector, mm |
| S | circumferential pitch for the grit, mm |
| T | thermodynamic temperature, $^{\circ}\text{C}$ |
| U | free stream velocity of fluid or the peripheral velocity of grinding wheel |
| V | volume of metal removal, mm^3/sec |
| V_E | volume of metal removed due to electrochemical action, mm^3/sec |
| V_M | volume of metal removed due to mechanical action, mm^3/sec |
| V_{DC} | applied DC voltage, volt |
| V_f | linear feed rate, mm/sec |
| V_g | grinding wheel surface velocity, mm/sec |
| V_w | workpiece feed velocity, mm/sec |
| W | weight of metal removed/deposited, gm/mm^3 |
| a | grinding wheel radius, mm |
| b | width of grinding wheel, mm |
| c | atomic weight, gm |
| d | set depth of cut, mm |
| d_i | actual depth of cut, mm |
| dp/dx | pressure gradient |
| dy | incremental depth at y , mm. |
| e | strain |

| | |
|-----------|---|
| h | machining gap width, mm, |
| h_1 | electrolyte film thickness, mm |
| h_m | maximum chip thickness, mm |
| i | current density, amp/mm ² |
| \hat{i} | unit vector along X-axis |
| \hat{j} | unit vector along Y-axis |
| k | constant for anode material |
| k_i | chip thickness coefficient |
| k_L | loading force coefficient |
| l_c | wheel peripheral contact length, mm |
| m | number of grits present along the width of the wheel |
| n | number of rows present in the angle $(\alpha - \tau)$ rad |
| q | electrochemical equivalent weight of the metal removed, mm ³ /amp.s |
| q_i | electrochemical equivalent weight of the element considered, mm ³ /amp.s |
| r | radius of abrasive grain, μm |
| s | linear feed rate of the wheel, mm/sec |
| s_n | total feed rate per revolution, mm/rev |
| s'_n | mechanical feed rate per revolution, mm/rev |
| t | time spent to cut the surface, sec |
| u | specific energy, Joule/mm ³ |
| u_i | weight fraction of an element at a given valency, % |
| v | table speed, mm/min |
| v_e | flow rate of electrolyte, cc/min |
| w | width of grinding wheel, mm |
| x_1 | displacement of X-axis with respect to initial position of the wheel, mm |
| y_1 | displacement of Y-axis with respect to final position from the top surface, mm |
| z | number of elements soluble in the electrolyte |

Greek Symbol

| | |
|------------|--|
| α | angle of contact between wheel and workpiece, rad |
| α_1 | stress coefficient for normal ploughing force, N/mm ² |
| α_2 | stress coefficient for tangential ploughing force, N/mm ² |
| ρ | density of workpiece, gm/mm ³ |
| ρ_1 | density of element, gm/mm ³ |
| μ | coefficient of friction |
| τ | angle of sliding, rad |
| μ_r | ratio of tangential to normal force |
| λ | coefficient of sliding friction between tip are and workpiece, N/mm ² |
| θ | angle swept in a small interval of time t, rad |
| θ_1 | chip cross sectional area, mm ² |
| ω | angular velocity of the wheel, rad/sec |
| η | current efficiency |
| η_E | percentage of electrochemical action |
| η_F | Faradaic efficiency |
| η_M | percentage of mechanical action |
| δ_r | radial deflection, μm |
| η_a | activation overpotential |
| η_c | concentration overpotential |
| η_r | resistance overpotential |
| μ_1 | absolute viscosity |
| ν | kinematic viscosity |

TABLE OF CONTENTS

| Contents | Page No. |
|--|----------|
| Certificate | iii |
| Acknowledgements | iv |
| Bio-Data | vi |
| Abstract | vii |
| List of Figures | ix |
| List of Tables | xii |
| Key Notes | xiii |
| Nomenclature | xv |
| Table of Contents | xix |
| | |
| Chapter 1 Introduction | |
| 1.1 Non-Conventional Machining Process | 2 |
| 1.2 Technology of Electrochemical Grinding Process | 8 |
| 1.2.1 Process Capabilities | 11 |
| 1.2.2 Advantages | 12 |
| 1.2.3 Disadvantages | 13 |
| 1.2.4 Applications | 14 |
| 1.3 Objectives | 14 |
| 1.4 Scope of the thesis | 15 |
| | |
| Chapter 2 Literature Survey | |
| 2.1 Introduction | 18 |
| 2.2 Electrochemical Grinding Process | 18 |
| 2.2.1 Material Removal Mechanisms | 18 |
| 2.2.2 Surface Finish and Surface Integrity | 25 |
| 2.2.3 Wheel Wear | 28 |
| 2.2.4 Optimization | 31 |

| | | |
|-------|----------------------------------|----|
| 2.2.5 | Influence of Process Parameters | 32 |
| 2.3 | Electrochemical Grinding Wheels | 34 |
| 2.4 | Electrochemical Grinding Machine | 38 |
| 2.5 | Summary | 41 |

Chapter 3 Some Electrochemical Aspects of ECG

| | | |
|------|---------------------------|----|
| 3.1 | Introduction | 43 |
| 3.2 | Electrochemistry | 43 |
| 3.3 | Electrolytes | 44 |
| 3.4 | Electrolytic Cell | 44 |
| 3.5 | Oxidation and Reduction | 47 |
| 3.6 | Electrolytic Conduction | 48 |
| 3.7 | Electrochemical Reactions | 51 |
| 3.8 | Anodic Passivity | 55 |
| 3.9 | Oxide Dissolution Process | 57 |
| 3.10 | Summary | 59 |



Chapter 4 Theoretical Analysis

| | | |
|-------|--|----|
| 4.1 | Introduction | 61 |
| 4.2 | Grinding Geometry and Kinematics | 63 |
| 4.3 | ECG Process Description | 70 |
| 4.4 | Process Parameters governing MRR | 70 |
| 4.5 | Feed Force Analysis | 74 |
| 4.5.1 | Introduction | 74 |
| 4.5.2 | Feed Force due to Sliding | 77 |
| 4.5.3 | Feed Force due to Ploughing | 80 |
| 4.5.4 | Feed Force due to Cutting | 82 |
| 4.5.5 | Feed Force due to Rubbing | 83 |
| 4.5.6 | Force Due to Viscous Effect of Electrolyte | 84 |
| 4.5.7 | Feed Force Equation | 86 |
| 4.6 | An Analysis for MRR | 87 |
| 4.6.1 | Introduction | 87 |

| | | |
|-------|--|----|
| 4.6.2 | Material Removal Rate due to Electrochemical Action | 88 |
| 4.6.3 | Material Removal Rate due to Mechanical Action | 91 |
| 4.6.4 | Total Material Removal Rate | 94 |
| 4.7 | Difficulties with Theoretical Calculations | 95 |
| 4.8 | Summary | 97 |

Chapter 5 Design and Development of Experimental Set-up

| | | |
|-------|--|-----|
| 5.1 | Introduction | 100 |
| 5.2 | Schematic Layout of the Machine Set-up | 101 |
| 5.3 | Principle of Operation | 102 |
| 5.4 | Development of Hydraulic and Electrolytic Circuits | 105 |
| 5.4.1 | Cylinder and Piston | 105 |
| 5.4.2 | Hydraulic Circuit | 106 |
| 5.4.3 | Electrolytic Circuit | 108 |
| 5.4.4 | Feed Mechanism | 109 |
| 5.5 | Electronic Device for Force Measurement | 109 |
| 5.6 | Design, Construction and Calibration of the Dynamometer | 112 |
| 5.6.1 | Introduction | 112 |
| 5.6.2 | Design Calculations | 112 |
| 5.6.3 | Fabrication | 114 |
| 5.6.4 | Mounting of Strain Gauges | 114 |
| 5.6.5 | Calibration | 117 |
| 5.6.6 | Summary | 119 |
| 5.7 | Development of the Experimental Set-up | 119 |
| 5.7 | Conclusion | 123 |

Chapter 6 Experimentation

| | | |
|-----|-----------------------|-----|
| 6.1 | Introduction | 125 |
| 6.2 | ECG System Components | 125 |

| | | |
|-------|---|-----|
| 6.2.1 | Electrolytic Solution | 125 |
| 6.2.2 | DC Power Supply | 126 |
| 6.2.3 | ECG Wheels (Cathode) | 127 |
| 6.2.4 | ECG Machine | 128 |
| 6.2.5 | Work Material (Anode) | 128 |
| 6.3 | Planning of Experimentation | 131 |
| 6.3.1 | Experimental Studies | 131 |
| 6.3.2 | Process Variables | 132 |
| 6.4 | Details of Experimentation | 133 |
| 6.4.1 | Performance Test of the Machine | 133 |
| 6.4.2 | Influence of Different Variables on MRR | 135 |
| 6.4.3 | Influence of Different Variables on Feed Force | 135 |
| 6.5 | Results and Discussion | 137 |
| 6.5.1 | Effect of Voltage on Current Density | 137 |
| 6.5.2 | Effect of Current Density on MRR | 140 |
| 6.5.3 | Effect of Voltage on Surface Finish | 141 |
| 6.5.4 | Effect of Voltage on Spindle Load | 146 |
| 6.5.5 | Effect of Electrolyte flow on Current Density | 146 |
| 6.5.6 | Effect of Depth of Cut on MRR | 148 |
| 6.5.7 | Effect of Current Density and Feed Force on Process Efficiency | 150 |
| 6.5.8 | Effect of Feed Rate on Grinding Force | 151 |
| 6.5.9 | Effect of Current on Feed Force | 152 |
| 6.6 | Verification of the Theoretical Results | 153 |
| 6.6.1 | Material Removal Rate | 153 |
| 6.6.2 | Feed Force | 155 |
| 6.7 | Summary | 156 |

Chapter 7 Epilogue

| | | |
|-----|-----------------------|-----|
| 7.1 | General Remarks | 159 |
| 7.2 | Conclusion | 159 |
| 7.3 | Scope of Further Work | 161 |

| | |
|-------------------|-----|
| References | 164 |
|-------------------|-----|

Appendices

| | | |
|--------|---|-----|
| A4.1 | Derivation of Equation of Contact Length | 175 |
| A4.2 | Determination of Chip Thickness | 175 |
| A4.3 | Derivation of Area A_1 , A_2 and A_3 | 177 |
| A4.4 | A Sample Calculation for Theoretical and Experimental MRR | 179 |
| A4.4.1 | Theoretical MRR due to Mechanical and Electrochemical Actions | 179 |
| A4.4.2 | Experimental MRR due to Mechanical and Electrochemical Actions | 180 |
| A5.1 | Resistance Load for Table Movement | 181 |
| A5.2 | Specifications of Hydraulic Cylinder and Operating Valves | 181 |
| A5.3 | Calculation of Minimum Load for Dynamometer | 182 |
| A5.4 | Thickness of the Ring of Dynamometer | 183 |
| A5.5 | Arm Length of the Ring of Dynamometer | 185 |
| A5.6 | Gap between Horizontal Members of Dynamometer | 186 |
| A5.7 | Specifications of Strain Gauge | 187 |

CHAPTER - 1
INTRODUCTION

CHAPTER 1

INTRODUCTION

1.1 Nonconventional Machining Process

With the rapid technological advancements in the field of conventional machining processes, the machining of carbides and other hard-to-machine materials has been limited to the diamond wheel grinding for a long time. Moreover, the development of the so-called technologically advanced industries like aerospace, nuclear power etc. has been accompanied by an ever increasing use of high-strength-temperature resistant alloys. In many cases, the only effective way to machine such materials is by using common energy forms in new ways or apply the forms of energy never used before. The processing of the parts of complicated shapes has been difficult, time consuming, and uneconomical by conventional methods of machining [1].

Inventions have been created to meet increasingly complex needs of modern society, and new tools have been devised to enable the creation of increasingly sophisticated inventions resulting the introduction of new manufacturing technologies used for material removal, forming, and joining etc. These technologies play an important role for their steadily improving capabilities and beneficial effects of computer control, adaptive control, and education.

These processes are used to reduce the number of rejects experienced by old manufacturing method by increasing repeatability, reduction in breakage of fragile workpiece or by minimizing detrimental effects on workpiece properties [2].

Till now, about thirty three nontraditional processes have been industrially exploited and grouped according to their primary energy modes as shown in Table 1.1 [3]. Different forms of energy like electrical energy, chemical energy, high velocity jet of liquids, or abrasives, electrochemical reactions, and high temperature plasma etc. are applied to process the materials. Table 1.2 gives the process modes on the

Table 1.1 Nonconventional Material Removal Processes

MECHANICAL

| | |
|----------------------------------|-----------------------------------|
| AFM - Abrasive Flow Machining | AJM - Abrasive Jet Machining |
| HDM - Hydrodynamic Machining | LSG - Low Stress Grinding |
| RUM- Rotary Ultrasonic Machining | TAM- Thermally Assisted Machining |
| TFM - Total Form Machining | USM - Ultrasonic Machining |
| WJM - Water Jet Machining | |

ELECTRICAL

| | |
|---|---|
| ECD-Electrochemical Deburring | ECDG-Electrochemical Discharge Grinding |
| ECG - Electrochemical Grinding | ECH - Electrochemical Honing |
| ECM - Electrochemical Machining | ECP - Electrochemical Polishing |
| ECS - Electrochemical Sharpening | ECT - Electrochemical Turning |
| ES TM - Electro-stream | EJ - Electro Jet |
| STEM TM - Shaped Tube Electrolytic machining | |

THERMAL

| | |
|--|-----------------------------------|
| EBM-Electron Beam Machining | EDG-Electrical Discharge Grinding |
| EDM-Electrical Discharge Machining | EDS - Electrical discharge Sawing |
| EDWG - Electrical Discharge Wire Cutting | LBM - Laser Beam Machining |
| LBT - Laser Beam Torch | PBM - Plasma Beam Machining |

CHEMICAL

| | |
|-------------------------------|--------------------------------|
| CHM - Chemical Machining | ELP - Electro-polish |
| PCM - Photochemical Machining | TCM - Thermochemical Machining |
| TEM - Thermal Energy Method | |

Table 1.2 Classification of Nonconventional Machining Processes

| Type of energy | Mechanism of metal removal | Transfer media | Energy source | Processes |
|-----------------|----------------------------|-------------------------|------------------------------|------------------------|
| Mechanical | Shear | Physical contact | Cutting tool | Conventional machining |
| | Erosion | High velocity particles | Pneumatic/hydraulic Pressure | AJM, USM, WJM |
| Electrochemical | Ion displacement | Electrolyte | High current | ECM, ECG |
| Chemical | Ablative reaction | Reactive environment | Corrosive agent | CHM |
| Thermoelectric | Fusion | Hot gases | Ionized material | IBM, PAM |
| | | Electrons | High voltage | EDM, EBM |
| | Vaporization | Radiation | Amplified light | LBM |
| | | Ion stream | Ionized material | PAM |

NOTE:

IBM- Ion Beam Machining

PAM- Plasma Arc Machining

basis of type of energy used, the mechanism of material removal and the source of energy requirements [4]. The process economy and the process capabilities of different methods are summarized in Tables 1.3 and 1.4 [4].

Table 1.3 Process Economy for Nonconventional Machining Processes

| Process | Capital investment | Tooling and fixtures | Power requirement | Efficiency | Tool consumption |
|------------------------|--------------------|----------------------|-------------------|------------|------------------|
| USM | B | B | B | D | C |
| AJM | A | B | B | D | B |
| ECM | E | C | C | B | A |
| CHM | C | B | D | C | A |
| EDM | C | D | B | D | D |
| EBM | D | B | B | E | A |
| LBM | C | B | A | E | A |
| PAM | A | B | A | A | A |
| Conventional machining | B | B | B | A | B |

NOTE: A- Very Low Cost B- Low C- Medium D- High E- Very High

Table 1.4 Process Capabilities for Nonconventional Machining Processes

| Process | Metal removal rate mm/min | Tolerance μm | Surface finish CLA μm | Surface damage depth μm | Corner radii mm |
|------------------------|------------------------------|----------------------------|-------------------------------------|---------------------------------------|--------------------|
| USM | 300 | 7.5 | 0.2-0.5 | 25 | 0.025 |
| AJM | 0.8 | 50 | 0.5-1.2 | 2.5 | 0.100 |
| ECM | 1500 | 50 | 0.1-2.5 | 5.0 | 0.025 |
| CHM | 15.0 | 50 | 0.4-2.5 | 50 | 0.125 |
| EDM | 800 | 15 | 0.2-12.5 | 125 | 0.025 |
| EBM | 1.6 | 25 | 0.4-2.5 | 250 | 2.50 |
| LBM | 0.1 | 25 | 0.4-1.25 | 125 | 2.50 |
| PAM | 75000 | 125 | Rough | 500 | - |
| Conventional machining | 50000 | 50 | 0.4-5.0 | 25 | 0.050 |

Before selecting any process for an application, the following aspects should be considered:

- i) physical parameters,
- ii) properties of work material ,
- iii) complex geometry of the work piece,
- iv) process capabilities,
- v) need for higher production rate,
- vi) closer tolerance , surface finish and surface integrity, and
- vii) economic considerations.

These processes are generally characterized by their high power consumption and lower material removal rate. As seen in Table 1.5, both USM and EDM require almost equal power. On the other hand, ECM is found to consume about forty times more power than EDM. Both ECM and EDM need electrically conductive material to machine. ECM has the advantage of a very low tool wear ratio[4]. Fig.1.1 demonstrates the relationship among conventional and nonconventional machining processes with respect to surface finish and dimensional tolerances [3].

Table 1.5 Physical Parameters of Nonconventional Machining Processes

| Parameters | USM | AJM | ECM | CHM | EDM | EBM | LBM | PAM |
|---------------|-------------------|-----------------|---------------|-----------------|-------------------|-----------------------|----------------------|-------------------|
| Potential (V) | 220 | 220 | 10 | - | 45 | 150,000 | 4500 | 100 |
| Current (Amp) | 12 (A.C.) | 1.0 | 10,000 (D.C.) | - | 50 (Pulsed D.C) | 0.001 (Pulsed D.C.) | 2 (average 200 peak) | 500 (D.C.) |
| Power (w) | 2400 | 220 | 100,000 | - | 2700 | 150(average 200 peak) | - | 50,000 |
| Gap(mm) | 0.25 | 0.75 | 0.20 | - | 0.025 | 100 | 150 | 7.5 |
| Medium | Abrasive in water | Abrasive in gas | Electrolyte | Liquid chemical | Liquid dielectric | Vacuum | Air | Argon or hydrogen |

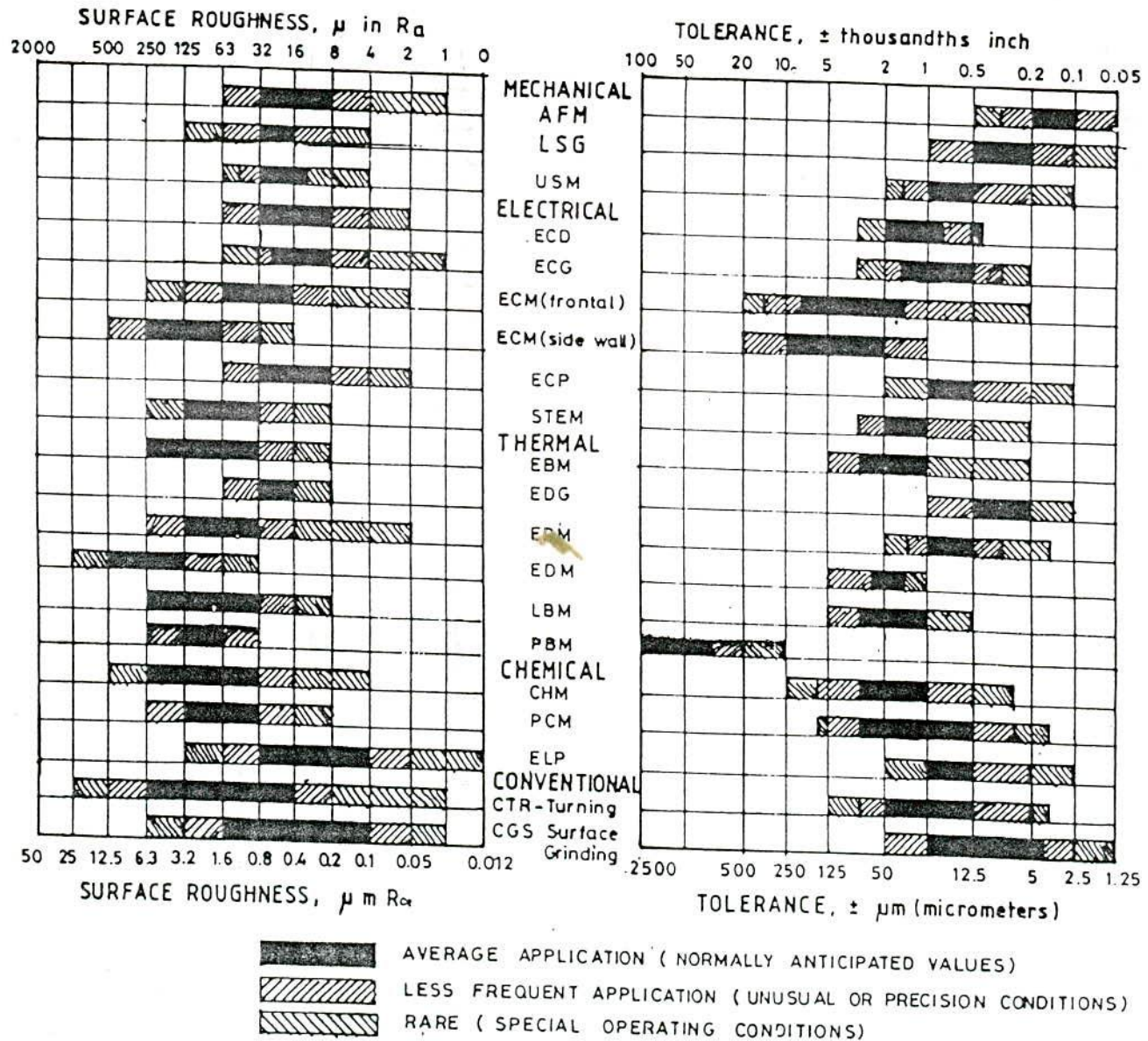


Figure 1.1 Surface Roughness and Tolerances Produced by
 Nonconventional Machining Processes[3]

1.2 Technology of Electrochemical Grinding

Electrochemical grinding is a special form of electrochemical machining in which the conductive workpiece material is dissolved by anodic action and any resulting films are removed by a rotating conductive abrasive wheel. The coolant used in abrasive grinding becomes the electrolyte in electrochemical grinding. Electrolyte is prepared by adding various salts of nitrates, chlorides, citrates etc. with water. The purpose of the abrasive particles is to maintain a working gap between the wheel bond and the work piece; and to remove the oxide film formed on the workpiece surface, if any. The wheels commonly used in ECG are: metal bonded diamond wheels for grinding tungsten carbide and other difficult-to-grind materials, metal filled resin bonded aluminum oxide wheels for grinding ductile metals [5, 6].

Brushes are used to bring the current from the power source to the spindle from which it flows to the grinding wheel. The dissolution rate of different substances is proportional to their chemical equivalent weights. The machining rate is affected by the workpiece passivity and current efficiency. Besides oxide films, the abrasive grit can also influence the stock removal significantly by mechanical action. To choose an electrolyte, the requirements should be taken into consideration are high electrical conductivity, high specific heat, high thermal conductivity, and the most important one is the chemical composition compatible with workpiece material not to cause preferential removal of different elements.

Theoretically, only a few volts are required for metal transfer in an electrolytic cell. The maximum voltage that can be served depends on the capacity of power supply unit employed and the current requirement. The material removal process internally influenced by wheel variables and externally regulated by operating voltage, feed rate, and the flow of electrolytes. Mechanical and electrochemical proportions of the total stock removal can be balanced for maximizing removal rate as well as working accuracy as summarized in Fig. 1.2 [8].

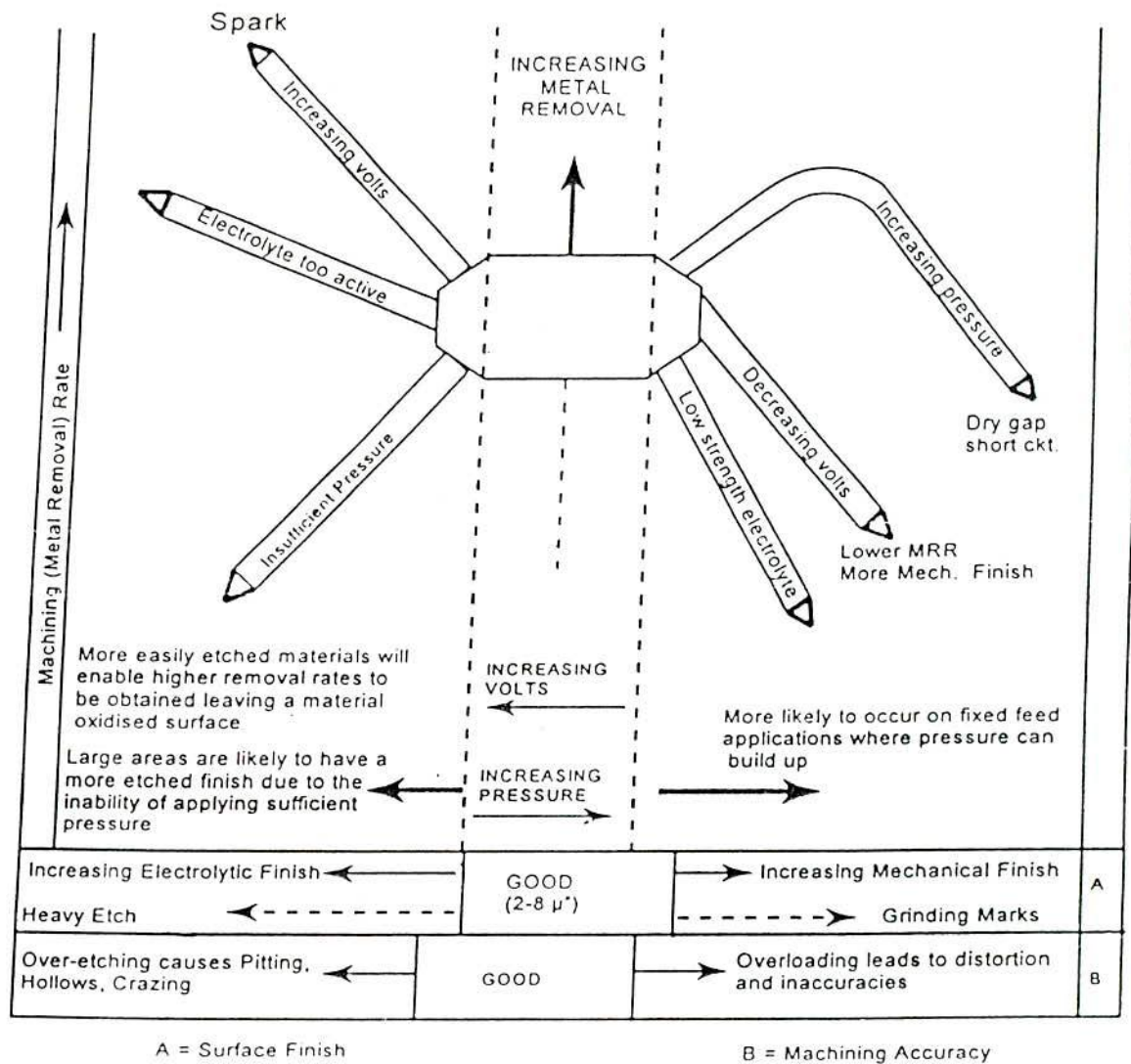


Figure 1.2 Summary of the General Effects of Electrochemical Grinding

A comparison between the ECG to precision milling and grinding process has been illustrated in Table 1.6. The superiority of ECG over conventional machining (conventional grinding) is exhibited for stock removal, tooling cost replacement. It also shows better machinability of fragile parts, lower heat damage, quality of surface finish and problems with burr [9]. The amount of current flowing through the gap and material removal rate are mainly determined by the applied potential difference (d.c. voltage), the machining gap, and engagement area between the wheel and workpiece. Fig. 1.3 represents the basic scheme of the process.

Table : 1.6 Comparison of ECG with Conventional Milling and Grinding [9]

| Material | Stock Removal (Milling) | Stock Removal (Grinding) | Tooling Cost & Replacement | Size Control | Production of Fragile Parts | Potential of Heat Damage | Quality of Surface Finish | Problems with Burrs |
|-------------------|-------------------------|--------------------------|----------------------------|--------------|-----------------------------|--------------------------|---------------------------|---------------------|
| Machinery steel | - | = | - | - | + | = | = | + |
| Tool steel, soft | - | = | - | - | + | + | = | + |
| Tool steel, hard | + | + | - | - | + | + | = | + |
| Cast iron | - | - | - | - | + | = | - | = |
| Copper | - | + | - | = | + | - | + | + |
| Brass | - | + | - | = | + | = | = | + |
| Aluminum | - | - | - | - | + | = | - | + |
| Tungsten | - | + | - | = | + | + | + | + |
| Tungsten carbide | + | + | + | = | + | + | + | = |
| Beryllium | - | = | - | - | = | = | - | + |
| 300 stainless | - | + | + | = | + | + | + | + |
| 400 stainless | - | + | + | = | + | + | + | + |
| Titanium | - | = | = | = | + | + | = | + |
| Waspaloy | + | + | + | = | + | + | + | + |
| Inconel 718 | + | + | + | = | + | + | + | + |
| Inconel X | + | + | + | = | + | + | + | + |
| Hastelloy alloy X | + | + | + | = | + | + | = | + |
| Udimet 500 | + | + | + | = | + | + | + | + |
| Udimet 700 | + | + | + | = | + | + | + | + |
| Greck Ascology | - | = | + | = | + | + | = | + |

= Processes about equal
 - ECG inferior to conventional machining
 + ECG superior to conventional machining

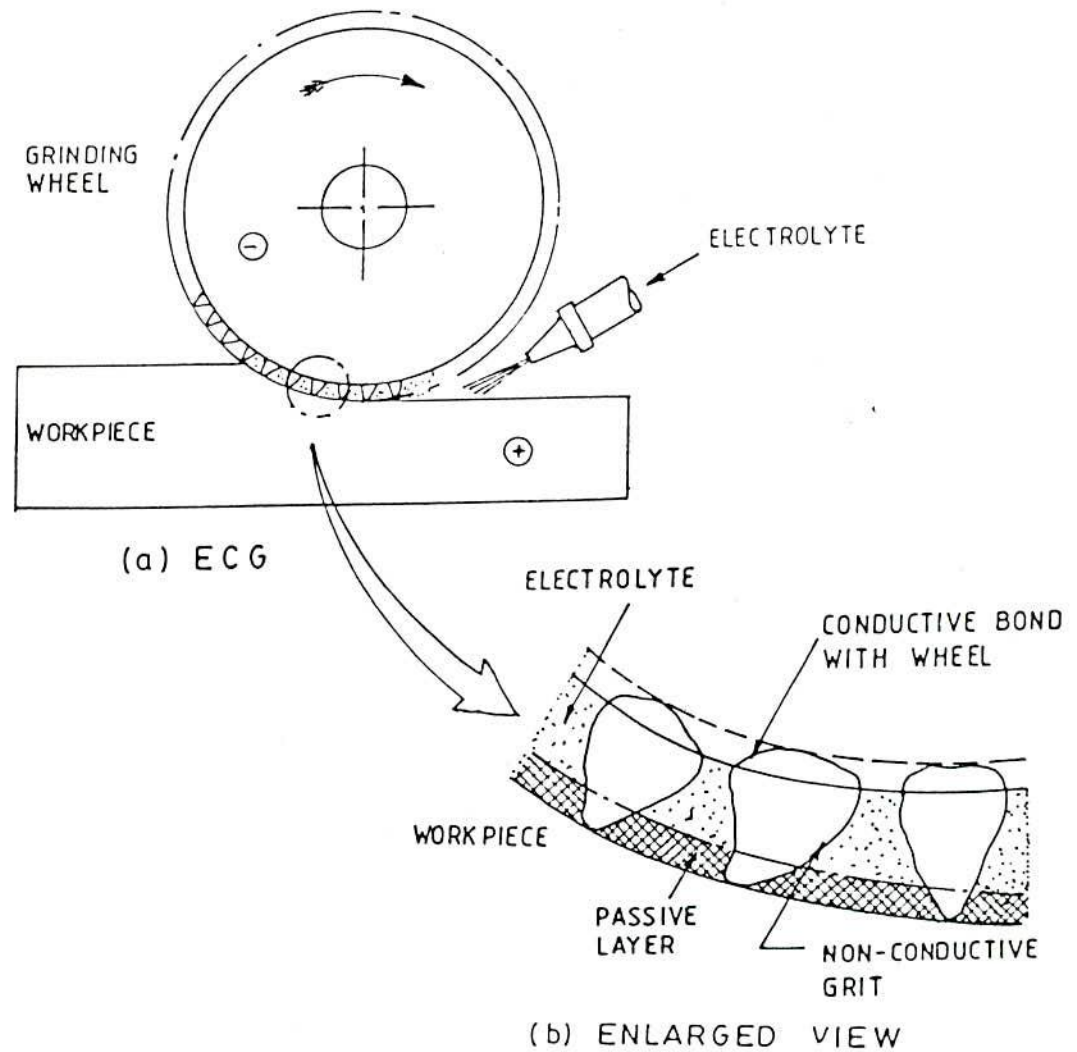


Figure 1.3 Basic Scheme of ECG Process

1.2.1 Process Capabilities

The process exhibits material removal rate that goes upto ten times faster than conventional grinding on materials harder than $HR_c 60$. The average value of metal removal rate is $1.6 \text{ cm}^3 / \text{min}/1000\text{A}$ [2]. The DC power supply provides voltage control from 0 to 15 volts and standard amperage ratings are 300, 600 and 1000A but

higher amperages are available. With proper application, tolerance of 0.05 mm can be achieved but with the extreme control of electrochemical grinding parameters, tolerances as close as 0.003 mm are possible [10].

Current densities range from 2 A/cm² in grinding tungsten carbide to about 3 A/cm² in grinding steel. The surface finish is affected by the metallurgy of workpiece. When electrochemical grinding is performed perfectly, the resulting surface is a microstructure of the workpiece crystalline structure. On tungsten carbide this generally provides a surface finish in the range of 0.4 to 0.5 micron for surface grinding, and 0.2 to 0.4 micron for plunge grinding. In case of steels and various alloys, it ranges from 0.4 to 0.6 micron [4].

Wheel speeds are most often found between 22 and 35 m/sec. The temperature of the electrolyte is usually maintained between 90- 110° F (32 - 43°C), pressure used to pump the fluid is about 5 - 10 psi (35-70 kPa) [11]. The longitudinal feed rate should not exceed 6m / min [41].

1.2.2 Advantages

Electrochemical grinding is best suited for fast machining very hard materials like carbide at major savings compared to that of conventional machining techniques. High strength materials in the range of 200,000 - 400,000 Psi tensile strength (1400 - 2800 Mpa) can be worked as readily as low strength materials. The machining of dissimilar metals such as brazed carbide tool assembly is highly productive in ECG process [12]. This machining process provides high metal removal rate specially with cobalt-nickel- alloys and high tensile strength materials. It does not affect the yield strength, sustained load strength, ductility or hardness of most alloys and metals (10, 13). Depending upon feed rate, size of wheel and other process variables, the wheel life can be increased from 500 to 1200 percent. Full-depth of cuts are made in one pass [19]. A program of quality improvement and cost reduction led to the use of electrochemical grinding which is associated with less force and power.

Hence the advantages offered by electrochemical grinding are higher material removal rate, practical elimination of mechanical or thermal cracking, deburring operations, stress-free in the component surfaces, undesirable reduction of wheel wear, independence of work material hardness, component accuracy, and capacity to grind assembled components consisting of different metals [14].

1.2.3 Disadvantages.

Electrochemical grinding needs contact area between anode and cathode to draw a current for which a DC power source is very much essential. Initial cost of the machine is comparatively high. Some applications are restricted to grinding geometries. Small I.D. grinding operations would be impracticable [14].

Since, only chemically conductive materials can be ground, the electrolyte used may corrode the workpiece. Therefore machine parts coming into contact with electrolyte must be anticorrosive (chrom plated). Holding of sharp corners is a major limitation of this process as the electrolytic action is nondirectional. Inside corners can not be ground sharper less than 0.25 to 0.40 mm radius because of the overcut and the accuracy is limited to 0.001 mm only [6,15]. ECG users usually accept the overcut which is really difficult to control. This is caused by over electrochemical dissolution of the workpiece which is not at all desirable [20].

It is not economical for soft materials and needs high preventive maintenance costs [2]. Copper-resin-bonded diamond wheels may be dressed to simple forms only. Intricate forms with multiple radius tangents and very deep forms require single-layer, plated-metal bonded diamond wheels [17].



1.2.4 Applications

Electrochemical grinding is applicable primarily where conventional abrasive grinding is unsatisfactory. Such areas include:

- i) form grinding of hard to grind ductile metals,
- ii) grinding of heat and stress sensitive materials,
- iii) generating burr and distortion free pieces, and
- iv) stock removal on extremely hard to grind materials[6].

This process has received wide application in the field of aircraft turbine industry for the production of blades, vanes, honey comb seal rings, and also employed in rail-road industry to profile worn locomotive traction motor gears. This has also been found for extensive use in the textile industries and automotive, instrumentation, and industrial knife market [2,10].

The increased use of stainless steel and new exotic materials such as medical devices, instruments and forceps, pace maker shells, precision nozzles, instrument coupling and air rotor motors, and grinding of carbide cutting tools have all successfully been accomplished with ECG [4,18]. It has long been adopted for use in grinding of cutting and turning tools [19].

1.3 Objectives

From the forgoing discussion it is clear that ECG process offers many advantages and applications over conventional processes. Though it can not replace any of the conventional processes, it has its own special features and advantages. Hence it is necessary to find out the optimum conditions under which most of the objectives like MRR, surface finish, surface integrity can be achieved. The present need of processing hard to machine materials with high surface finish, stress and crack-free surface required is demanding import of electrochemical grinding machines. The high import cost of such machine has forced to initiate the

development of a machine.

Keeping the above facts in view, the objectives of this research program are as follows:

- a) development of an electrochemical surface grinding machine with automatic hydraulic feed drive retrofitting an existing obsolete conventional peripheral surface grinder with manual feed, in house,
- b) design, construction and calibration of a two component octagonal extended type grinding dynamometer for measurement of vertical and horizontal force components, to measure forces subsequently on a transducer for adaptive control,
- c) development of a mathematical model to quantitize material removal rate due to electrochemical and mechanical actions,
- d) development of a mathematical model for feed force,
- e) performance evaluation of the developed machine set-up, and
- f) corroboration of the model with experimental results.

1.4 Scope of the Thesis

The thesis consists of seven chapters of which the present one is Chapter 1. This chapter introduces the subject and contains the development of the electrochemical grinding process and illustrates its technology. The fundamentals, importance, and applications of the process along with its drawbacks are furnished. The main objectives of the thesis have also been included.

An up-to-date past research work encompassing all the areas involved related to the "Studies on some aspects of electrochemical grinding" has been

briefly discussed in Chapter 2. It provides a comprehensive literature review for material removal mechanism, surface finish and surface integrity, influence of process parameters, ECG machines, grinding wheels and process optimization.

Some important electrochemical aspects are provided in Chapter 3 which illustrates electrochemistry, electrolyte phenomenon, electrochemical reactions, anodic passivity and dissolution phenomena.

Chapter 4 describes the details of the analytical part of the thesis including kinematics of the process, process parameters governing MRR, a theoretical model developed for predicting material removal rate due to electrochemical action and that of mechanical action. A generalized feed force equation has also been developed and presented.

Chapter 5 contains the details of main experimental test-rig. It deals with the design and development of the set-up that includes:

- i) the schematic layout of the machine,
- ii) principle of operation,
- iii) development of hydraulic and electrical circuits,
- iv) electronic device for force measurement, and
- v) design, construction and calibration of a grinding dynamometer.

Chapter 6 describes the experimental investigation which includes studies on the effect of different process parameters. Experimental designs, procedures, and set up for experimental studies can be found in this chapter. Towards the middle of the chapter the major parameters involved during experimental studies have been highlighted. Important results are discussed and developed models are corroborated.

Chapter 7 briefly summarizes the major observations drawn from the present investigation and concludes the work. It enlightens the scope of future work which is followed by references and appendices.

CHAPTER - 2
LITERATURE SURVEY

CHAPTER 2

LITERATURE SURVEY

2.1 Introduction

The electrochemical grinding process was introduced in the early 1950's evolving from the developments in the USSR on electrical discharge machining [13]. Its first appearance in the west was in the form of a machine built in Gloucester, UK following which a patent was filed, covering the use of tool electrode containing particles of insulating material projected from the surface of the tool. To remove metal from a workpiece utilizing the electrochemical method, the commercial machine tools used were grinding machines. Ilhan [20] reported that the electrochemical grinding machine appeared in the USA around 1953 for grinding of tungsten carbide cutting tools. Since then the use of ECG has been replaced by several other methods including conventional grinding and electrodischarge grinding.

It was also reported by Thompson [6] that ECG first became known to industry as a process using metal bonded diamond wheels to grind tungsten carbide in 1950, and using electrically conductive resin bonded aluminum oxide wheels to grind ductile metals in 1960. The productivity of ECM was increased by modifying the process into 'Anode Machining' and then to electrochemical machining. Past research pertaining to material removal mechanisms, surface finish and integrity, influence of various parameters, and recent development in the grinding wheel and ECG machines are included in the following sections.....

2.2 Electrochemical Grinding Process

2.2.1 Material Removal Mechanisms

The principle and mechanism of the process have been illustrated very extensively by De Barr [16] and McGeough [65].

Phillips [10] presented the principle of electrochemical grinding process and reported that variables influencing ECM would also influence the electrochemical grinding process.

The basic mechanism of the process was studied by Jones[42] and explained the basic electrochemical reactions which might occur in the process. To get optimum results from ECG, the function of the wheel and the different ways that could be used were needed to be considered.

The fundamental removal modes involving mechanical abrasion, and one, having no mechanical contribution viz. (i) totally mechanical removal (ii) electrochemical removal combined with mechanical and zero overcut (iii) electrochemical removal combined with mechanical removal and an overcut greater than zero and (iv) totally electrochemical removal were studied by Atkinson and Noble [21]. Nimonic 105 and AISI01 tool and die steel were machined with single pass peripheral electrochemical grinding using a diamond grit wheel. They also tested with mild steel. A 100/120 non-formable diamond grit wheel was used and electrolyte solution was supplied using a front and rear entry nozzle. They concluded that with zero electrochemical contribution, changes in applied voltage could not influence the workpiece surface. The electrochemical removal for surface roughness was found to increase slightly with the increase of applied voltage.

The relative amount of material removal due to electrochemical and conventional grinding actions were investigated by Cole[22]. The interrelationship amongst electrolyte flow rate, voltage, current density, MRR and the efficiency of the process was also investigated by him. Several phenomena of the process were explained on the basis of hydrogen gas pressure in the work-wheel interface. During ECG of hot rolled plain carbon steel by diamond embedded wheel, a combination of potassium nitrate (KNO_3) and potassium nitrite (KNO_2) in aqueous solution of strength 10% and 5% by weight respectively was used. The Faradaic efficiency appeared to be almost 100% while the process efficiency was about 97.5%. A formula was presented for hydrogen gas pressure in the work-wheel interface as follows:

$$\Delta P = \frac{12\mu L Q_a P_a}{3bd^2 P_i}$$

Where,

L = average path length of superimposed gas-electrolyte flow, in

μ = viscosity of gas-electrolyte mixture, lb.sec/in³

d = work-wheel interface gap, in

P_i = average pressure in work-wheel interface, lb/in²

P_a = atmospheric pressure, lb/in²

Q_a = volume of flow rate of gas-electrolyte mixture at atmospheric pressure, in³/s

Physical aspects of the electrochemical grinding process were studied by a number of researchers. Colwell [62] studied experimentally the dependence of many variables like current, feed rate, feed force, voltage, spindle power and gap resistance with each other. A physical model of the gap between the grinding wheel and the workpiece was suggested. In his study, he focussed on the relationship between the gap resistance and the feed force. Analysis of experimental data against the physical model for a broad range of operating conditions suggested somewhat more explicit conclusions.

Investigation on electrochemical grinding of WC-Co cemented carbides, with particular consideration of their heterogeneity was carried out followed by an analysis of the electrochemical removal process [24]. It was shown that electrochemical dissolution penetrating into cobalt phase occurred initially at a much faster rate than that of the carbide phase. The interaction between the electrochemical and mechanical processes was illustrated based on experimental results.

The quantitative characterization of surface damage to WC-Cobalt composites by ECG process was studied by Malkin and Levinger [25]. A method for measuring the degree and depth of damage in the surface layer was developed. The degree of

weakening was expressed as the ratio of the specific grinding energy of the material in the surface layer to the normal specific grinding energy. They also stated that surface damage from electrochemical grinding could reduce the specific grinding energy by as much as factor of 10 at the finished surface. They concluded that the depth of damaged layer was shallower with a lower current density and a faster infeed velocity.

The grinding mechanism for WC-Co cemented carbides, with particular consideration of the role of plastic flow was studied in more detail, by many researchers [25,26]. Their investigations were to relate measurement of grinding forces, energies to the grinding wheel topography. The experiments were performed on various types of WC-Co cemented carbides with different grinding wheels over a wide range of workpiece velocities and depths of cut. An analysis of the specific ploughing energy relationship obtained from grinding model suggested that plastic deformation of the cemented carbide workpiece occurred by a ploughing force along the abrasive grain cutting edges, which was proportional to the engaged cutting edge length.

The electromechanical grinding of alloy tool steel and some other alloys was investigated at a higher work feed rate than that used in ECG by Hasegawa et al [28]. An experimental analysis of grinding forces showed a slight decrease in mechanical removal and a severe loss of mechanical properties. Additional contributions of the electrolytic action to a reduction of grinding forces were also clarified.

Action of a non-grit wheel was first examined by Noble [29] to determine inter-electrode gap values with different set depth of cuts and machining parameters. He mentioned that in peripheral electrochemical grinding, the surface of the rotating disc has non-conducting grits protruding above the surface of the conductive bond. At any angular position where mechanical action was included, the resistance in the inter-electrode gap would be constant.

Kaczmarek et al [30] investigated the electrochemical and mechanical actions on the material removal rate of grinding cemented carbide and high speed steel tool

materials. Electrochemical penetration velocity based on Faraday's first law, and mechanical removal rate depending on the peripheral velocity of the wheel, the feed rate, the pressure, and the depth of cut were studied. From theoretical studies some recommendations of the optimization of the process were provided. It was reported that the process efficiency was highest with a diamond wheel and lowest with alundum (Al_2O_3) wheel for machining sintered carbides. The magnitude of process efficiencies for carbide and HSS, when ground by diamond wheel were about 80% and 60% respectively. But when the same work materials were ground by aluminum oxide wheel the process efficiencies came down to about 25% and 12% respectively.

A theoretical analysis of electrochemical grinding process was introduced by Shan [31]. Equations for material removal due to electrochemical dissolution and that of mechanical grinding were derived as:

$$V_E = b \left[-\frac{r}{2t} R^2 + (2rt)^{\frac{1}{2}} R \right]$$

and

$$V_M = bft - V_E$$

Where,

f = longitudinal table feed,

r = radius of the wheel

t = depth of cut,

V_E = material removal due to electrochemical action, and

V_M = material removal due to mechanical action.

Electrochemical plunge-in-grinding of small-diameter carbide specimens brought about the enveloping surfaces of the multi-point cutting tools made of solid [32]. A model that was developed could be considered as the cutting and burnishing rings of a multi-component broach. In his investigation on material removal, the function of current versus depth of cut was determined. To measure the concentricity of the produced broach, the machining deformation was found to be due to the

dissolution of stock, the inaccuracy of main spindle and the mechanical load due to contamination of electrolyte. The experiment was carried out with high speed steel (grade R6).

Okhten [33] reported that the electrolytic diamond grinding process was highly affected by variations in contact area between the wheel and workpiece in the direction of electrolyte motion. A method for calculating stock removal rate was also proposed for the process.

The role of electrochemical dissolution of a surface on the mechanical properties of copper specimens in electrolytic diamond grinding was studied [34]. That lead to the proposition that micro cutting took place due to the decrease in limiting strength of the metals.

Electrochemical cylindrical grinding of small diameter specimens made of tungsten carbide, were theoretically analyzed by Kaldos [35]. The arc and area of contact, as well as material removal are of great importance. The experiments proved that the electrochemical external deep grinding technique was advantageous for tungsten carbide of size of 15 to 20mm diameter. Predictions obtained from the theoretical analysis showed a correlation to the experimental results. For cylindrical grinding, removal rate was found to be a linear function of width of wheel, number of revolutions, diameter of specimen, and a quadratic function of depth of cut.

Experiments were carried out on various grades of WC using diamond grinding wheel and aqueous solution of NaNO_3 15% by weight as electrolyte. The effect of magnetic field on material removal rate, power consumption, current density, Faradaic and process efficiencies were discussed [36,37]. They concluded that material removal was increased at lower and higher ranges of feed forces. The volume of metal removed by ECG process was proportional to the current flow across the gap between workpiece and the wheel. This did not take into account the metal that was removed mechanically by the abrasive grits in the wheel [9]. It is generally accepted as a rule of thumb that the volume of material removed electrolytically by ECG is $7.3 \text{ mm}^3/\text{s}$ ($0.1 \text{ in}^3/\text{min}$) for each 1000 amps of

current flow through the gap [9,4,3]. Two fundamental factors: i) the ionization rate of the electrolyte and ii) the relative affinity of the electrolyte anion for the workpiece metal, directly result in establishment of any specific current density in the area of electrolytic action [9].

The principal operating features of the vertical spindle surface grinding machine were illustrated through the analysis of process electromechanics on the basis of simple dynamic behaviour [38]. The current waves developed during machining were evaluated.

The supply and distribution of electrolyte is important not only with regard to removal rate but also with unwanted side-effects [99]. The effect of operating parameters on efficiency, accuracy and controllability was pointed out. The main problems associated with electrochemical surface grinding were summarized. Effect of edge erosion and variation of depth of cut or set depth of cut ratio with transverse feed were analyzed.

Material removal of cemented carbides and dissolution were investigated and it was presumed that cobalt binder was removed first by anodic dissolution leaving the skeleton carbide structure having 1/3 rd of the original strength [41]. His concluding report includes that ECG of carbide when metal bonded diamond wheel is used, provides a very fast MRR with high process efficiency. The effect of operating conditions on surface finish and wheel was presented by using different wheel parameters.

McMillen [12] investigated the ECG process from his own experience as a research and development engineer. He pointed out its major complaints and benefits. The ability to grind burr free parts was a welcome relief and the possibility to grind dissimilar materials without loss of dimension or surface integrity added much to the liberty of the design engineer.

2.2.2 Surface Finish and Surface Integrity

Surface integrity is mainly governed by differential electrochemical activity of the micro-structural constituents, by the process voltage, and by the amount of mechanical contribution to the process [40]. Finish grinding under suitable conditions permits close dimensional control and yields a good surface quality for tungsten and composite carbide systems but not for the titanium carbide systems because of local activation.

Geva et al [40] briefed about the effect of peripheral electrochemical grinding process on surface finish, in case of sintered carbides. The different wheel-workpiece regions- the 'contact' region, characterized by a simultaneous electrochemical action, abrasive action, and 'after-wheel' action in which only the electrochemical aspect is present were examined. Geometrical surface parameters such as overcut and surface roughness were found related to those of the main process. The electrochemical surface parameters such as selective etching, oxide layer formation, and local activator were also evaluated.

Ranganathan [61] worked on the electrolytic grinding of titanium, and reported that ECG damaged work surface forming pits which act as crack-initiation sites for fatigue failure. In ECG, the surface integrity and fatigue strength were found to decrease when titanium based materials were machined. On the other hand, no inter-granular attack was observed which implied that there was no electrochemical corrosion due to the electrolyte.

The surface effect and residual stresses in electrochemical grinding were studied by Frisch and Cole [63]. Their principal observations are as follows:

- i) ECG with low feed rate and low feed force does not induce any appreciable residual stress, and the normal condition results small compressive stress compared to large tensile stress.



ii) Surface finish and accuracy improve with feed force and flow rate within certain limits.

It was reported [21] that, under purely electrolytic condition, surface roughness increased with increasing applied voltage and decreased feed rate. Surface finish was not influenced by wheel variables but with some proportion of mechanical removal, surface finish improved as voltage was decreased and feed rate was increased. A better surface finish was obtained by using a fine rather than a coarse grit wheel and a formable bond aluminum oxide wheel rather than diamond impregnated wheel. The resulting surface finish was found to exhibit remarkably consistence characteristics with the material removal modes. It was stated that the surface finish data was very useful to identify appropriate operating parameters. With increasing applied voltage, the non-uniformity of electrolyte flow had increasingly aggravated the deterioration of surface finish.

The effect of magnetic field on surface roughness was investigated by Kuppuswamy and Venkatesh [37]. They showed that magnetic field increased the activity of electrolytic process, and the roughness was the outcome of complex dynamic process of anodic dissolution. The grinding wheel abrasives aided the process by removing the oxide layers, carbide skeleton, and the extent of mechanical removal.

Workpiece hardness is not a dependable factor but the type of material can affect the roughness values. It is mentioned that the surface texture was found to be similar to that obtained with a metallographic polish. There is no heat-affected zone and the surface is free from any induced residual stress contributing to the production of workpieces with high surface integrity [3]. Current density is an important factor to determine the electrochemical action and surface finish. A chart, for determining contact length and feed rates with respect to different depths of cut, is shown in Fig. 2.1.

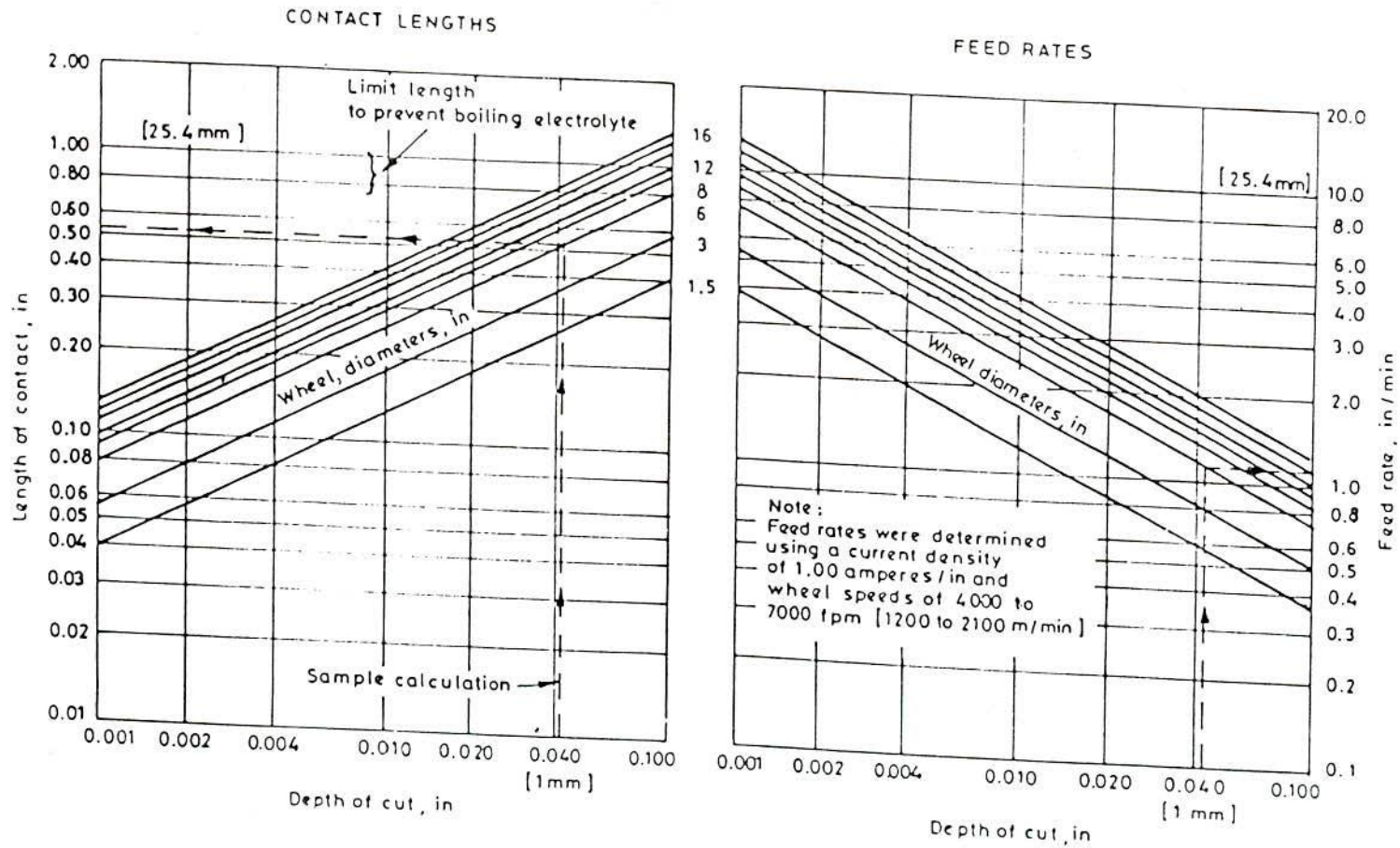


Figure 2.1 The Chart for Surface ECG to Determine Contact Length and Feed Rates

It is provided in [4] that, the higher the hardness of an alloy, the better is the surface finish. Surface finish depends on the type of grinding and the workpiece material. Most steels and other alloys when electrochemically ground, have a surface finish of 0.37 to 0.7 micron [9].

The electrochemical grinding may be widely used in production, if the grinding wheels have sufficient mechanical cutting ability that leads to the finer surface finish of high accuracy. A nickel coated vitrified wheel was developed by Kubota [58]. He reported that in working hardened steel, a metal bond CBN wheel and a nickel coated vitrified wheel would have sufficient cutting ability [58].

Different applications of electrochemical grinding were described, and machining time was compared for electrochemical grinding to conventional grinding by Knight et al [79]. The process was found to reduce the grinding time per specimen for several hours to a few minutes and resulted superior surface finish and dimensional tolerances.

Gutt et al [93] studied the mass and energy balance sheet in grinding of cemented carbide bits and expressed that the higher the current density the lower ^{is} the total specific energy consumption. The work specimen of P-25 cemented carbide was used.

2.2.3 Wheel Wear

Wheel wear comprises of wear of abrasive grits, wheel bond, micro-fracture of abrasive grains, corrosive wear etc.. They are increased significantly as the feed rate increases but not much affected by any operating variables at low feed rate. Ilhan [44] observed that the wheel wear was mainly caused by the breakdown of abrasive grains during operation and affected by the attrition resistance and the friability of the grit material. The wheel wear was found to increase with the process conditions that led to short-circuiting and anodic passivity. Attrition resistance is the degree of area in contact with the material being machined.

The impact of the forces created due to mechanical contact of the grains with the workpiece, the corrosive grits were broken down causing the wheel radius to change [97].

The bond metal along with the impregnated abrasive grits may be found as a 'welded deposit' on the workpiece surface which consequently fuses to the wheel surface [7].

Grit concentration on different parameters, and the relationship between wheel wear and pressure for diamond wheels were investigated by Veromen [101].

Sfantsikopoulos and Noble [102] suggested an electrochemical wheel dressing method so that it could remove the mechanical debris, conductive bond 'peaks' and expose the diamond grits on the working surface of the wheel. They claimed that this method would significantly extend the useful life of the wheel and assured stable ECG, at least when grinding tungsten carbide. Electrochemical dressing was shown to remove conductive products from the inter-grit spaces.

Nankov [55] explained the effect of specific wheel wear for different sets of voltage and depth of cut specially in grinding hard alloy workpiece by diamond wheel.

A formula was proposed by Balashov [41] to determine wheel wear, and the metal bonded diamond wheels were found to be the most suitable wheels for electrochemical grinding.

Opitz and Heitmann [97] reported that in ECG there was a tool wear caused by mechanical metal removal component. Increasing pressure caused increasing tool wear. The wheel bond, not being in contact with workpiece material, showed a wear caused by spark formation and lapping activities of chips.

The wheel wear considerations were extended by the machine and labor costs due to economic calculations in electrochemical grinding [56]. The maximum

wheel pressure or minimum gap width was limited by the maximum current density values.

The most economic process is ECG with metallic-bond abrasive wheels for machining parts of nickel-based creep-resisting alloys. The life of an abrasive wheel depends mainly on the rate at which it becomes embrittled as a result of electrochemical process. Relationship between the wheel wear, wheel bond and type of electrolytes was made by Antipov et al [57].

Gavrilov [48] discussed the wheels used for both conventional and nonconventional grindings. Electrochemical grinding tests were performed with direct and inverse supply-source polarity. The test specimens of cemented carbide, Ti4K8 were plunged ground. The grinding force was determined for wheels of various bonds. The effect of wheel bond on electrochemical diamond grinding was also explained.

An experimental research project aimed at developing the electrochemical deep diamond grinding process with the cemented carbide dies was conducted with a modified model 3/2M universal cylindrical grinding machine. Polynomial expressions were derived for linear grinding wheel wear [103].

Kubota [58] studied a newly developed nickel coated vitrified wheel which possessed cutting ability sufficient to remove hardened steel. In electrochemical grinding, mechanical cutting ability of wheel electrode was important to get a finer surface of high accuracy.

Ranganathan [61] discussed the effect of process parameters on grinding wheel ratio and experimentally found that G-ratio was very sensitive to table speed and cutting fluid.

An experimental study was conducted to analyze the performance of the electrochemical grinding process by Kuppuswamy et al [37,67]. They discussed the effect of magnetic field in the electrode gap during the process. Faraday and process

efficiencies were best observed with the diamond wheel with significant improvement in metal removal. They successfully tried to control passivation by accelerating the ion-transfer rate with the help of externally applied strong magnetic field.

The electrochemical grinding process is characterized mainly by its faster material removal rate and its best economical application, may be carbide tool grinding. Experimental investigations were carried out to evaluate the role of some parameters on its overall performance. Banerjee and Chattopadhyay [71] concluded that ECG of carbide of grade TTW by diamond wheel could raise MRR by about 8 to 10 times compared to conventional grinding.

2.2.4 Optimization

Different combinations of control techniques can be applied to improve the process, and approach economic and technological optimum. Here, optimum means the attainment of maximum electrolytic current. Colwell [62] introduced an automatic adaptive control system with some adjustment of the control parameters. Environmental conditions that determine or influence the attainment of optimum systems in electrochemical grinding can vary rapidly with passing of time. On the basis of experimental results he concluded a maximum current criteria for the process optimization to have maximum metal removal rate.

Another adapting control method for various process variables was suggested by Lenz and Levy [59]. They incorporated a performance index that indicated the quality of process behaviour. The optimization criteria could be adjusted by affecting several control constants.

In order to get the effective tight tolerances and minimum production time, the ECG process was optimized by Maksoud and Brooks [92]. The optimization criteria was based on the tolerances of the machined form, surface topography of both the electrodes and the grinding time. The operational parameters such as feed rate, electrolyte flow and current density were investigated.

Kaczmarek and Zachwieja [30] presented the basic principle of the process for both mechanical and electrochemical actions. Their theoretical studies gave a general idea for the optimization of the process responses.

An adaptive control system was made by Shpitalni et al [73] to control overcut in the process. They described overcut as a function of the dominant parameters, the voltage and feed rate. The results obtained with and without the control system were compared by them.

Thompson [6], on the basis of empirical models, presented an approach to predict the operating parameters involving the gram equivalent weight of the alloy to be estimated in an electrochemical grinding process.

Agasaryan et al [100] studied the workpiece material removal, wheel wear, grinding force components and surface roughness. They found that the productivity in electrochemical grinding was more than that of conventional abrasive grinding.

Surface grinding with electrochemical technique proved that the toughness, stringiness, and hardness of the material in no way affected stock removal rate. This fact suggested that ECG might be an economical and accurate means of thread grinding of super alloys such as waspaloy, stellite, hastelloy, inconel etc. [104].

2.2.5 Influence of Process Parameters

In electrochemical grinding, the electrochemical gap has been shown as a critical parameter which is influenced by four main factors: the principle of operation, the grinding wheel condition, the geometrical accuracy of the machine tool, and the vibration level [29]. A short fundamental analysis and related experimental work were conducted to establish the contributing role of the factors for process control.

The process variables for peripheral ECG with a formed wheel were discussed and some experimental results were presented by Geddam et al [46]. They used Nimonic 105 as work material using sodium nitrite aqueous electrolyte solution. They

concluded that it was possible to vary the operating parameters, viz. applied voltage, feed rate and set depth of cut, over a wide range in order to meet the various requirements used as stock removal and form accuracy. The most desirable operating conditions for rough forming in single pass plunge grinding was also investigated.

Pearlstein [60] experimentally showed that sparking potential was found dependent largely upon the area of contact and applied pressure. The arc and the area of contact, and material removal were investigated.

The effects of various variables on surface finish, spindle load, and overcut were studied for machining 304 stainless steel work materials [44].

The significance of operating variables such as abrasive grain material, grit concentration, grit feed rate, and electrolyte flow rate were analyzed [50]. It was reported that spindle load and wheel wear were found to increase as the feed rate was increased but material removal rate was found to be decreased. Higher feed rates caused abrasive grits to penetrate deeper into the metal, and the working gap between the wheel and the workpiece became smaller [20].

The effect of process variables on grinding ratio was briefly discussed and mentioned that it was very sensitive to table speed and cutting fluid for the wheel speed of 30.5 m/sec [61].

A study of the independent and dependent variables experienced in the application of metal filled resin bonded aluminum oxide wheels was developed into a mathematical description of the process and compared that with actual test results. A method for predicting operating parameters in electrochemical grinding was also presented [6].

Investigation of an external cylindrical ECG process with the face of a cup wheel was performed by utilizing the synthetic superhard materials such as diamond and hard face wheels [55]. The specific consumption of diamond, and surface finish were studied by considering the process variables: electrolyte flow rate, voltage,

wheel velocity, transverse feed rate, and different types of electrolyte compositions. Their investigations were carried out using a retrofitted universal machine for cylindrical grinding. From their tests and observations it was concluded that in grinding hard alloys by diamond wheels, the voltage should not exceed 4V.

Performance of electrochemical grinding process was found to affect by the passivation in the electrolytic cell during anodic dissolution. Banerjee et al [47] experimentally investigated that after a certain voltage, the rate of increase in current density decreased indicating the onset of passivation. Comparison between pulsed and conventional ECG was made and concluded that pulsed ECG appeared to be more efficient than conventional ECG.

2.3 Electrochemical Grinding Wheels

Though most of the materials in ECG is removed by electrochemical action, some are ground away in the conventional manner as the protruding abrasive grains move across the surface of the workpiece. The abrasive grains serve three major purposes:

- i) To wipe the oxide layer from the workpiece exposing new metal and allowing the process to continue,
- ii) To act as a spacer to keep the conductive media in the wheel from making direct contact with the workpiece and generating a short circuit, and
- iii) To act as a carrier in bringing electrolyte to the work area between the workpiece and the wheel, making the process continuous [13].

Phillips [43] concluded that the wheel life in ECG was 8-10 times larger than that of in conventional grinding. Less time was spent on wheel truing and dressing operations, and important savings could be made if diamond tools were used.

The wheels used in electrochemical grinding mainly for cemented carbides and conventional abrasive wheels were metal bonded. Among the diamond wheels, the most suitable wheel was the cast metal M5 bond, with an ASV (8 to 12) grain size with 100 to 150% concentrations. Tsofin [81] mentioned that diamond abrasive of the ASP type reduced the stability of the process.

Two types of wheels were commonly used in ECG process. They were metal bonded diamond wheels for grinding tungsten carbides, and metal filled resin bonded aluminum oxide wheels for grinding ductile metals. Thompson [6] reported that metal bonded aluminum oxide wheels were found unsuccessful as the metal bond would not wear away when aluminum oxide abrasive eventually became too dull to grind away the metal oxide filled on the workpiece. Metal filled resin bonded diamond wheel would grind tungsten carbide at about 50% higher stock removal rates than metal bonded diamond wheels but the wheel life would be decreased.

The wheel bond was found to wear simultaneously with the grit, thereby uncovering new sharp edges so that the electrolyte process was not interrupted when the gap between the wheel and the workpiece was maintained [4].

The diamond grinding wheels used for conventional grinding were also used for electrochemical grinding. Here, in addition to the base metal, the bonds contain non-metallic constituents those were added to improve the cutting properties of the wheel. The intersection of the bond and the electrolyte, and the possibility of an oxide film formation on the wheel were to be taken into account in selecting the wheel bond for ECG [45].

A new type of ECG wheel made of electroless plating of nickel was developed by Kita et al [49]. The influence of the characteristics of nickel coated wheel on ECG phenomena was investigated. An experimental analysis to get the best condition of making that new type of wheel was described. It was reported that the wheel had the same capability of metal removal by itself.

It is provided in Benedict [51] that the geometrical arc length of an electrochemical grinding wheel is smaller than that of a conventional grinding wheel.

Ilhan [50], of course, introduced a new design of electrochemical grinding wheel which could provide constant current, hence preventing overcuts.

Sorkhel et al [51] suggested that the wheel eccentricity should be less than 0.02 mm and the contact area should be as large as possible.

The performance of Al_2O_3 , SiC and diamond wheel for machining of tungsten carbide was compared with each other, and high MRR was observed in case of diamond wheel [36].

ECG of tungsten-free hard alloys using SHM wheels was investigated by Lavrinenko et al [54]. When using wheels based on Cu-Sn-Sb bonding materials (MO20, MO20 -2), the edges of the machined surface suffered from chipping while, in the case of Cu-Al-Zn based bonding materials (MO4, MO13E, and MVI), there was no chipping. It was also established that with the increase of voltage the current in deep, ECG of the alloy TN 50 with wheels based on MO20 -2 bonding material, was found to increase, reaching its maximum within the 5-6 V range. The current was found to decrease when voltage was above 5 to 6 volts, was caused due to formation and growth of anode oxide films on the machined surface.

Sfantsikopoulos and Noble [39] introduced an electrochemical wheel conditioning method to remove mechanical debris, conductive bond 'peaks', and to expose the diamond grits on the working surface of the wheel. They also claimed that the method increased the wheel life and assured stable ECG, especially for grinding WC.

The change in specific wheel wear for diamond wheels was studied by Nankov et al [55] for different levels of voltage and depths of cut. An approximate formula was also presented to determine this specific wheel wear by Balashov [41]. The formula is

$$S = 2.82 (P/K)^{1/4}$$

Where,

P= pressure on the wheel surface

K= the diamond concentration in the wheel

The maximum wheel pressure or minimum gap width was shown to be limited by the maximum current density values or the formation of arcing that occurred when the gap became too small. Increase of wheel pressure, for constant level of current, resulted in excessive wheel wear [56].

The ECG wheels contained abrasive particles in a current carrying bond. Copper, brass, and nickel were the most commonly used materials for metal bond wheels [27].

Both metal bonded and carbon bonded wheels were available with diamond abrasives for carbide grinding and aluminum oxide for non-carbide materials softer than Rc65. Brandi [9] reported that carbon bonded wheels were available with silicon-carbide abrasive for work, on both hard and soft materials. The metal bonded wheels were more difficult to dress than the carbon types and often require a deplating operation after dressing.

Metal bonded wheels were susceptible to spark damage and constant wear out in the form of disappearance of grit protrusion [7].

The process of electrochemical grinding when used to machine profiles of metal-bonded diamond composite wheels was investigated by Maksoud [92]. The most common of the metal-bonded types are those with mild steel and bronze bonds. Direct nickel-plated diamond composite form tools were used to machine such kind of wheels in case of ECG. The process was optimized based on the tolerances of the machined form, on the surface topography of both the metal bond wheel segments and the plated form tool. Operational parameters such as feed rate, electrolyte flow and the current density were investigated, and evaluated the optimum operating conditions.

Economics of using metallic-bond abrasive wheels for electrochemical grinding of creep-resisting nicrome alloy were discussed. The effect of the physiochemical characteristics of the electrolyte and the wheel bond in ECG were explained by Antipov et al [91].

Coleman [19] reported that the most common wheel was a resin bond, copper impregnated, aluminum oxide grit wheel. Other wheels found in service were metal bond diamond, resin bond diamond, diamond-plated, and silver impregnated wheels. Silver was found the most common bond material used in ECG wheels for grinding carbide tooling. The metal has a threefold purpose:

- i) It bonds the diamonds in a uniform matrix,
- ii) It acts as a current conductor, and
- iii) It brazes diamonds and nonconductive fillers to steel core (back plate).

The different types of wheels used for ECG process were studied by Kubota [58]. He reported that mechanical cutting ability of ECG wheels led to the finer surface finish of high accuracy. A nickel coated vitrified wheel was found to have the property to remove hardened steel. It was reported that sodium sulfide in sodium nitrate electrolyte would decrease the pollution problem of ECG.

2.4 Electrochemical Grinding Machine

In ECG, the grinding machine is more or less of conventional form but employs an abrasive grinding wheel with a current carrying bond and is provided with electrolyte instead of coolant. ECG power supplies upto 3000 amps are available but power supplies greater than 1000 amps are seldom economical for this process.

Voltage control upto 15 V is sufficient because spark occurs in most of the operations when voltage is exceeded. ECG machines are available with either vertical or horizontal spindle for external and internal cylindrical grinders. Five

different methods namely face grinding, surface grinding, internal grinding, form grinding, and cylindrical grinding can be performed with different types of ECG equipments [43]. Two methods are currently used to carry power through the spindle through brushes and mercury coupling. Most ECG machines generally use metal wire brushes to provide a sliding electrical connection but its ability to carry high current is limited. The most effective method to deliver high current is the mercury coupling, as this type of coupling can carry more current [2,44]. Amperage adjusts automatically with the change in contact area between the wheel and the workpiece to maintain constant current density, thus constant metal removal rates are provided. The feed rate must be absolutely steady and slow, with a variation less than 1% in set speed.

Electrolytes are generally the mixtures of alkaline metal salts, and various formulations are available from different manufacturers. The most commonly used electrolytes for electrochemical grinding process are sodium chloride and sodium nitrate at concentrations of 0.12 to 0.36 kg/litre [2]. The most efficient electrolyte for ferrous, nickel and cobalt alloys is sodium chloride solution [11].

There is no non-corrosive electrolyte available, but there are some that contain corrosion inhibitors. The less corrosive electrolyte exhibits lower ionization rates and metal removal rate would be slower with these non-corrosive electrolytes [9]. For most conventional ECG applications, the electrolyte is passed through a nozzle placed behind the wheel with respect to the feed direction.

Very small amount of inhibitor was required to make the electrolyte anticorrosive (from 10^{-5} to 10^{-1} of normal solution) [41].

ECG machines operate in the following different ways according to the method of maintaining the clearance between the workpiece and the working surface of the wheel:

- i) With constant pressure of the grinding wheel against the surface being machined,
- ii) With small depth of cut,

- iii) When constant contact is maintained between the work surface and the wheel, and
- iv) With large depth of cut when all the allowance is removed in one pass [45].

Phillips [10] pointed out the requirement of ECG machine. According to him the feed rate must be absolutely steady with a speed regulation of less than 1% variation in set speed. Slipstick conditions could not be tolerated.

Many types of ECG machines are now available including surface grinders, vertical spindle cylindrical grinders, burr-free cut-off machine, and many special machines including automatic part transfer types. They are also available with both manual digital input (MDI) and with DNC and CNC [11].

The construction of grinding machine must be rigid enough to maintain precision under the deflecting forces which can reach 150 psi (1MPa) between the workpiece and the wheel. The spindle must be insulated and capable of conducting the low voltage, high current d.c. power to the wheel [3].

Geddam and Noble [46] commented that peripheral grinding was of great importance in production engineering, and their experimental investigations proved the capability of electrochemical grinding in this field of machining.

The design and development of an ECG machine was carried out by Banerjee et al [47]. The role of principal parameters involved in this process was studied. They used diamond grinding wheel and tungsten carbide, brass, copper, stainless steel, and HSS as work materials. They reported that MRR could be raised by diamond wheel by 8 to 10 times as compared to mechanical grinding, and process efficiency might be raised up to 85 to 90%.

2.4 Summary

Literature survey pertaining to material removal mechanism in electrochemical grinding process, surface integrity and surface finish, grinding wheel and wheel wear, ECG machine and influences of different parameters have shown that worse surface finish and dimensional control are the basic problems with the process. Little attempt has been made theoretically but practical investigations are performed mostly. This study considers a large number of parameters by using stainless steel and tungsten carbide. Theoretical analysis of electrochemical grinding process has to be considered separately for electrochemical and mechanical actions. For the analysis of MRR due to electrochemical action, the longitudinal feed movement should be same as that of radial rate of metal dissolution so that the dissolution front would always be at a particular distance. It is also necessary to find out the optimum conditions under which most of the objectives like MRR, surface finish and integrity are achieved. Present research is for the development of the technology to investigate the electrochemical grinding process.

The effects of parameters on process responses are utilized by a comprehensive experimental study. ECG geometry and kinematics are also analyzed and the mechanistic behaviour of the process is explained with different cutting dynamics in the next chapter. An analysis for MRR in ECG process, and the theoretical model developed for representing the feed force have also been included.

CHAPTER - 3
SOME ELECTROCHEMICAL
ASPECTS OF ECG

CHAPTER 3

SOME ELECTROCHEMICAL ASPECTS OF ECG

3.1 Introduction

The electrochemical aspects of electrochemical grinding are very complicated and sometimes become out of control. These aspects basically involve the electrochemistry of the process. The important factors that affect the process are: the electrolyte and its flow rate, temperature and concentration of electrolyte, interaction time, chemical properties of the anode (work material), and applied dc voltage. The electrolyte solution, of course, should suit the anode material to be machined and provide a continuous electrochemical action at high feed rates. The objective of this chapter is to explain these electrochemical aspects so that the electrochemistry, electrolysis phenomena, reactions, and anodic passivity etc. can easily be understood.

3.2 Electrochemistry

Electrochemistry is concerned with the study of mutual conversion of chemical and electrical forms of energy, and also of the laws of regularities associated with the process. It deals with reactions proceeding at the expense of external electrical energy or serving as a source of this energy. Such reactions are known as electrochemical reactions. Electrochemical grinding basically is the applied electrochemistry dealing with following fundamentals as^{they} generally happen in cells. It implies that,

- i) electrochemical reactions occur at the neutral electrolyte boundary layer, and
- ii) chemical reactions occur in the bulk of the electrolyte solution.

This is also the basic electrochemistry of ECM_λ^{and} reveals that a sizeable potential has to be supplied. In addition to that it is required to break and ionize the electrolyte resulting in the flow of current through the electrode so as to provide the decomposition potential.

3.3 Electrolytes

The solution containing mobile ions move under the influence of an electric potential and thereby carries electric charge is called an electrolyte. The electrolyte has three main functions:

- i) it carries the current between the wheel and workpiece,
- ii) it removes the products of the reactions from cutting region, and
- iii) it removes the heat produced in operation.

Pure water is not a good conductor of electricity. When some substances make the solution in water that does not conduct electricity are known as non-electrolytes. Weak electrolytes have a greater conductivity than that of water. The most common electrolyte contains ionizable salts, acids or bases dissolved in water. For example, with the combination of iron-anode and sodium chloride salt solution, the electrolysis will evolve the dissolution of iron from the anode, and the generation of hydrogen at the cathode, no other reaction taking place at the electrode [65].

The electrolytes generally used for different metals in electrochemical grinding process could be found in Table 3.1 [3].

3.4 Electrolytic Cell

The basic requirements for a successful electrochemical cell are: the cell is composed of two half cells each of which contains a solution, a metallic conductor so that redox reaction can take place smoothly. The solutions of the two half cells are connected in some way that allows ions to move between them. Three principal types of electrochemical systems or cells can be distinguished as physical, concentration, and electrochemical cells.

Table 3.1 Parameters for ECG of Various Materials

| Work Material | Wheel Type | Electrolyte | |
|-------------------|----------------|--|-----------------------|
| | | (Base Chemical) | g/L. H ₂ O |
| Tungsten Carbide | Diamond | Potassium Nitrate | 180-200 |
| Titanium Carbide | Diamond | Potassium Nitrate | 180-200 |
| High Speed Steel | Diamond | Sodium Nitrate | 120-180 |
| Tungsten | Diamond | Potassium Hydroxide or Sodium Hydroxide | 120-180 |
| Low Carbon Steel | Aluminum Oxide | Potassium Nitrate and Potassium Nitrite | 60-120 |
| High Carbon Steel | Aluminum Oxide | Sodium Nitrate | 120-180 |
| Stainless Steel | Aluminum Oxide | Sodium Nitrate | 180-200 |
| Silicon Iron | Aluminum Oxide | Sodium Chloride | 120-180 |
| Aluminum Alloys | Aluminum Oxide | Sodium Nitrate | 120-140 |
| Titanium Alloys | Aluminum Oxide | Sodium Nitrate | 120-140 |
| Nickel Alloys | Aluminum Oxide | Sodium Nitrate | 120-140 |
| Cobalt Alloys | Aluminum Oxide | Sodium Nitrate | 60-80 |
| Zirconium Alloys | Aluminum Oxide | Sodium Nitrate | 120-180 |
| Stellite Alloys | Aluminum Oxide | Sodium Nitrate | 210-240 |
| Copper Alloys | Aluminum Oxide | Sodium Nitrate or Potassium Nitrate | 180-200 |

The cell in which the electrodes differ only in their physical properties are termed as physical cells, and when differs in the activity (concentration) of the participants in the electrode reactions are called concentration cells. When the electrodes differ both in chemical and physical properties are known as electrochemical cells [88].

When an electric current is passed between the two electrodes immersed in a conductive solution the chemical process is termed as electrolysis. The system

consisting of two dissimilar electrodes in the electrolyte is termed as an electrolytic cell or simply a cell where electric charges are exchanged at the electrodes. When an electric current is supplied externally to the electrolyte, the reactions will occur at the electrode surfaces, and in the electrolyte solution. The electrolyte is the resistance of the circuit if one neglects the resistivity of the cables between generator and electrodes. Electrolytes are different for metallic conductors of electricity, in the sense that the current is carried not by electrons but by atoms, or group of atoms, which have either lost or gained electrons thus acquiring either positive or negative charges such atoms are known as ions [65]. Cations, being positively charged ions, are attracted by, and migrate to negatively charged electrode from which they gain electrons and are consequently reduced. On the contrary, anions, being negatively charged, and thereby, are attracted by and migrate to the positively charged electrode, and thereby give up electrons and consequently oxidized. The movement of ions has been shown in the Fig. 3.1. The solution with charged particles moves under the influence of electric potential and is continuous so long as un-reacted ions migrate to each electrode and reacted ions move away from the electrode. Different electrode materials exhibit different electrode potentials, and the difference in electrode potentials becomes the electromotive force (emf) of the cell which may assist or oppose the current flow [105].

It is convenient to consider the total emf as the sum of the two "single electrode potentials". That means,

$$E_{\text{cell}} = E_{\text{ox}} + E_{\text{red}} \quad \dots 3.1$$

At equilibrium the potential for the overall reaction is zero [86]. Where, E_{ox} is the single electrode potential of the electrode forming the negative pole of the cell, and E_{red} is the single electrode potential of the electrode forming the positive pole of the cell. If a particular substance is more easily oxidized than hydrogen, its E_{ox} is assigned a positive value and its E_{red} a negative value. When a substance is not oxidized as easily as hydrogen then E_{ox} will be negative and E_{red} positive.

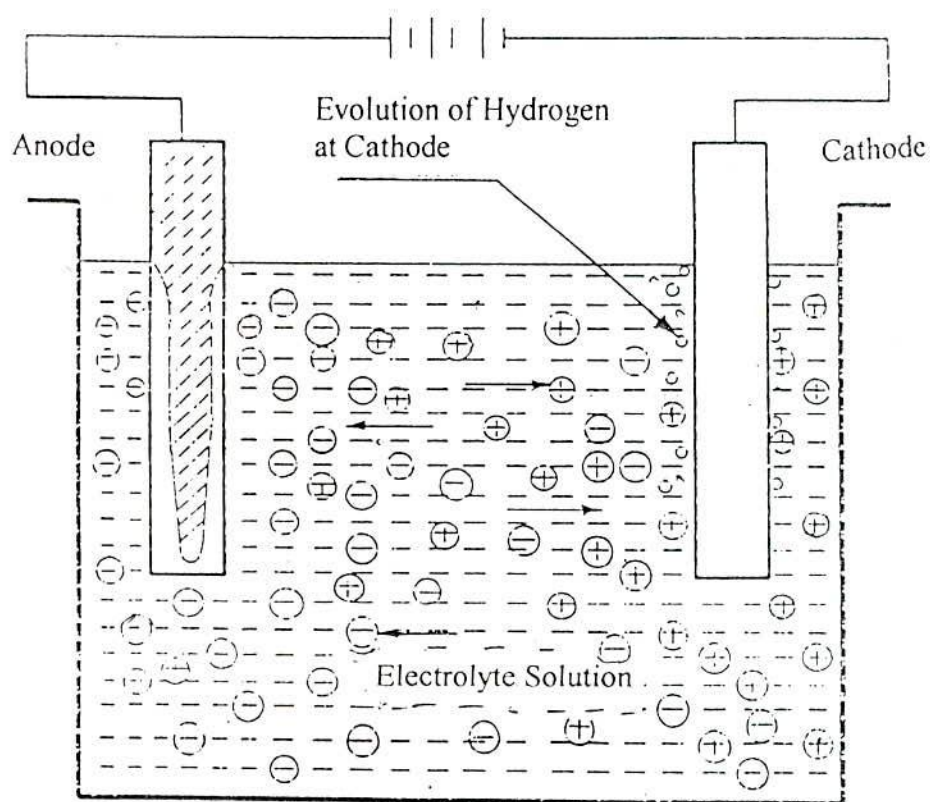


Figure 3.1 Electrolytic Cell Showing the Movement of Ions

3.5 Oxidation and Reduction

When an atom loses one or more electrons, it is said to be oxidized and is characterized by an increase in the positive charge of an atom. When the atom gains one or more electrons it is then reduced, characterized by an increase in the negative of an atom. The degree to which an atom is oxidized is its state of oxidation, reduction being considered as negative oxidation, and oxidation numbers are used to describe the state of oxidation. The oxidation number of atoms in various compounds are determined taking into account the oxidation numbers of hydrogen and oxygen in water^{as} $+1$ and -2 respectively as a fundamental reference.

Oxidation and reduction potential expresses the strength of an oxidizing and reducing agent. Oxidation is always accompanied by an equivalent reduction. As all the chemical systems are electrically neutral, there should be a simultaneous an equivalent gain of electrons by one atom or loss by another. An oxidizing agent is being reduced in the process and causes the oxidation of the material. On the other hand, the reducing agent affects the process in reverse. Oxidation-reduction can take place in different manners. In case of direct oxidation, reaction can take place simply by placing the reactant together. During oxidation in aqueous media, the reactants are dissolved in water to ionize them and initiate the electron migration. The reactants may involve here in both the ions and molecules. In electrochemical reduction-oxidation reactions, the individual oxidation and reduction reactions can be physically separated (in electrochemical reaction) with the charge transfer occurring through an external wire [106].

3.6 Electrolytic Conduction

The conductivity of electrolyte is the degree with which an electrolyte conducts an electrolytic current and depends upon the number and type of ions present, and how easily they move through the electrolyte. An ion may not carry the same fraction of the current due to various mobilities of different ions. The ions that move faster will carry larger fraction of the electricity [105]. This fraction of the total electricity carried by an ion is termed as "transference or transport number". The current is carried by negative ions towards the anode, and by positive ions towards the cathode. The ionic conduction in an electrolyte obeys Ohm's law. The conductance of a solution between two electrodes is nothing but its equivalent conductance that depends on the concentration of the solution. For example, more current carrying electrolyte will be more dilute solution. But beyond a certain point, dilution of the electrolyte does not make any notable change of equivalent conductance. For proper electrolytic conduction, electrolytes should possess the following characteristics [56,105]:

- i) high electrical conductivity,
- ii) high electrochemical aggressiveness towards the material to be machined,
- iii) ability to dissolve the reaction products,
- iv) no detrimental physiological reactions,
- v) chemical inactivity towards the machine components,
- vi) ability to suppress over cut, and
- vii) ability to permit accurate sizing and dimensional control of workpiece.

No single electrolyte provides all the properties for all metals. For example, sodium chloride provides high stock removal efficiency, but it does not provide the passivation protection of oxidizing electrolyte such as NaNO_2 or NaClO_3 . The difference between the two electrode potentials in the electrolytic cell becomes the electromotive force of the cell. Of course, different electrode materials possess different electrode potentials. When the electrodes are not polarised the emf is usually just larger than the difference in electrode potential [105]. There are some phenomena that occur at the electrode surfaces to produce emf to oppose the vary cause of flow of current. They are known as anode and cathode overvoltages, and include activation polarization, concentration polarization, and ohmic overvoltage. Figure 3.2 shows the potential profile in the machining gap. The decomposition potential is comprised of reversible potential 'E' and overpotential ' η ' at the electrode, as shown in Fig. 3.3. The total overpotential is the summation of all these over potentials namely activation overpotential ' η_a ' due to difference in the rate of metal ionization and ion discharge, concentration overpotential ' η_c ' due to concentration polarisation, and the resistance overpotential ' η_v ' due to film layer deposited on the electrode.

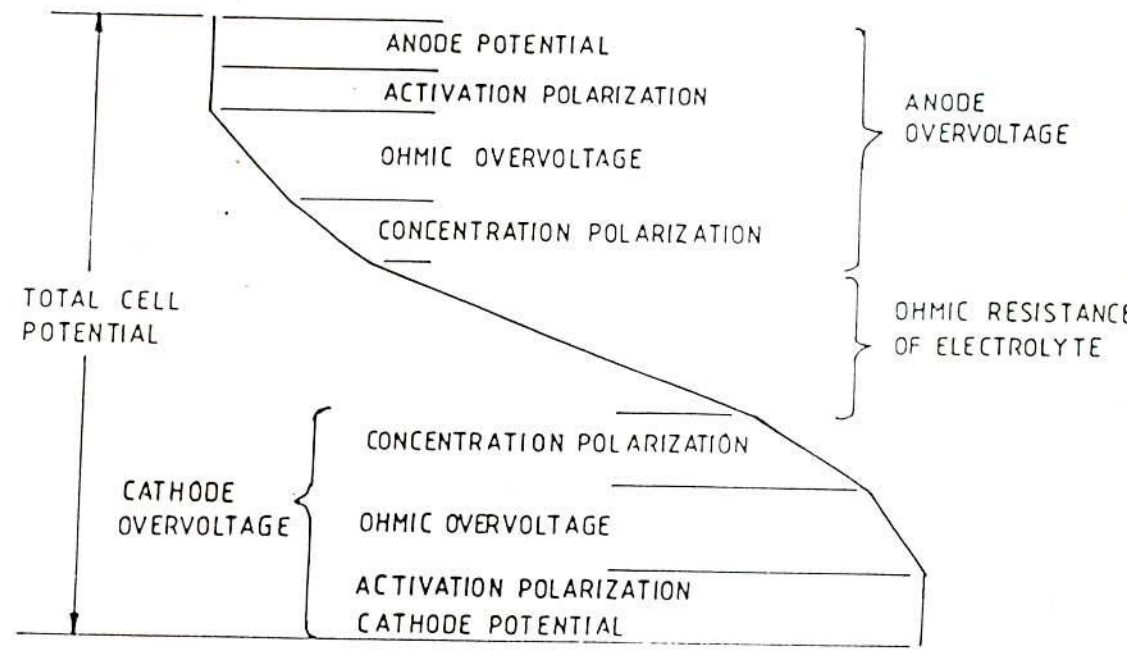
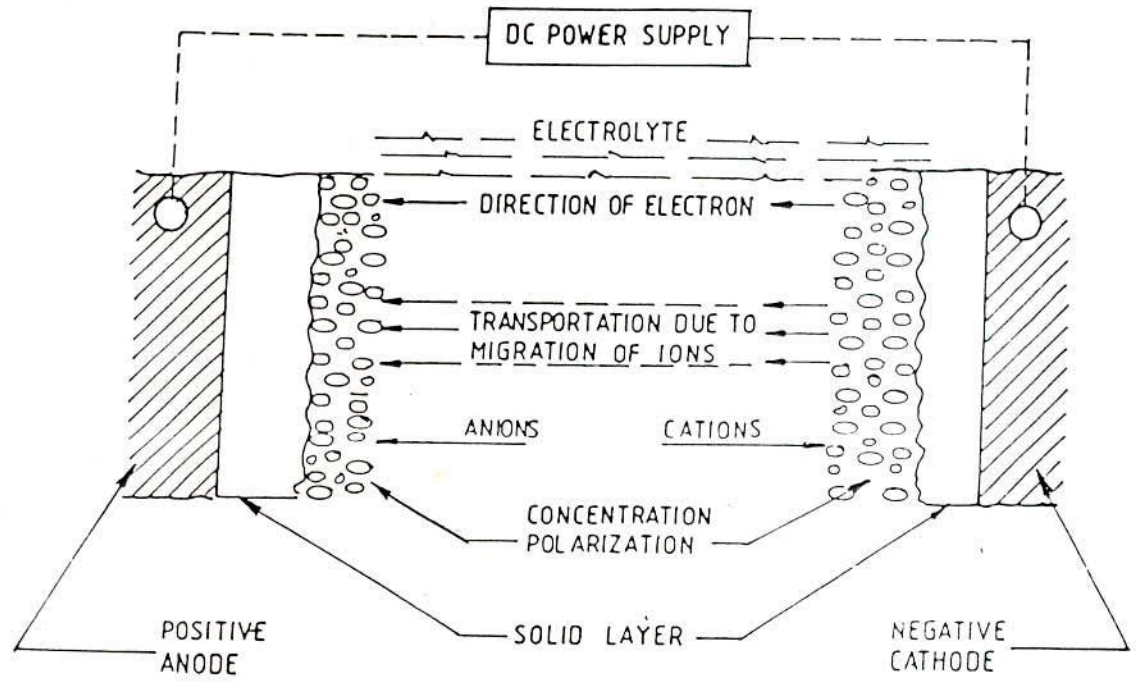
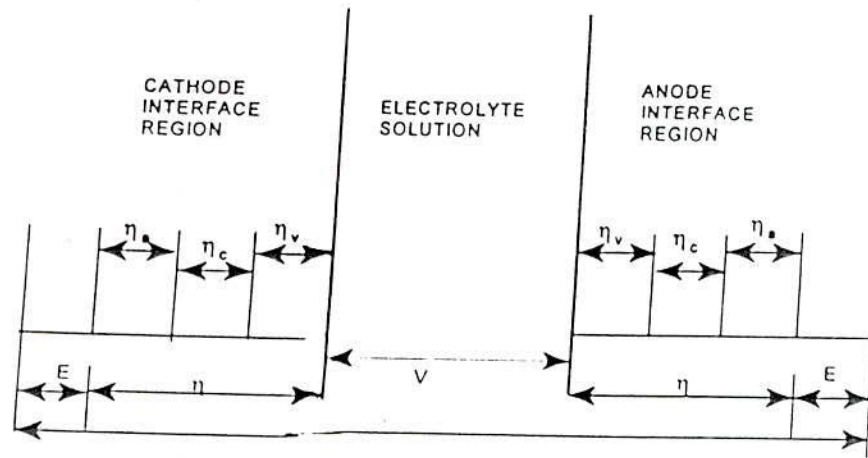


Figure 3.2 Potential Profile in the Machining Gap



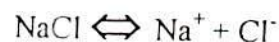
- E Reversible Potential
- η Total Overpotential
- η_A Activation Overpotential
- η_c Concentration Overpotential
- η_v Resistance Overpotential

Figure 3.3 Potential Distribution in the Machining Gap

3.7 Electrochemical Reactions

When no current flows, electrochemical reactions occurring at an electrode are in equilibrium. However, to make the dissolution proceed one has to apply a voltage in excess to the electrodes and activation polarization potentials. Electrolyte reactions are influenced by the exchange of electric charges. They may be classified according to their locations at which they occur: at the anode surface, at the cathode surface, and in the bulk of electrolytes [42, 86]. The reactions will vary in accordance with electrolytic condition whether it is acidic, neutral or basic.

If one performs electrolysis experiment taking steel specimen as anode and a metal as cathode using sodium chloride solution as an electrolyte, and when high current flows through the solution ions are formed and will proceed to produce the following effects:



3.2



The positive ions move towards the cathode and negative ions move towards the anode to react. The possible reactions at the anode and cathode are analyzed.

Cathodic Reactions:



By neutralizing charge on hydrogen ions, the free hydrogen is the main reaction in acidic electrolytes. It is a chemical transformation involving a net electron transfer, and it can be written in familiar style as:



The hydrogen ions are discharged on the electrode and there is an evolution of hydrogen gas. There is no deposition on tool but only gas is formed. In electrochemical grinding, the metal ions are deposited in the electrolyte before reaching the cathode as



Anodic Reactions:

The anodic reactions those occur during machining operations are in the present example, the dissolution of iron. As the metal dissolves from the anode, electrons are left behind at a rate depending on the valence of the metal as follows:



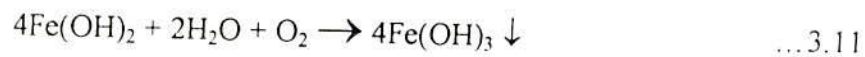


Reactions within the Electrolyte:

The outcome of the electrochemical reaction is that, the metal ions combine with the hydroxyl ions to precipitate out as an iron hydroxide so that the net reaction becomes



If ferrous hydroxide reacts further with water and oxygen to form ferric hydroxide

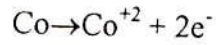


Although it is stressed that this reaction does not form any part of the electrolysis i.e, this is independent of metal removal process. With this metal-electrode combination, the electrolysis involves the dissolution of iron from the anode, and the generation of hydrogen at the cathode, and no other reaction takes place at the electrodes [65]. The reactions within the electrolyte become

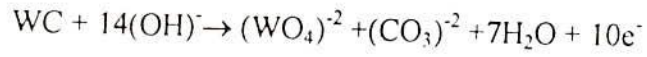


This shows that iron (Fe) goes into the solution and hence machined to produce reaction products as iron-chloride and iron-hydroxide as precipitate.

For grinding tungsten carbide, as an experimental investigation the primary reactions are [36]:



3.14



3.15

The role of electrochemistry in electrochemical grinding process can be presented as shown in Fig. 3.4.

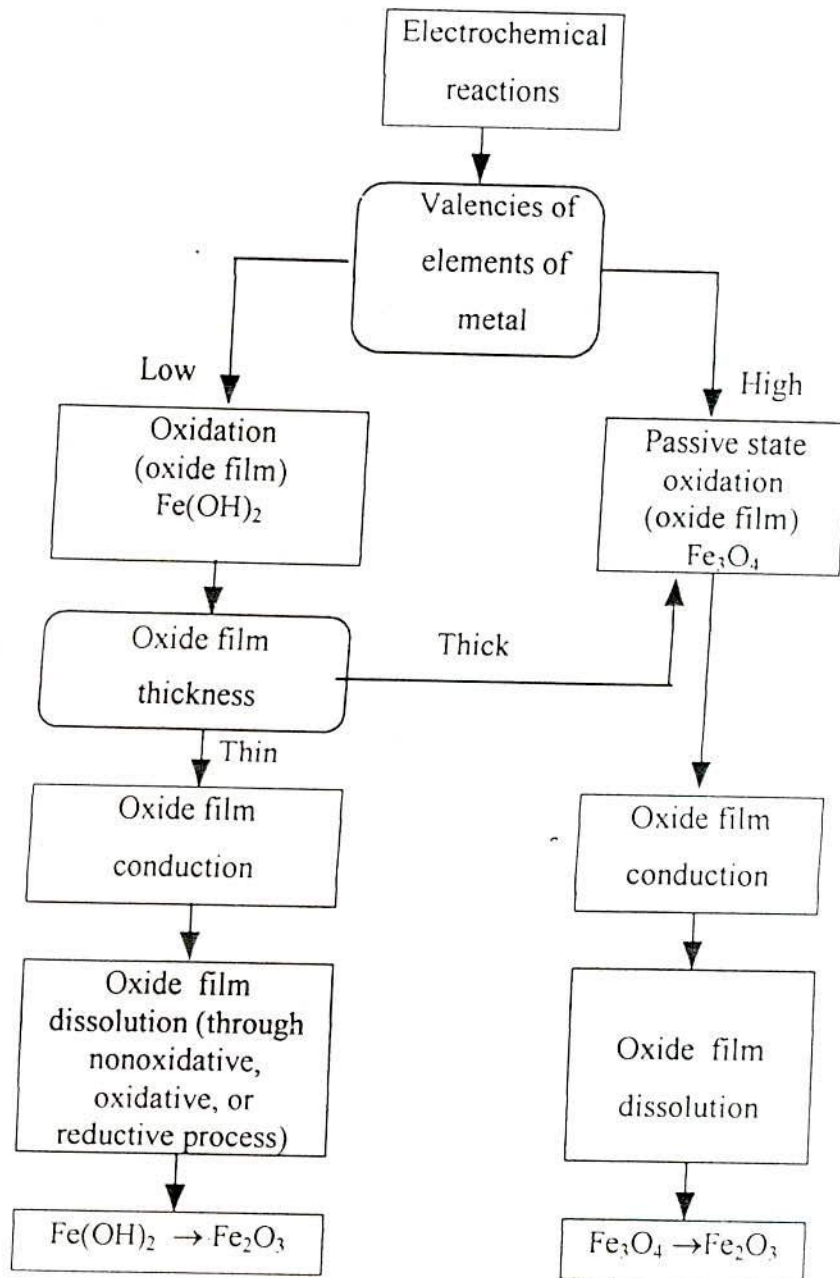


Figure 3.4 Effects of Electrochemistry in ECG Process

3.8 Anodic Passivity

The effective technique of metal removal from a work surface requires the evaluation of optimal machining parameters subject to the constraints of various physio-chemical phenomena which take place during the machining operation. One of such phenomena that affects the MRR of the process is the passivation of the work surface. It is generally considered as a special condition of anode polarization that results in either a substantial reduction in current or an increase in valency of anodic dissolution. Concentration polarization can produce such condition where there is an insufficient velocity of electrolyte flow, especially at low feed rate [105]. This inadequate flow of electrolyte also tends to produce passivity. The electrolyte selection is a very important factor to control it. Passivity evolves out of a change in the chemical and electrochemical behaviour of a metal due to the formation of a protective film on the work surface. It may be classified as:

- i) Mechanical passivity, and
- ii) Chemical passivity.

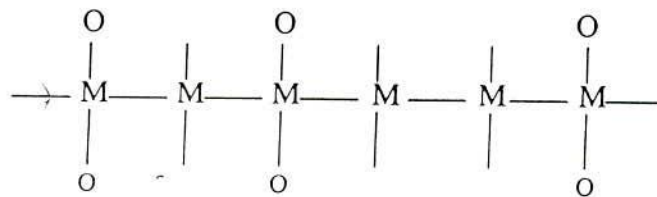
The mechanical passivity occurs due to the formation of a protective thick visible layer from an excess of metal ions in the metal-electrode diffusion layer. As soon as this layer is being saturated, metallic salt begins to precipitate onto the anode surface. But this passive layer is usually porous due to the formation of the salt. As a result, the electrode continues to cause electrochemical reactions at a slow pace. The protective layer gradually increases to a considerable thickness resulting in a short circuit disrupting the machining process, and producing worse surface finish. On the contrary, the chemical passivity occurs due to the formation of a very thin invisible layer of metallic oxide. These metallic oxides are insoluble in the electrolyte. The oxygen evolution at the metal surface becomes impervious to the passage of metallic ions which results a complete passivation of the anode surface.

Oxidizing condition tends to increase passivity while reducing condition develops activity. In ECG process, passivity can occur at high electrolyte flow

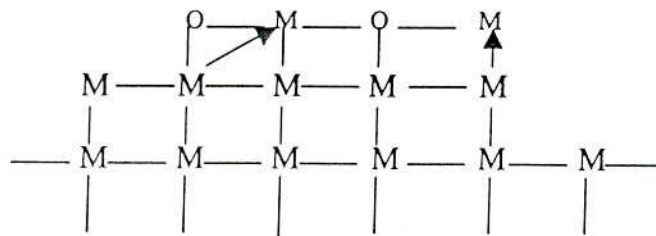
velocity. As acidity increases, the metal ions freed at the anode move further into the electrolyte before forming the hydroxides, are removed by the turbulence flow of electrolyte. Hence the rate of electrochemical reaction and the oxide film thickness vary on the work surface [50].

In case of anodic passivity, the higher reaction rates decrease the total free energy of the chemical system within a shorter time than is expected. The most favourable theories for passivation in electrochemistry are adsorption theory and oxide film theory. In adsorption theory, passivity is described as a phenomena of the change in the kinetics of an electrochemical reaction because of the activated adsorption of the oxygen of water. At this point, the different opinions regarding movement of the metal atoms are:

- i) explains the formation of chemical bonds which satisfies the surface affinities without metal atom leaving their lattice site (Fig. 3.5a)
- ii) concentrates on the mono-molecular oxide layer at which metal atoms leave their regular position to form a new, alternating arrangement of oxygen and metal together with oxygen atom in the lattice (Fig. 3.5b)



(a)



(b)

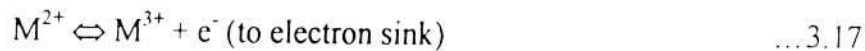
Figure 3.5 Passivating Film Characterization

On the other hand, the oxide theory describes the state of improved corrosion resistance through the formation of a protective film on the metal substrate. These theories do not contradict with each other but supplement with regard to the initial passivation condition. In an oxygen atmosphere, molecular oxygen is absorbed, dissociated, and chemisorbed in the initial stage of the process. But for an aqueous solution, water molecules of hydroxyl ions will be absorbed and chemisorbed. The passive state may be prevented by reducing the potential to a value where an ion of less positive charge, and soluble, results the surface to become active. And by raising the potential to a value where an ion of more positive charge, soluble, resulted from an anodic reaction, makes the surface active. Failure of passivity may occur if the oxygen concentration drops or pH value varies from that in the electrolyte solution [109].

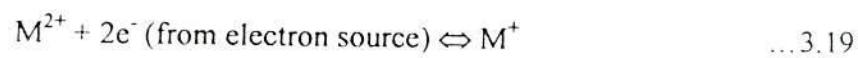
3.9 Oxide Dissolution Process

Oxide dissolution processes are specialized by the rate determining step that may involve electronic charge transfer. The basic sub-divisions are oxidative, reductive, and non-oxidative. The electrochemical dissolution process is either oxidative or reductive depending upon experimental condition and the oxide. When the charge transfer is not rate determining, the dissolution is chemical, and sub-classified as oxidative and reductive. For covalent oxides, some form of charge transfer is usually involved in dissolution, and thus dissolution can be classified as electrochemical if the charge transfer is rate determining [90].

For a metal oxide (MO), chemical oxidative mechanism is



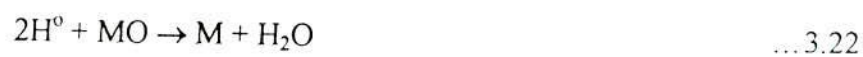
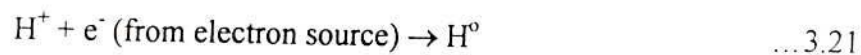
Similarly, the chemical reductive mechanism may be written as



Predominantly for ionic oxide, dissolution that involves ion transfer under the influence of electrostatic field, is termed as chemical non-oxidative, the mechanism of which is



Oxide dissolution may also be classified as hydrogen atom-oxide combination mechanism and a solid-state mechanism. Hydrogen atom-oxide combination can be stated as



Solid-state mechanism may be represented as



The relative importance of the electronic state of the oxide can be an important clue in differentiating between electrochemical or oxidative chemical dissolution and non-oxidative chemical dissolution [90].

3.10 Summary

The electrochemical aspects governing the ECG process are very complicated and sometimes it is found beyond control. This study has provided the information regarding the insides of the process. The oxide film characteristics are generally affected primarily by the composition of the workpiece material and electrolyte solution, the flow of electrolyte, and by machining parameters such as supplied voltage, feed rate, abrasive grains. The oxide film initially termed as insoluble metal hydroxide, which transforms into soluble metal oxide (Fe_2O_3). The fundamental knowledge gained from these studies gives better concept of the process so that efficient operations can be achieved easily.

CHAPTER - 4
THEORETICAL ANALYSIS

CHAPTER 4

THEORETICAL ANALYSIS

4.1 Introduction

Material is removed in grinding process mainly by chip formation, whereas in ECG, the material is removed mainly by electrochemical action. The grinding scheme geometry for straight surface grinding is illustrated in Fig. 4.1, where the depth of cut corresponds to the machine down feed.

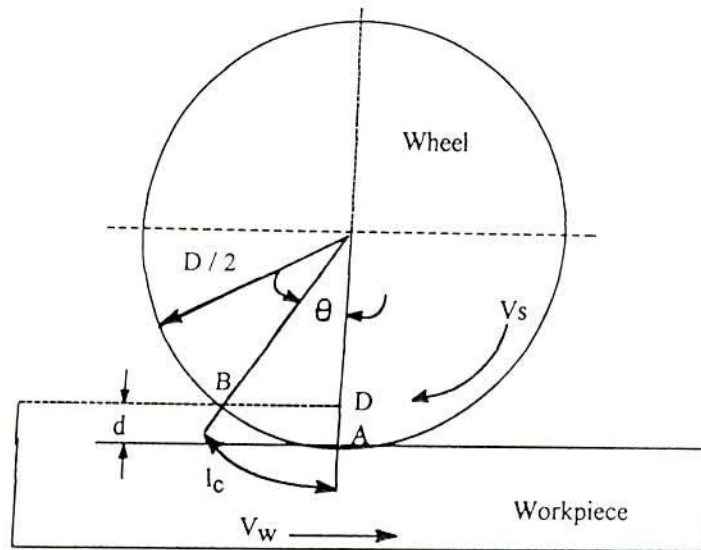


Figure 4.1 Scheme for Straight Surface Grinding

In electrochemical process, the grinding wheel acts as cathode electrode consisting of abrasive particles bonded with an electrically conductive metal. Since the abrasive particles of electrochemical grinding wheel protrude beyond the conductive bond surface they established a small gap between the wheel and the workpiece (Fig. 4.2). These particles not only act as insulators to maintain individual electrolytic cells between wheel bond and the workpiece but also removes some material as chips during machining action, and wipes away the oxide layers.

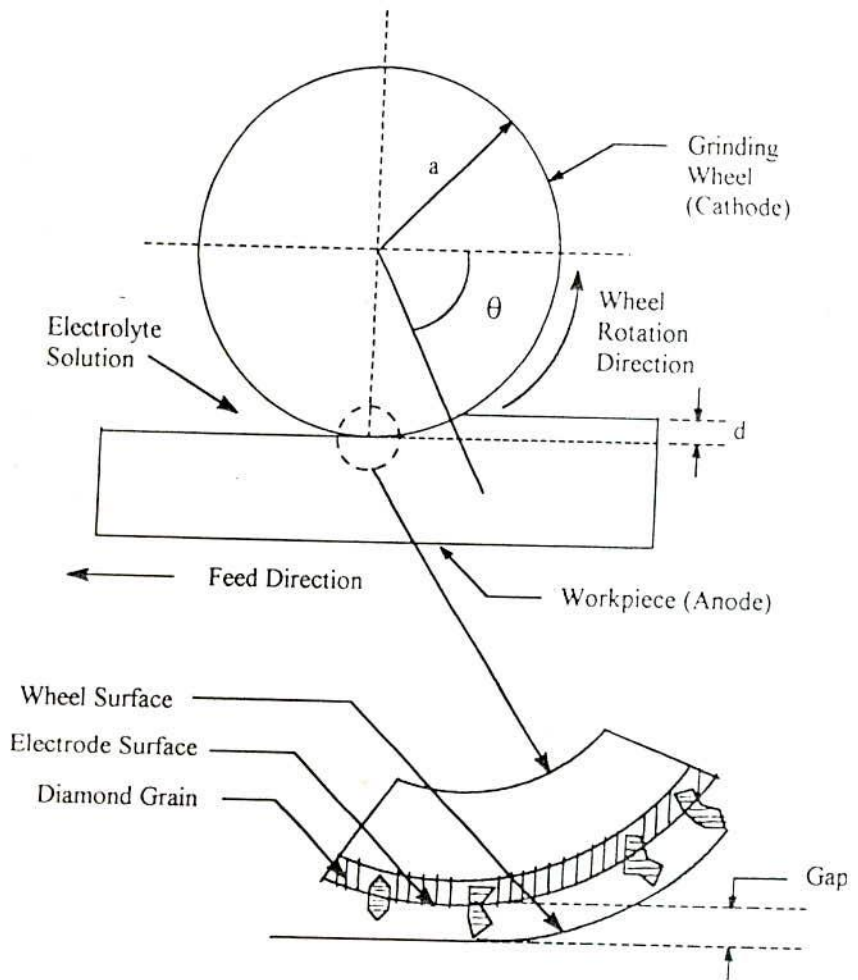


Figure 4.2 Electrochemical Grinding Scheme

The wheel is to produce an electrolyte pressure in the machining zone resulting the required amount of flow of electrolyte between the wheel and the workpiece for grinding operation. This flow of electrolyte entirely depends on the speed of the wheel. For very slow speed the electrolyte cannot be carried to the zone even also at very high speed. At a very high speed, the wheel will throw the electrolyte off the wheel before coming in contact with the gap between the wheel and workpiece.

The electrolyte will cause the desired reactions to occur for machining and will take away the heat and reaction products from machining zone. Prime requirement of an abrasive is that it should be harder than the material, it is to abrade. This hardness is generally defined in terms of its static indentation hardness. The other important properties of abrasives are its dynamic strength and toughness which

are inversely proportional to friability and attrition resistance, the degree of solubility of the abrasive when in contact with the material being machined [44].

4.2 Grinding Geometry and Kinematics

Materials subject to electrochemical grinding are removed by both mechanical and electrolytic actions. This removal having a low work feed rate and large depth of cut is mainly performed by an electrolytic action. About 90% of the total removal is removed due to electrochemical action and only about 10% is by mechanical grinding [89]. With increasing work feed-rate, workpiece materials are mainly removed by mechanical cutting action of abrasive grains.

As in Fig. 4.1, for any straight surface grinding, a wheel rotating with a peripheral velocity ' V_s ' takes a wheel depth of cut, ' d ' from the workpiece as it moves at velocity ' V_w '. The grinding wheel penetrates into the workpiece resulting in apparent area of contact, where grinding due to mechanical action occurs.

Considering, motions as well as deformations of the wheel and the workpiece neglected, the contact arc length ' l_c ' for any type of grinding can generally be expressed as (considering θ to be small):

$$l_c = \text{ArcAB} \cong \frac{D\theta}{2} \quad \dots \quad 4.1$$

Where,

$$\cos\theta = \left(1 - \frac{2d}{D}\right) \quad \dots \quad 4.2$$

Since $2d \ll D$, the small-angle approximation would apply

$$\cos\theta = 1 - \frac{\theta^2}{2}$$

The metal removed in a single cut is represented by area ABCEA. But since AB/BC is equal to v/V_s . We may neglect AB and take the area 'BCF' as the metal

removed. Then the length of the undeformed chip is equal to the arc length BC or to a very good approximation to the chord length BC, since angle θ is very small. The equation of the contact arc length becomes as in Fig. 4.3

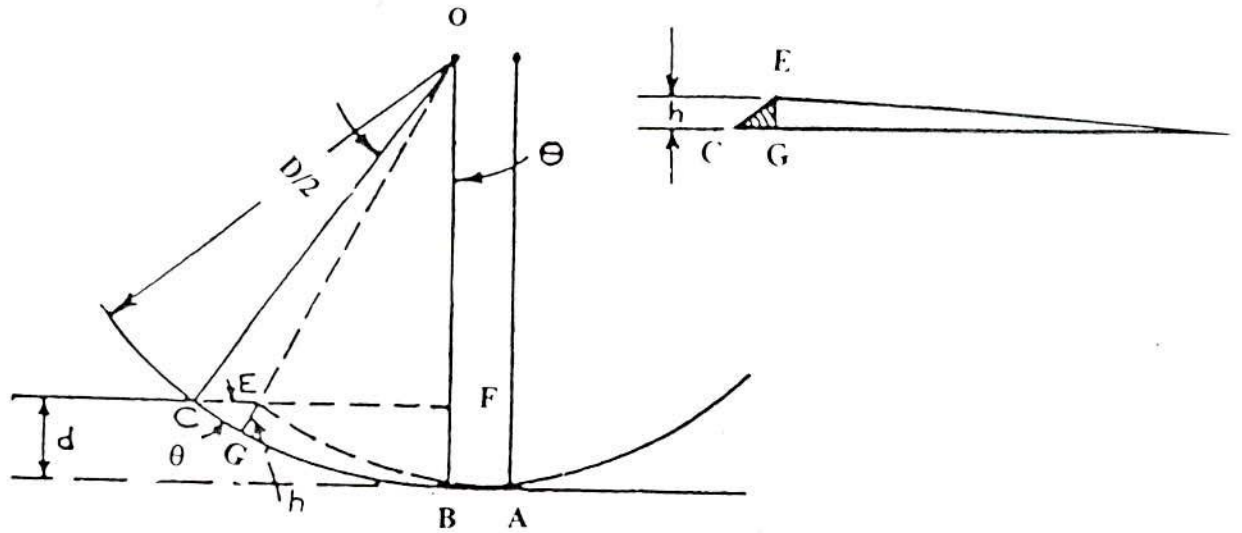


Figure 4.3 Grinding Geometry

Thus

$$l_c = BC = \sqrt{CF^2 + d^2} \quad \dots 4.3$$

Where,

$$d = D/2 (1 - \cos\theta) \quad \dots 4.4 \text{ a}$$

$$\text{and } CF = \frac{D}{2} \sin\theta \quad \dots 4.4 \text{ b}$$

From Eqns. (4.3) and (4.4), it becomes (refer A4.1)

$$l_c = (D \cdot d)^{1/2} \quad \dots 4.5$$

The curvature of the chip may be negligible and the cross section of the undeformed chip will appear as in Fig.4.3b, which may be considered as a long thin triangle.

The maximum chip thickness is

$$h_m = CE \left(\frac{CF}{D/2} \right)$$

The value of CF can be found out from Eqns. (4.3) and (4.4) as

$$CF = \sqrt{(D.d - d^2)}$$

Hence,

$$h_m = 2CE \sqrt{\left\{ \frac{d}{D} - \left(\frac{d}{D} \right)^2 \right\}} \quad \dots 4.6$$

Since $d/D \ll 1$, $(d/D)^2$ may be neglected.

$$\text{But } CE = v / N_t N_w$$

Where, N_w is the spindle speed in rpm and v is the table speed in min/sec, N_t is the number of teeth (abrasives).

Then,

$$h_m = \frac{2v}{N_w N_t} \left(\frac{d}{D} \right)^{1/2} \quad \dots 4.7$$

It is assumed that chip of constant width exists throughout its length, s and taper section yields the average depth of cut.

Thus, for surface grinding, the value of 'h' can be expressed as [83]

$$h_m = \left[\frac{4v}{\pi DN_w C_r} \sqrt{\left(\frac{d}{D}\right)} \right]^2 \quad \dots 4.8$$

Where,

C = no. of grains (no. of cutting points),

$r = \frac{b}{h/2}$, width to depth ratio of an average cut, and

b = width of each cut.

But the chip width is proportional to chip thickness, then 'h' (refer A4.2) becomes

$$h = \left[\frac{6v}{\pi DN_w C_r} \left(\sqrt{\frac{d}{D}}\right) \right]^2 \quad \dots 4.9$$

In general, the grain depth of cut is an order of magnitude less than the wheel depth of cut in surface grinding [83].

In Fig. 4.4, the length of the cutting path F'B'A' for straight grinding can be obtained from the equation of the cutting path motion. The length F'B' in each case can be taken as half the feed per cutting point. The total cutting path length 'l_k' is also provided in [89] as

$$l_k = \int_0^{\theta} dl_k + \frac{s}{2} \quad \dots 4.10$$

Where,

$$dl_k = \left[\left(\frac{dx}{d\theta'}\right)^2 + \left(\frac{dy}{d\theta'}\right)^2 \right]^{\frac{1}{2}} d\theta'$$

$$x = \left(1 \pm \frac{V_w}{V_s}\right) \frac{D\theta'}{2}$$

and $y = \frac{D\theta'^2}{4}$

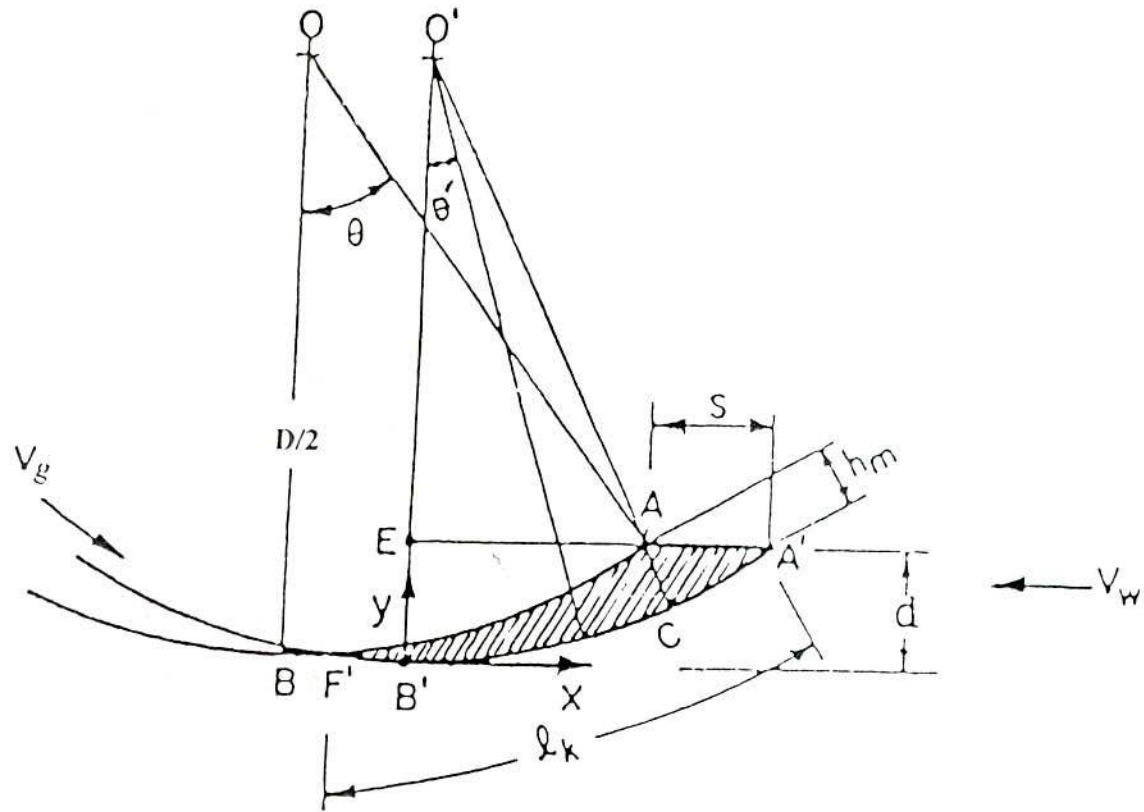


Figure 4.4 Undeformed Chip Geometry for Straight Surface Grinding

Substituting the values of x and y and integrating leads to the results

$$l_k = \left(1 \pm \frac{V_w}{V_s}\right) \frac{D\theta}{2} + \frac{\theta^3}{6 \left(1 \pm \frac{V_w}{V_s}\right)} + \frac{s}{2} \quad \dots 4.11$$

Here, + ve sign indicates up-grinding, and
- ve sign indicates down-grinding.

Since θ is small angle the second term is very negligible compared to the first one and omitted. The quantity $\frac{D\theta}{2}$ corresponding to the arc length AB can be approximated by its chord length.

Therefore,

$$l_k = \left(1 \pm \frac{V_w}{V_s}\right) (d.D)^{1/2} + \frac{s}{2} \quad \dots 4.12$$

It can also be written as

$$l_k = \left(1 \pm \frac{V_w}{V_s}\right) l_c + \frac{s}{2}$$

The cutting path length ' l_k ' is shown in Eqn. (4.12) may be considered as a kinematic correction to the static contact length ' l_c ' in which case ' l_k ' is called the kinematic contact length.

For straight grinding the maximum undeformed chip thickness ' h_m ' corresponds to the length AC as

$$h_m = 2s \left(\frac{d}{D}\right)^{1/2} - \frac{s^2}{D} \quad 4.13$$

when $d/D \ll 1$

The maximum possible value of h_m is equal to the set depth of cut in surface grinding as shown in Fig 4.5.

According to Thompson [6], total contact area can also be calculated as:

$$A = A_p + A_s \quad \dots 4.14$$

Where,

$$A_p = \frac{\pi D.b.}{360} \cos^{-1} \left(1 - \frac{2d}{D}\right)$$

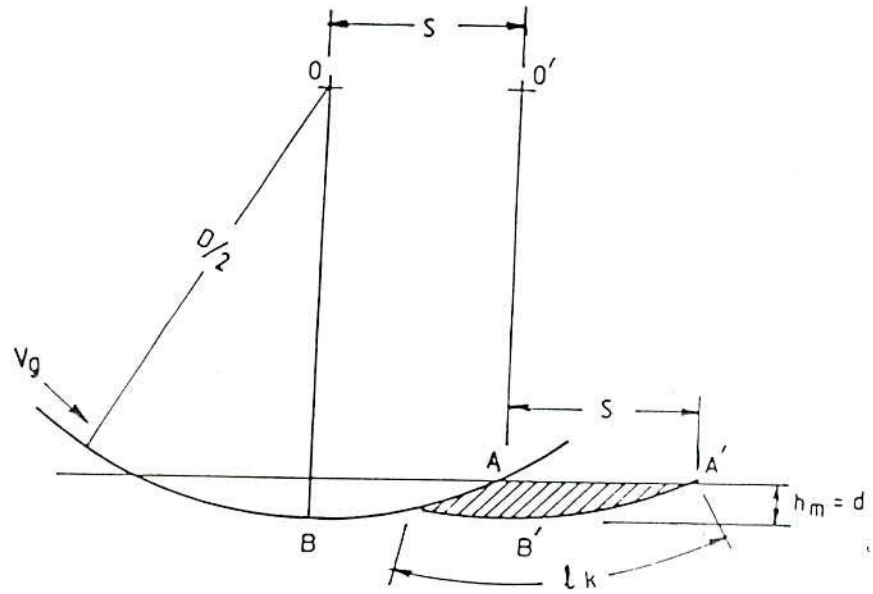


Figure 4.5 Undeformed Chip Shape for Maximum Possible Value of Chip Thickness

Total side contact area is

$$A_s = 2 \left\{ 2\pi \frac{(D/2)^2}{360} \cos^{-1} \left(1 - \frac{2d}{D} \right) - \left(\frac{D}{2} - d \right) \sqrt{(D \cdot d - d^2)} \right\}$$

The angle between the infeed direction and the normal to workpiece surface corresponding to the initial contact point is [6, 21]

$$\theta = \cos^{-1} \sqrt{\left(\frac{4 \cdot d}{D} \right)} \quad \dots 4.15$$

The feed per abrasive cutting point for the idealized wheel where the cutting points are equally spaced apart by a distance L is given by [89]

$$s = \frac{L \cdot V_w}{V_s} \quad \dots 4.16$$

Where,

$$\frac{L_c}{v_s} = \text{time between two successive cuts, and } L_c = \frac{V_s}{V_w} J_c$$

That means, the feed per abrasive cutting point is equal to the product of the workpiece velocity and the time between two successive cuts.

4.3 ECG Process Description

Electrochemical grinding process employs the principle of anodic dissolution. The experimental set up used is very similar to a conventional type grinding machine. The main difference is that the grinding wheel and spindle are insulated electrically from the rest of the machine. When this process is carried out in presence of an electrolyte, DC power supply and electrically conductive abrasive grinding wheel, then it is called ECG process. It is an important type of electrochemical machining in which the material removal phenomenon consists of two different processes namely electrochemical action and mechanical action. The oxide deposit coated on the surface of the workpiece is removed by the rotation of the abrasive wheel. A spring loaded carbon brass is connected with a copper disk fitted to the other end of the grinding wheel spindle to make negative connection of the DC supply. The positive side of the DC source is connected to the job holding vice. The process is governed by some process parameters as explained hereafter.

4.4 Process Parameters Governing MRR

The process parameters that affect the mechanical metal removal mechanism are:

- i) type of bond and abrasive, grain size and concentration, and profile of the grinding wheel,
- ii) structure, pre-treatments and shape of work material, and

- iii) different machining conditions such as feed rate, wheel speed, and depth of cut etc.

The aim of adopting the electrochemical grinding process is to get higher material removal rate and grinding ratio coupled with better dimensional control and surface integrity. To achieve those goals, identification of the significant parameters that affect the process are necessary. The following parameters are found to influence the MRR very significantly:

- i) the voltage input across the two electrodes,
- ii) the equivalence of atomic weight and valency of elements of work material,
- iii) the conductivity and strength of the electrolyte,
- iv) the width of the machining gap,
- v) the degree of polarization or passivation,
- vi) the presence of gas in the machining gap, and
- vii) the process durability.

The increase in input voltage increases the current, thereby causes higher electrolytic action and consequently increases MRR. However, too much increase in the voltage will cause rise to gas pressure which throws the electrolyte out of the machining gap, decreases the overall conductivity and thereby current density. At some point, severe electric sparking may occur damaging the wheel and workpiece and possibly cracks the workpiece, impairs dimensional accuracy and surface finish. Fine red sparks at exit side of the wheel indicates optimum voltage setting, bright blue audible sparks at inlet end of the wheel indicates too high voltage setting. The effect of decreasing volts is to reduce the electrolyte action thus reducing the overall metal removal rate.

Increased pressure will cause increase in electrolytic action. With the increase in feed force the abrasive grits penetrate more into the workpiece. More penetration of the grits into the work surface means the material removal is by abrasive action thus increases MRR. But excessive feed force will result intensive

mechanical rubbing, shortens the process efficiency. Slow feed rate results in large overcut and poor surface finish. Fast feed rate results in shortening of wheel life.

The composition of work material decides the molecular weight. Different constituents have different valencies, and one element may have more than one valence. Hence the composition of anode material is very important to determine MRR. Increase in pressure increases mechanical scuffing. Initially higher over all material removal rate occurs, but further increase in pressure leads to a quite a number of disadvantageous effects, culminating in short circuiting and a rapid drop in removal rate.

Specific conductivity of electrolyte depends on the type of electrolyte, its concentration and the presence of the additives. The viscosity determines the energy required to flow through the machining gap. The width of the machining gap depends upon the grit size and its projection from bond surface. It also depends on the feed rate and depth of cut in case of constant feed grinding and on the feed force in constant feed force grinding, and electrolyte flow rate. The proper design of nozzle is important to assure the continuous flow of electrolyte through the gap.

The passivation created by the high pressure gas bubbles due to high current densities can be controlled by the surface speed and electrolyte flow rate. Excessive surface speed may over throw the electrolyte due to centrifugal action, and excessive flow rate may cause stray machining.

The wheel properties also play an important role in electrochemical grinding. Since the abrasives maintain the machining gap and remove passive layer, the size-shape-concentration of abrasives must be considered. The bond material influences the conductivity, binding strength, wheel wear, and the principle of wheel dressing.

The relationship among different process parameters has been illustrated in the following Fig. 4.6.

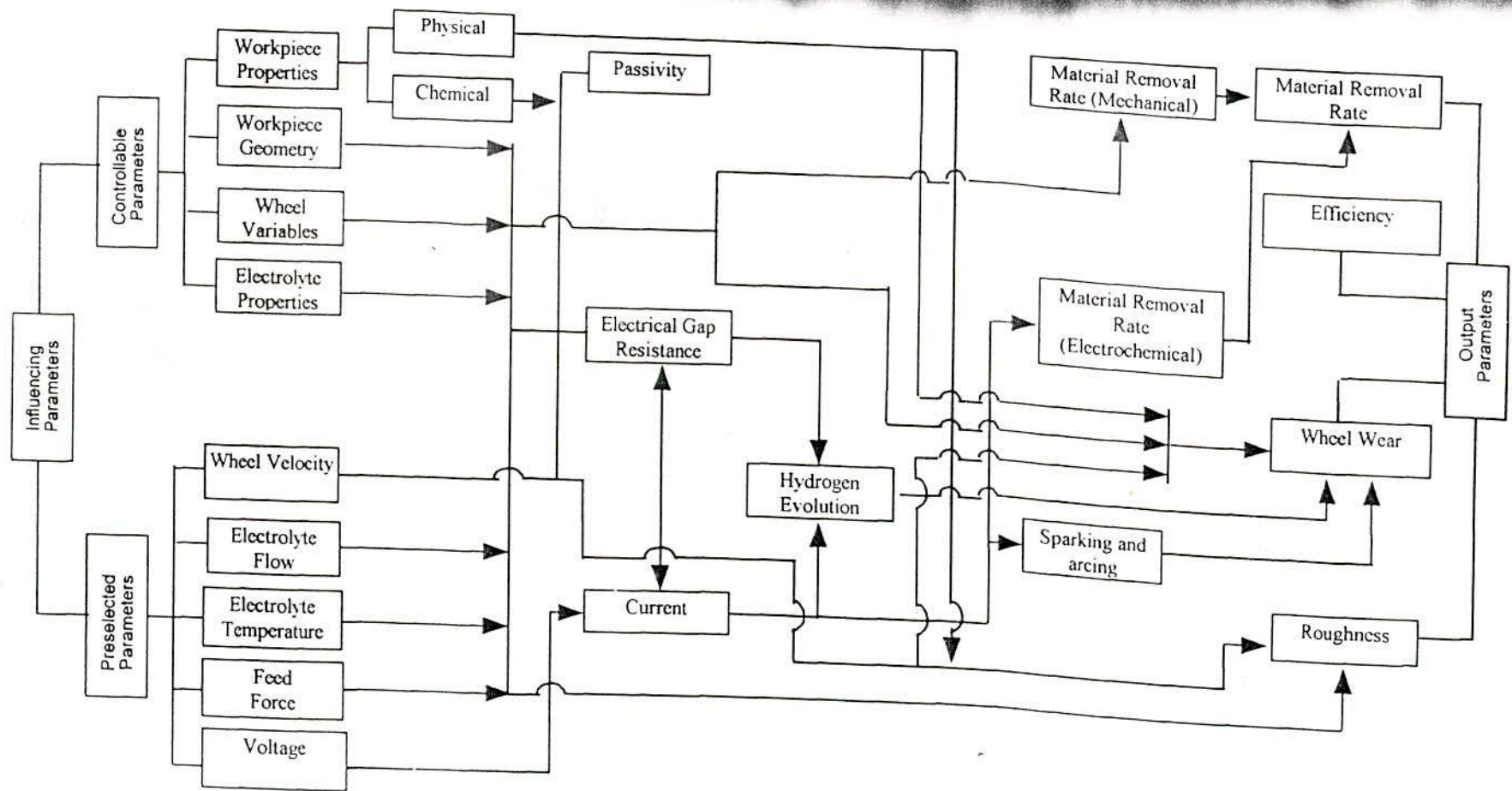


Figure 4.6 Inter-relationship Amongst ECG Process Parameters

4.5 Feed Force Analysis

4.5.1 Introduction

Different types of forces are involved in different stages of grinding. Ploughing deformation occurs as the abrasive initially cuts into the workpiece, as illustrated in Fig. 4.7. As the cutting point passes through the grinding zone, its depth of cut increases from zero to maximum value ' h_m ' at the end of the cut. On the average, chip formation commences only when the cutting point has penetrated to some critical depth of cut. Even after chip formation begins, ploughing may still persist with some of the form of cutting path being pushed aside into ridges rather than removed as chip. The effect of material removal rate on ploughing contribution has been shown in Fig. 4.8. In up-grinding as in Fig. 4.9, there will be rubbing and plastic flow to the side without removal (ploughing) until the undeformed chip thickness reaches a critical value sufficient for penetration. Rubbing occurs from A to B; then chip formation occurs from B to C. As the workpiece advances towards the grinding wheel, in first stage, a force comes into existence between the grinding wheel abrasive grain and the workpiece till the workpiece feed movement is equal to the radius of the tip. Then chip formation starts which is associated with three types of forces namely ploughing, cutting and rubbing forces. Normal and tangential component of all the forces are found out. All the horizontal components are combined to get the total feed force. The following assumptions are taken for the calculation of feed force:

- a) Each abrasive grain is considered as a single point cutting tool,
- b) The grains are arranged along the width of the wheel in parallel rows and those are on the circumference of the grinding wheel with definite circumferential pitch,
- c) Sliding of abrasive grain takes place in the time interval in which, the workpiece movement is equal to the radius of the tip of the abrasive grain.
- d) Constant pressure exists between interacting surfaces during sliding.

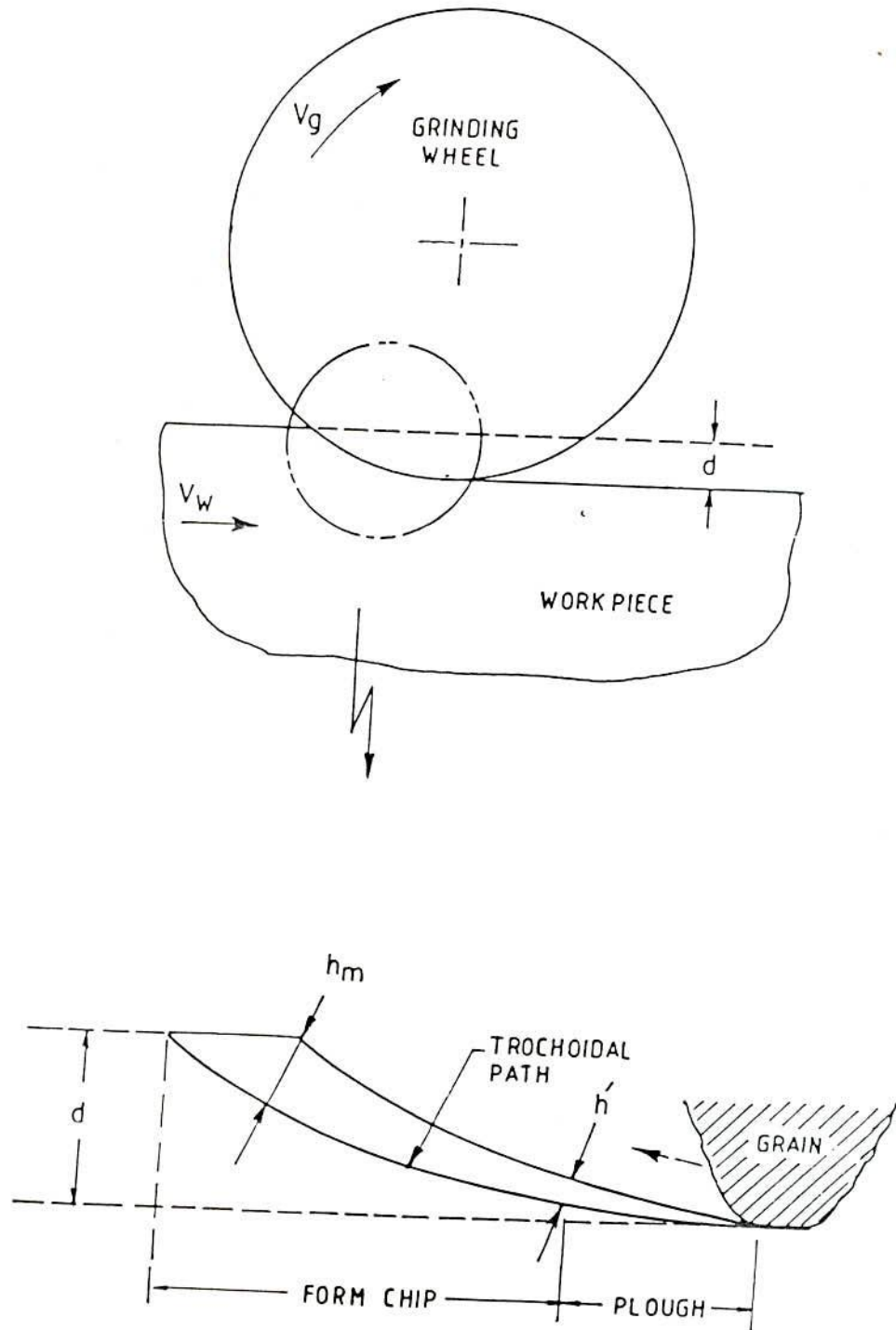
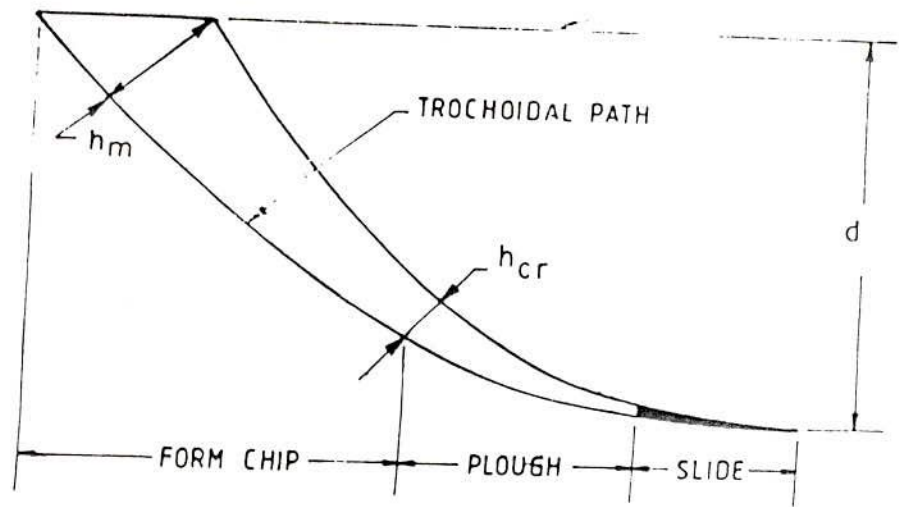
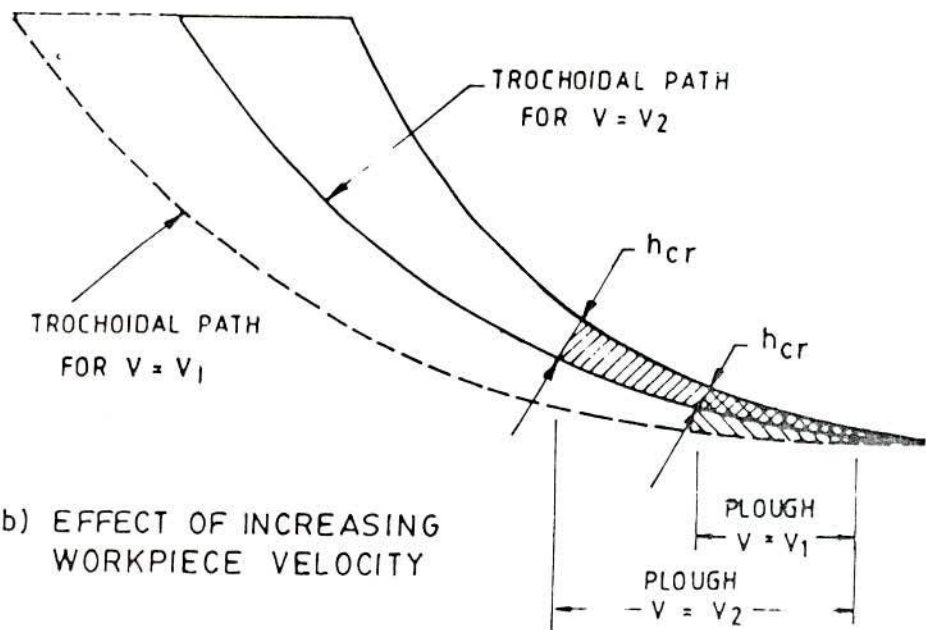


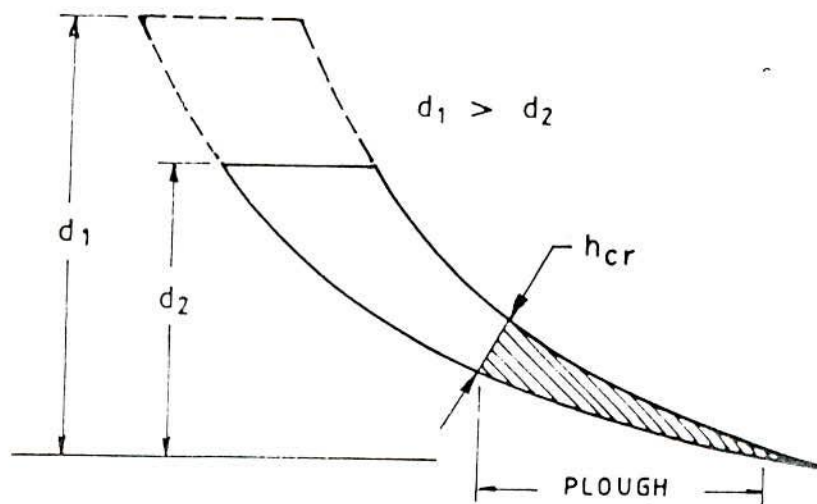
Figure 4.7 Illustration of Ploughing Followed by Transition to Chip Formation



(a) SLIDING, PLOUGHING AND CHIP FORMING REGIONS



(b) EFFECT OF INCREASING WORKPIECE VELOCITY



(c) EFFECT OF INCREASING DEPTH OF CUT

Figure 4.8 Effect of Metal Removal Rate on the Ploughing Contribution

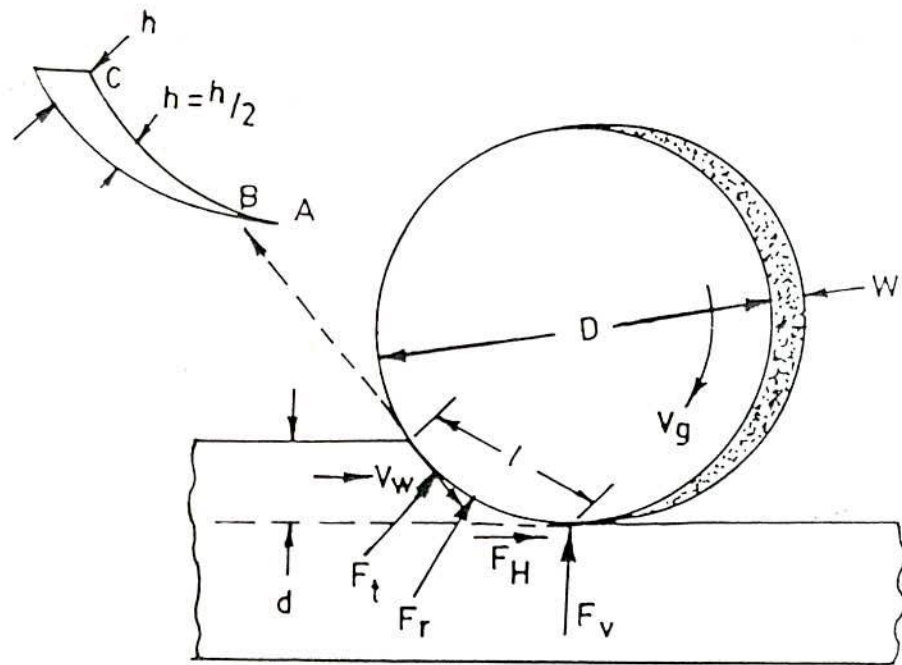


Figure 4.9 Schematic Diagram of Surface Operation Showing Individual Undeformed Chip in Insert

For the analysis of the feed force, a single grain on the surface of the grinding wheel is considered. The following forces are discussed individually.

- i) Sliding force,
- ii) Ploughing force,
- iii) Cutting force,
- iv) Rubbing force, and
- v) Force due to viscous effect of electrolyte.

4.5.2 Feed Force due to Sliding

In Fig.4.10 the point A_1 represents the initial point of contact of grinding wheel abrasive grain with the workpiece. In the first phase, sliding will take place

between abrasive grain and workpiece till workpiece feed movement is equal to the radius of the tip. During the time of sliding the wheel rotates through an angle, τ .

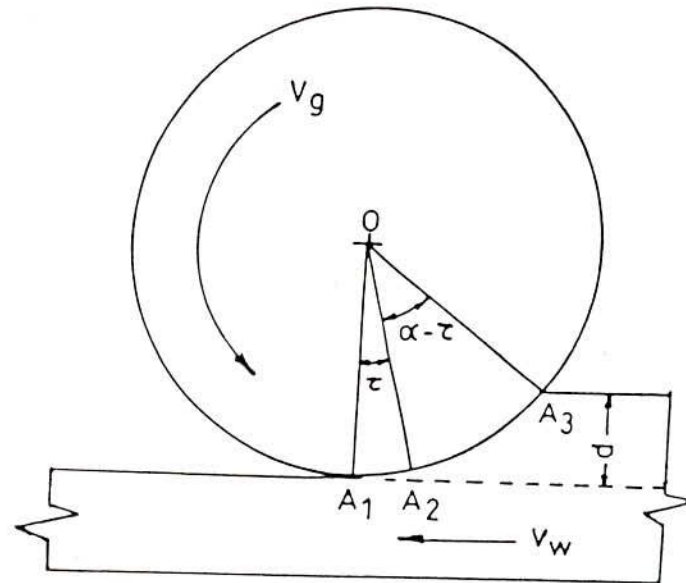


Figure 4.10 Geometry of Sliding Action

The point A_2 represents the end point of sliding action. Since the worktable feed velocity is V_w mm/s, so for a travel of $r \mu\text{m}$, the worktable will take a time equals to $\frac{r \times 10^{-3}}{V_w}$ sec. And the angle described by the abrasive grain is equal to

$$\left(\frac{r \times 10^{-3}}{V_w} \times \frac{2\pi N_w}{60} \right)$$

Hence,

$$\tau = \left(\frac{r \times 10^{-3}}{V_w} \times \frac{2\pi N_w}{60} \right) \quad \dots 4.17$$

Within this angle the sliding force acts on each abrasive grain. The projected area of action for sliding force is given by :

$$A = \pi (r \times 10^{-3})^2 \quad \dots 4.18$$

To know the normal and tangential component of sliding force at any point within the angle τ , the angle can be magnified for simplicity as shown in Fig. 4.11. The angle θ is considered to vary from 0 to τ radian and the normal sliding force for a single grain is then PA , P being the pressure intensity.

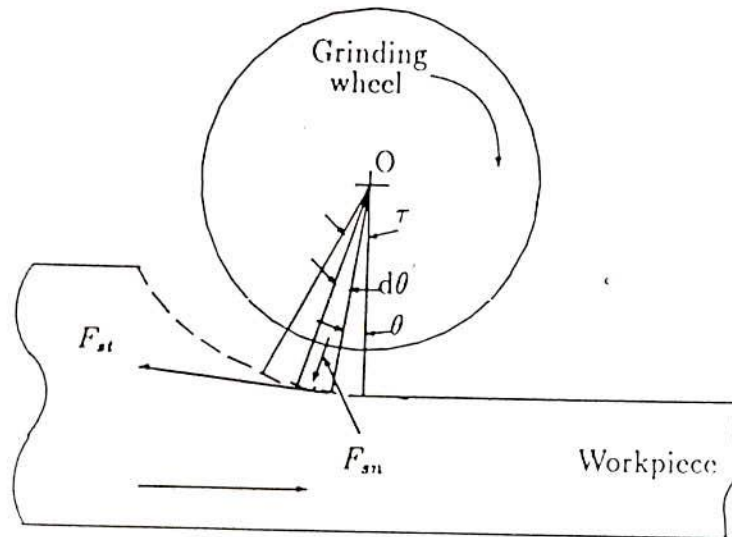


Figure 4.11 Enlarged View of Sliding Angle

If 'm' number of grains are present along the width of the wheel, the total normal sliding force $(F_s)_n$ is as follows :

$$(F_s)_n = m P A \quad \dots 4.19$$

Hence, the tangential component will be

$$(F_s)_t = \mu m P A \quad \dots 4.20$$

The component $(F_s)_n$ along horizontal direction is $(F_s)_n \sin\theta$ and that of $(F_s)_t$ along the same direction is $(F_s)_t \cos\theta$

Hence, the total horizontal force is given by ,

$$(F_s)_{TH} = \int_0^{\tau} (mPA \sin \theta + \mu mPA \cos \theta) d\theta$$

$$\therefore (F_s)_{TH} = mPA[1 - \cos \tau + \mu \sin \tau] \quad \dots 4.21$$

4.5.3 Feed Force due to Ploughing

The chip formation consists of three observed stages viz, ploughing, cutting and rubbing as in Fig.4.7. Considering a single grain along a single row, in the first stage, the only deformation of the workpiece is elastic and that occurs as the cutting edge first comes in contact with workpiece surface. As the cutting edges form the surfaces, the deformation continues, thereby the normal and tangential forces increase steadily.

During this phase of grinding, the temperature of the workpiece increases until a critical point is reached. When the normal stress exceeds the yield stress of metal the cutting edge penetrates into the plastic matrix. The plastically deformed metal is displaced sideways and ahead of the grit thus resulting a surface of up-heaval (a violent disturbance) i.e. a ploughing effect. The force experienced for this is the ploughing force. The total horizontal component due to all rows present in the angle $(\alpha - \tau)$ region can be analyzed as follows:

It is considered that 'n' number of rows present within an angle of $(\alpha - \tau)$ rad. For a circumferential pitch 'S' mm, the angle subtended by a single row is equal to S/r rad.

So within the angle $(\alpha - \tau)$ rad, the number of rows present are:

$$n = \left[\frac{(\alpha - \tau)}{S/r} \right] + 1 \quad \dots 4.22$$

The normal and tangential component of ploughing force due to first row are found as follows:

Normal force for a width, dw

$$F_n = \alpha_1 \cdot dA$$

Where,

dA = elementary area of the grit

$$\text{So, Normal force} = \alpha_1 \left(\frac{l_c V_w}{V_g} dw \right) \quad \dots 4.23$$

The resultant normal ploughing force for all active grits in contact area along with one row is

$$\left(F_p \right)_n = \alpha_1 \sum_0^w l_c \frac{V_w}{V_g} dw = \alpha_1 l_c w \frac{V_w}{V_g} \quad \dots 4.24$$

Similarly, tangential ploughing force is

$$\left(F_p \right)_t = \alpha_2 \sum_0^w l_c \frac{V_w}{V_g} dw = \alpha_2 l_c w \frac{V_w}{V_g} \quad \dots 4.25$$

The horizontal component of both the forces due to first row i.e. the contribution of both the forces for feed force is

$$\alpha_1 w l_c \frac{V_w}{V_g} \cdot \sin \tau + \alpha_2 w l_c \frac{V_w}{V_g} \cos \tau$$

Similarly, for the second row,

$$\alpha_1 w l_c \frac{V_w}{V_g} \sin\left(\tau + \frac{S}{r}\right) + \alpha_2 w l_c \frac{V_w}{V_g} \cos\left(\tau + \frac{S}{r}\right)$$

and so on.

Hence, total contribution due to ploughing effect is given by

$$(F_p)_{TH} = w l_c \frac{V_w}{V_g} \left[\alpha_1 \left\{ \sin \tau + \sin\left(\tau + \frac{S}{r}\right) + \sin\left(\tau + 2\frac{S}{r}\right) + \dots + \sin\left(\tau + n\frac{S}{r}\right) \right\} \right. \\ \left. + \alpha_2 \left\{ \cos \tau + \cos\left(\tau + \frac{S}{r}\right) + \cos\left(\tau + 2\frac{S}{r}\right) + \dots + \cos\left(\tau + n\frac{S}{r}\right) \right\} \right] \quad \dots 4.26$$

4.5.4 Feed Force due to Cutting

If the deformed surface ahead of the cutting grit edge comes in contact with the cutting edge profile, a transition from ploughing to chip formation occurs. During the chip formation, the cutting component is expected to vary due to the change of the number of geometry of the cutting grits will directly affect the cutting coefficient. The normal component of the cutting force imposed by a single grit can be determined as a function of undeformed chip cross sectional area which can be expressed as

$$(F_c)_n = k_i Q_i \quad 4.27$$

For a single row of grit, the normal component of the cutting force,

$$(F_c)_n = w \cdot k_i \sum Q_i$$

Where,

$\sum Q_i$ = total value of all simultaneous chip cross sectional area per unit width of grinding,

$$= w.k_i \frac{V_w}{V_g} s'_n \quad \dots 4.28$$

Similarly, tangential component will be

$$(F_c)_t = \mu_r . w.k_i \frac{V_w}{V_g} s'_n \quad \dots 4.29$$

Hence, net horizontal component of cutting force is

$$\begin{aligned} (F_c)_{TH} = & w.k_i \frac{V_w}{V_g} s'_n \sin \tau + \mu_r . w.k_i \frac{V_w}{V_g} s'_n \cos \tau + w.k_i \frac{V_w}{V_g} s'_n \sin \left(\tau + \frac{S}{r} \right) \\ & + \mu_r . w.k_i \frac{V_w}{V_g} s'_n \cos \left(\tau + \frac{S}{r} \right) + \dots \end{aligned}$$

which implies

$$\begin{aligned} (F_c)_{TH} = & w.k_i \frac{V_w}{V_g} s'_n \left\{ \left[\sin \tau + \sin \left(\tau + \frac{S}{r} \right) + \dots + \sin \left(\tau + n \frac{S}{r} \right) \right] \right. \\ & \left. + \mu_r \left[\cos \tau + \cos \left(\tau + \frac{S}{r} \right) + \dots + \cos \left(\tau + n \frac{S}{r} \right) \right] \right\} \quad \dots 4.30 \end{aligned}$$

4.5.5 Feed Force due to Rubbing

The normal and tangential force components resulting from rubbing action at the actual area of contact between active grit and the workpiece are derived. The normal component, $(F_r)_n$ is $a_1 k_l$, where a_1 represents the average percentage tip area per active grit, and k_l represents average contact pressure.

For 'm' number of grits, the normal rubbing force is

$$(F_r)_n = m . a_1 k_l \quad \dots 4.31$$

The tangential rubbing force component can similarly be found as

$$(F_r)_t = \lambda m. a_1 k_L \dots 4.32$$

Therefore, the total horizontal force due to rubbing force is

$$\begin{aligned} (F_r)_{TH} = & m. a_1 k_L \sin \tau + \lambda m. a_1 k_L \cos \tau + m. a_1 k_L \sin \left(\tau + \frac{S}{r} \right) \\ & + \lambda m. a_1 k_L \cos \left(\tau + \frac{S}{r} \right) + \dots + m. a_1 k_L \sin \left(\tau + n \frac{S}{r} \right) \\ & + \lambda m. a_1 k_L \cos \left(\tau + n \frac{S}{r} \right) \end{aligned}$$

On simplification,

$$(F_r)_{TH} = m. a_1 k_L \sum_{n=0}^{n=n} \sin \left(\tau + n \frac{S}{r} \right) + \lambda \sum_{n=0}^{n=n} \cos \left(\tau + n \frac{S}{r} \right) \dots 4.33$$

4.5.6 Force due to Viscous Effect of Electrolyte:

The viscous drag could essentially be due to the movement of the wheel within a fluid medium, in this instance, a salt solution. Considering the two dimensional steady and laminar flow of incompressible viscous fluid through the space between grinding wheel and the workpiece, the Navier-Stokes equation for the x direction becomes [6]

$$\frac{dp}{dx} = \mu_1 \frac{d^2 u}{dy^2} \dots 4.34$$

Integrating

$$u = \frac{1}{2\mu_1} \frac{dp}{dx} y^2 + c_1 y + c_2$$

The boundary conditions are

at $y = 0, u = 0$

at $y = h_1, u = U$



Then,

$$c_2 = 0, \text{ and}$$

$$c_1 = \frac{U}{h_1} - \frac{1}{2\mu_1} \frac{dp}{dx} h_1$$

Where,

h_1 = electrolyte film thickness

$$\text{Hence, } u = \frac{1}{2\mu_1} \frac{dp}{dx} y^2 + \left[\frac{U}{h_1} - \frac{1}{2\mu_1} \frac{dp}{dx} h_1 \right] y$$

Which implies

$$u = \frac{1}{2\mu_1} \frac{dp}{dx} h_1 y \left[\frac{y}{h_1} - 1 \right] + \frac{U}{h_1} y \quad \dots 4.35$$

$$\text{Now, } Q = \int_0^h u w dy \quad \dots 4.36$$

Where,

w is the width of workpiece and Q is the flow rate of electrolyte.

$$Q = w \left[-\frac{1}{2\mu_1} \frac{dp}{dx} \frac{h^3}{6} + \frac{U h_1}{2} \right] \quad \dots 4.37$$

For the case where p is maximum, $dp/dx = 0$

$$\text{Therefore, } Q = w \frac{U H}{2} \quad \dots 4.38$$

Where, H = film thickness at the point of maximum pressure

On simplification, it becomes

$$\frac{dp}{dx} = 6 \mu_1 U \left(\frac{h_1 - H}{h_1^3} \right) \quad \dots 4.39$$

If dF is the horizontal force acting on the area dA of the workpiece surface,

$$\text{Then, } dF = 6 \mu_1 U \left(\frac{h_1 - H}{h_1^3} \right) dx w dx$$

Integrating

$$F_c = 6 \mu_1 U l_c^2 w \left(\frac{h_1 - H}{h_1^3} \right) \quad \dots 4.40$$

4.5.7 Feed Force Equation :

The feed force equation for electrochemical grinding process has been determined by summing up all the horizontal components of the individual force components namely sliding, ploughing, cutting and rubbing forces, and the force produced due to viscous electrolyte. This equation can be represented as

$$\begin{aligned} F_f &= (F_s)_{TH} + (F_p)_{TH} + (F_c)_{TH} + (F_r)_{TH} + F_e \\ &= m p A (1 - \cos \tau + \mu_r \sin \tau) + (w \cdot l_c \cdot \frac{V_w}{V_g} \alpha_1 + w \cdot k_1 \cdot \frac{V_w}{V_g} s'_n + m a_1 k_1) \\ &\quad \left\{ \left(\sum_0^n \sin \left(\tau + \frac{nS}{r} \right) \right) \right\} + (\alpha_2 w \cdot l_c \cdot \frac{V_w}{V_g} + w \cdot k_1 \cdot \frac{V_w}{V_g} s'_n \mu_r + m a_1 k_1 \lambda) \\ &\quad \left(\sum_{n=0}^n \cos \left(\tau + \frac{nS}{r} \right) \right) + 6 \mu_1 l_c^2 U w \left(\frac{h_1 - H}{h_1^3} \right) \end{aligned} \quad \dots 4.41$$

The value of s'_n may be assumed to be 10% of the s_n value. Because the MRR value due to mechanical action in ECG is about 10% [2].

Since the process is in micro level, all the possible aspects of the machining process are taken into account in this equation. As a result, the equation expressed becomes larger and that could be made simpler form if the negligible force components are omitted.

4.6 An Analysis for MRR

4.6.1 Introduction

Material removal rate for electrochemical grinding process is required to be analysed. The amount of material removed is due to a combined effect of electrochemical and mechanical actions. It has already been discussed, the electrolyte when passes through the working zone, the conductive workpiece is dissolved by anodic action and the resulting oxidised layer on the surface is removed by the abrasives held by rotating conductive wheel. As long as the oxide film is removed continuously, the electrochemical grinding process is at a constant rate. The MRR in ECG is determined by current density that involves the removal of material from workpiece and the anodic dissolution is fairly in accordance with Faraday's laws of electrolysis. The two laws are:

- a) The first which states the process condition, that the amount of chemical changes 'W' produced (i.e. dissolved or deposited) is proportional to the amount of charge 'Q' passed through the electrolyte, i.e. $W \propto Q$.
- b) The second law proposes the condition stating the dependency on material property, that amount of change produced is proportional to its electrochemical equivalent, ECE of the material, i.e. $W \propto ECE$.

The total cutting phenomenon is very complicated as the process is accompanied by electrolytic action. An analysis for MRR due to electrochemical action and that of mechanical action is intended to be carried out.

4.6.2 Material Removal Rate due to Electrochemical Action

Material removal rate has been calculated on the assumption that the rotating grinding wheel is provided with both rotational speed as well as linear feed. The other assumptions are : conductivity of electrolyte remain constant, and the potential remains unchanged over the entire surface area and throughout the machining periods, at both the electrodes. For any small interval of time ' Δt ', linear amount of dissolution or rather depth of penetration in a direction perpendicular to the surface is (Fig. 4.12)

BG equals to $R \cdot \Delta t$ and is perpendicular to the wheel surface. Since the anodic dissolution takes place between wheel and workpiece, the perpendicular distance between them is considered.

For, $\Delta t = 1$ unit time, $BG = R$

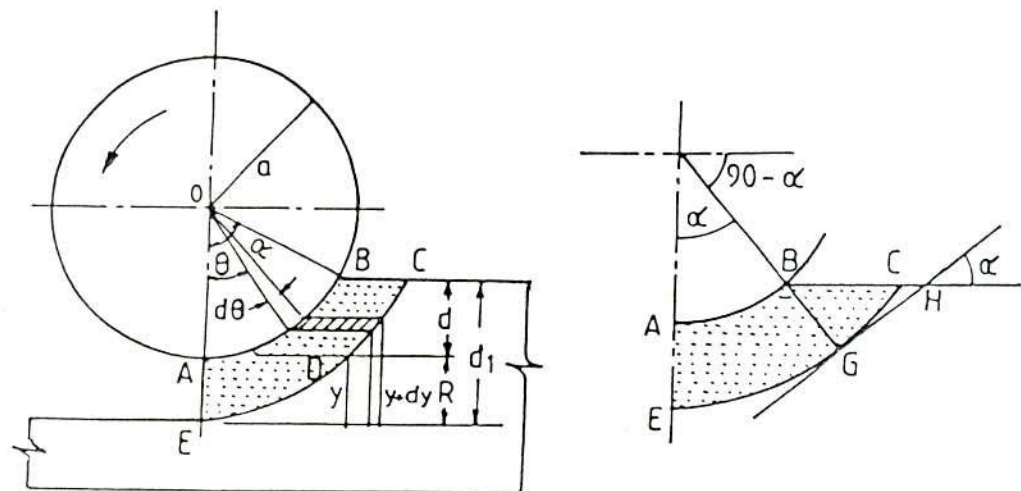


Figure 4.12 Electrochemical Action on the Grinding Wheel

From Faraday's laws of electrolysis it can be stated that the amount of material dissolved from anode is proportional to the current, passage time t , and electrochemical equivalent of anode material, which can be written as

$$W \propto E I t$$

or
$$W = \frac{E I t}{F} \quad \dots 4.42$$

Hence, volume of metal removed, (V) is

$$V = \frac{W}{\rho}$$

or,
$$\frac{L}{t} = \frac{E}{\rho} \cdot \frac{I}{A} \cdot \frac{1}{F} \quad \text{since } V = L.A \quad \dots 4.43$$

The linear rate of dissolution (L/t) on active area through which current flows is R and that may be written in the form

$$R = k \cdot i \quad \dots 4.44$$

Where,
$$k = \frac{E}{\rho} \cdot \frac{1}{F}$$

This equation yields the rate of metal dissolution in a direction perpendicular to workpiece surface. But during this interval of time, the wheel also moves linearly with respect to workpiece through a distance $s \cdot \Delta t$ so that

$$BH = s \cdot \Delta t$$

Where,

s = linear feed rate of the grinding wheel, mm/s

Geomerically it is found

$$\frac{BG}{\sin \alpha} = \frac{BH}{\sin 90^\circ} = R \cdot \Delta t = R, \text{ as } \Delta t = 1 \text{ and } BH = BC$$

$$\therefore \sin \alpha = \frac{R}{s} \quad \dots 4.45$$

Again, $\sin \alpha$ can be expressed as

$$\sin \alpha = \frac{\sqrt{a^2 - (a-d)^2}}{a}$$

$$\text{which implies, } \sin \alpha = \left[\frac{2d}{a} \right]^{1/2} \quad \dots 4.46$$

(neglecting d^2 , as $d^2 \ll 2.a.d$)

The relationship among wheel radius and depth of cut with wheel feed rate and also with the rate of linear dissolution is determined by combining Eqns. (4.45) and (4.46) as follows :

$$R = s \left[\frac{2d}{a} \right]^{1/2} \quad \dots 4.47$$

To analyze the volumetric removal rate for electrochemical action only, the horizontal feed rate of the wheel is assumed to be equal to radial rate of anodic dissolution. The total area 'BCDEAB' as shown in Fig. 4.12 has been calculated to determine volumetric removal rate. The area can be splitted up into two parts, one is 'ADCBA' and the other is 'ADE'. The horizontal distance BC varies along the depth. In general, the length of the hatched parallelogram is equal to $R/\sin\theta$

Hence,

$$\begin{aligned} BC &= \frac{R}{\sin \alpha} \\ &= R \left(\frac{a}{2d} \right)^{1/2} \end{aligned}$$

The area 'ADCBA' has been calculated by integrating from $y = R$ to $y = d$, that means

$$\text{Area ADCBA} = \Delta t \int_{y=R}^{y=d} R \cdot \sqrt{\frac{a}{2y}} dy \quad \dots 4.48$$

Where, $d_1 = d + R \Delta t = d + R$

Similarly, length $AD = R \Delta t \left[\frac{a}{2y} \right]^{1/2}$ since $R = \Delta E$

Considering contour ED as a contour of parabola, and the area EDF to be one third of the rectangle ADFE, the area ADE becomes

$$\text{Area ADE} = \frac{2}{3} \left[\Delta t \cdot R \left\{ \frac{a}{2R \Delta t} \right\}^{1/2} \right] \cdot R \Delta t \quad \dots 4.49$$

Therefore, the total area for material removal rate due to electrochemical action is

$$A = \frac{2}{3} \left[R^2 \sqrt{\frac{a}{2R}} \right] + R \left(\sqrt{\frac{a}{2}} \right) \int_R^{d_1} \sqrt{\frac{dy}{y}}$$

On simplification, it becomes

$$A = \frac{2}{3} R^2 \sqrt{\frac{a}{2R}} \left[1 + 3 \left(\sqrt{\frac{d_1}{R}} - 1 \right) \right] \quad \dots 4.50$$

Referring to Fig. 4.12 and assuming 'b' as the width of the grinding wheel, the volume of metal removed per unit of time due to electrochemical action can now be written as

$$\text{MRR}_E = 2 \cdot b \cdot R^2 \left(\frac{a}{2R} \right)^{1/2} \left\{ \left(\frac{d_1}{R} \right)^{1.2} - \frac{2}{3} \right\} \quad \dots 4.51$$

4.6.3 Material Removal Rate due to Mechanical Action

The grinding wheel has a rotational motion about its own axis as well as linear feed motion relative to workpiece. Any particle on the periphery of the wheel would have tangential and linear velocities in feed direction. The simulated position of the

wheel considering the mechanical material removal part only (of the total removal in ECG) has been shown in Fig. 4.13.

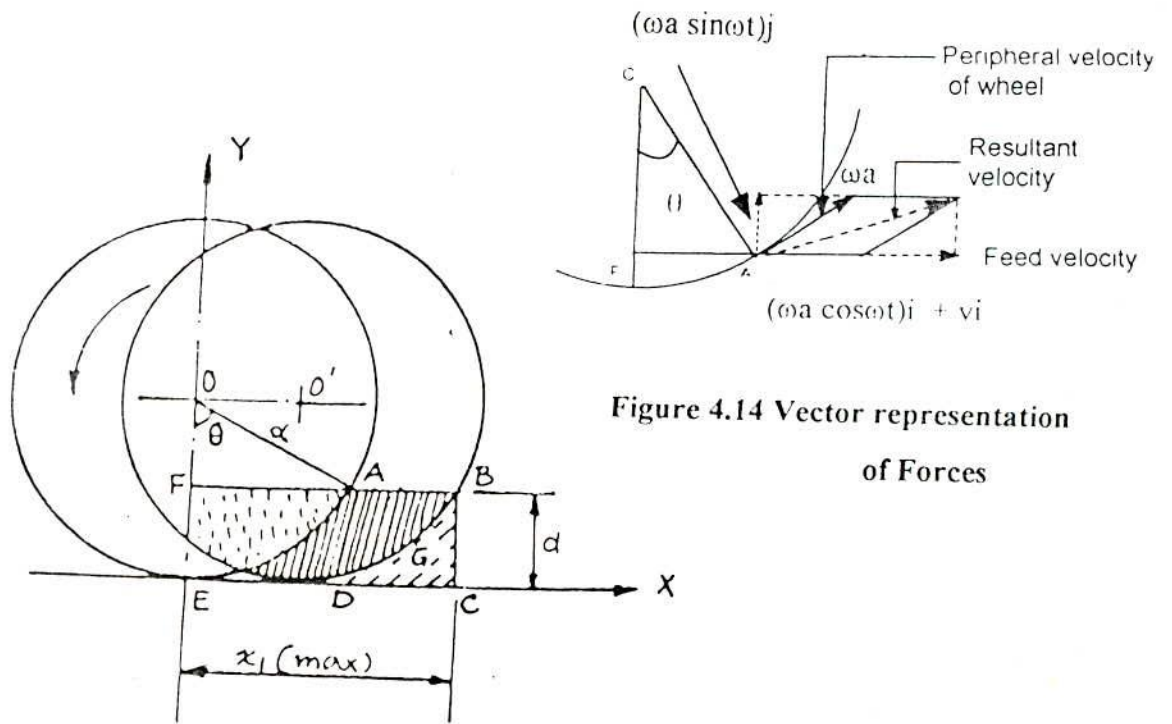


Figure 4.14 Vector representation of Forces

Figure 4.13 Simulated Position of the Grinding Wheel in Mechanical Action

A is any point on the periphery of the grinding wheel with ' O ' as its centre. If ' θ ' be the angle through which the wheel turns and the cutting point A traces out the locus, the components of the tangential velocity are $\omega a \cos \omega t$ and $\omega a \sin \omega t$ in X and Y directions respectively. The angle swept in a small interval of time t is ' ωt ' which is equal to ' θ '. The resultant velocity is nothing but the time rate of change of displacement vector (R)

$$\text{So, } \frac{dR}{dt} = \omega a (\cos \omega t \hat{i} + \sin \omega t \hat{j}) + v \hat{i} \quad \dots 4.52$$

Where, v is the feed velocity along +ve X direction

Integrating Eqn. (4.52) it becomes,

$$\vec{R} = (a \sin \omega t + vt)\hat{i} - a \cos \omega t \hat{j} \quad (\text{with respect to centre of the wheel})$$

$$\text{Again, } R = (a \sin \omega t + vt)\hat{i} + (a - a \cos \omega t)\hat{j} \quad (\text{with respect to point E of the wheel})$$

So, the values of x_1 and y_1 (components of displacement) are

$$x_1 = a \sin \omega t + vt \quad \dots 4.53$$

$$y_1 = a - a \cos \omega t \quad \dots 4.54$$

Since x_1 is a function of time its value increases from 0 to maximum. That is, if ω rad/sec is the angular velocity of the wheel, then α radian covers in $\frac{\alpha}{\omega}$ sec.

For small angle, $\sin \alpha = \alpha$

$$\text{Then } x_1(\text{max}) = a \sin \alpha + \frac{v_f}{\omega} \cdot \sin \alpha \quad \dots 4.55$$

Geometrically it can be written as

$$\cos \alpha = \frac{a-d}{a}, \quad \sin \alpha = \sqrt{\frac{2d}{a}}$$

Since $d^2 \ll 2ad$, d^2 may be neglected.

Putting the value of $\sin \alpha$ is Eqn. (4.55)

$$x_1 (\text{max}) = \sqrt{\frac{2d}{a}} \left(a + \frac{v_f}{\omega} \right) \quad \dots 4.56$$

The total cutting area 'EHABGDE' due to mechanical action is splitted into three parts as

$$\text{EHABGDE (A)} = \text{FBCE (A}_1\text{)} - \text{DGBCD (A}_2\text{)} - \text{FAHEF (A}_3\text{)} \dots 4.57$$

The areas A_1 , A_2 , and A_3 are calculated separately as given in Appendix (A4.3) and presented in the following:

$$A_1 = \sqrt{\frac{2d}{a}} \left(a + \frac{v_f}{\omega} \right) \times d$$

$$A_2 = \frac{a \cdot d}{2} \sqrt{\frac{2d}{a}}$$

$$A_3 = \frac{1}{2} \cdot \sqrt{\frac{2d}{a}} \cdot a \cdot d$$

Substituting the values of A_1 , A_2 , A_3 in Eqn.(4.57), the net area becomes

$$A = \sqrt{\frac{2d}{a}} \times \frac{v_f d}{\omega} \quad \dots 4.58$$

Hence, the volume of metal removed, $V = A \cdot b = v_f \cdot d \cdot b \cdot t$

$$\text{Since } \sqrt{\frac{2d}{a}} = \sin \alpha = \sin \omega t \cong \omega t$$

$$\text{MRR}_M = \frac{dV}{dt} = v_f \cdot d \cdot b \quad \dots 4.59$$

Where, v_f = linear feed rate during mechanical grinding.

4.6.4 Total Material Removal Rate

Since in ECG process, a combined effect is to be considered, the assigned feed would be apportioned between the two mechanisms depending on the current level. It may also be pointed out that when current 'I' takes the maximum value depending on stock removal i.e. when it is purely ECM, mechanical process is assumed to be completely absent (feed on radial forces are absent). It also states that feed and radial forces are maximum when current is zero, stating that the process is purely mechanical.

For a given feed 's', if both processes exist and let ' χ ' be the fraction of the feed responsible to contribute to ECM, then $(1-\chi)$ is the fraction that contributes for mechanical abrasion .

The total material removed per unit of time due to combined action of both electrochemical and mechanical actions can be written by summing up the Eqns.(4.51) and (4.59) with appropriate apportionment as

$$MRR_{\text{Total}} = 2.b.R^2 \times \left(\frac{a}{2R}\right)^{1/2} \left\{ \left(\frac{d_1}{R}\right)^{1/2} - \frac{2}{3} \right\} + v_r.d.b(1-\chi) \quad \dots 4.60$$

4.7 Difficulties with Theoretical Calculations

The theoretical model developed for the feed force is mostly based on the different actions, such as sliding, ploughing , cutting, rubbing, and viscous effect of electrolyte. Besides the above, the size, shape, and the arrangement of abrasive grains in the wheel are also responsible for the contribution of feed force which involves many unknown terms in the final expression. These unknown terms are to be put carefully to obtain an acceptable value. This also bears some finite series and the analysis is in the order of micron level. It is true that all the abrasive grains can not be identical, that means there is a great possibility of deviation of theoretical findings with the experimental results. Prior to the above limitations a rigorous study is carried out to reach a final expression. In the theoretical analysis, some factors are left to be considered (specifically in electrochemical action for example, the valency of the constituting elements in workpiece material are mostly not known until the exact valencies displayed by elements during electrochemical dissolution), the theoretical machining rates can only be considered as a rough guide. Material removal rates for various metals are provided in Table 4.1 [10].

Table 4.1 Metal Removal Rates for Various Metals

| Metal | Valency | Density | | Metal-removal Rate at 1000A | |
|------------------------|---------|----------------------|-------------------|-----------------------------|----------------------|
| | | lb/ in. ³ | g/cm ³ | in ³ /min | cm ³ /min |
| Aluminum | 3 | 0.098 | 2.67 | 0.126 | 2.06 |
| Beryllium | 2 | 0.067 | 1.85 | 0.092 | 1.50 |
| Chromium | 2 | 2.260 | 7.19 | 0.137 | 2.25 |
| | 3 | | | 0.092 | 1.51 |
| | 6 | | | 0.046 | 0.75 |
| Cobalt | 2 | 0.322 | 8.85 | 0.125 | 2.05 |
| Niobium (Columbium) | 3 | 0.310 | 8.57 | 0.132 | 2.16 |
| | 4 | | | 0.103 | 1.69 |
| | 5 | | | 0.082 | 1.34 |
| Copper | 1 | | | 0.268 | 4.39 |
| | 2 | | | 0.134 | 2.20 |
| Iron | 2 | | | 0.135 | 2.21 |
| | 3 | | | 0.090 | 1.47 |
| Magnesium | 2 | 0.324 | 8.96 | 0.265 | 4.34 |
| Manganese | 2 | 0.284 | 7.86 | 0.139 | 2.28 |
| | 4 | | | 0.070 | 1.15 |
| | 7 | | | 0.040 | 0.66 |
| Molybdenum | 3 | 0.369 | 10.22 | 0.119 | 1.95 |
| | 4 | | | 0.090 | 1.47 |
| | 6 | | | 0.060 | 0.98 |
| Nickel | 2 | 0.322 | 8.90 | 0.129 | 2.11 |
| | 3 | | | 0.083 | 1.36 |
| Silicon | 4 | 0.084 | 2.33 | 0.114 | 1.87 |
| Silver | 1 | 0.379 | 10.49 | 0.390 | 6.39 |
| Tin | 2 | 0.264 | 7.30 | 0.308 | 5.05 |
| | 4 | | | 0.154 | 2.52 |
| Titanium | 3 | 0.163 | 4.51 | 0.134 | 2.19 |
| | 4 | | | 0.101 | 1.65 |
| Tungsten | 6 | 0.697 | 19.3 | 0.060 | 0.98 |
| | 8 | | | 0.045 | 0.74 |
| Uranium | 4 | 0.689 | 19.1 | 0.117 | 1.92 |
| | 6 | | | 0.078 | 1.29 |
| Vanadium | 3 | 0.220 | 6.1 | 0.106 | 1.74 |
| | 5 | | | 0.064 | 1.05 |
| Zinc | 2 | 0.258 | 7.13 | 0.174 | 2.85 |

It is assumed that the gap between wheel and anode material is constant. During the machining process different actions such as activation polarisation, concentration polarisation, ohmic over voltage, passivity activity etc. will also be present, for which Faradaic efficiency can not be calculated accurately. In ECG operation, there is also a chance of sparking and/or short circuiting, would lead to flow more current than the expected value.

The intergranular attack decreases the strength of a part, even though it affects a very little percentage of material. When this attack occurs, the first process variable to be considered is the electrolyte. In such a case, sodium nitrate or nitride alone or, in certain cases mixed with chloride is to be used. Lower electrolyte temperature and lower operating voltage can decrease this type of attack. (It has been reported by many researchers [10, 77] that there is no such effect observed in ECG process).

The anode material may be attacked by certain solutions, fails by corroding at individual spots, known as 'pit' corrosion. The presence of dents, rough spots, foreign particles deposited on the metal surface can increase this formation of pits. At the time of severe electrical arcing and sparking, the process suddenly changes from electrochemical grinding to electrodischarge machining as well and results in severe pitting [10].

4.8 Summary

In this study, the grinding geometry and kinematics are explained for straight surface grinding. The process parameters which influence the material removal rate very significantly are discussed. The theoretical models for determining material removal rates due to both mechanical and electrochemical actions are developed. Feed force analysis has been included in this study for general surface grinding conditions. The amount of the mechanical and electrochemical actions are determined by the process variables that affect the peripheral contact length, contact area, and the cutting path. The mechanical contact length and cutting path is shorter in case of electrochemical grinding process. But the total contact length and cutting

path is larger than that of conventional grinding. The penetration of abrasive grains into the workpiece and feed per abrasive cutting point at initial contact point is higher with higher cutting forces. The depth of cut for combined mechanical and electrochemical action can be used as a tool to calculate material removal rate without considering them independently. The basic idea gathered from this theoretical analysis results in better understanding of the process with which electrochemical grinding parameters can be chosen properly. For the verification of the analysis and experimental works, a set up has been developed from an obsolete surface grinder, details of which is explained in Chapter 5.

CHAPTER - 5

DESIGN AND DEVELOPMENT OF

EXPERIMENTAL SET-UP

CHAPTER 5

DESIGN AND DEVELOPMENT OF EXPERIMENTAL SET-UP

5.1 Introduction

The present need of processing super alloys and hard materials with high surface finish as well as with stress and crack free surface required by Indian Industries, is demanding for the import of ECG machines. The high import cost of such machine (to be approximately of 50 lac to 1 crore rupees) has forced to initiate the development of such rarely available machine. The project has been undertaken to develop a prototype, industrial electrochemical grinding machine with hydraulic feed control system and inbuilt force measuring transducers, for experimentation to corroborate the theoretical and practical analysis.

Among the non-conventional methods of machining, this ECG system has also been chosen due to its higher material removal rate, independent of work material hardness, practical elimination of mechanical or thermal cracking and stresses, economical method of machining for intractable materials. Due to high electrochemical action, the cutting force applied to the workpiece is minimal and no heat is generated resulting in negligible metallurgical damage or distortion.

An existing obsolete structure of a grinding machine is utilized as the main frame and retrofit for the present machine set-up. The design of hydraulic cylinder and piston, the development of hydraulic and electrolytic circuits and the modification of bed and machining chamber are also included. The aim behind designing and fabricating the set-up of the ECG machine is that one should be able to vary the principal parameters desirably and as far as possible independently within suitable ranges. The work also deals with the design, construction and calibration of a grinding dynamometer, which can be treated as an important element of the ECG machine to ease adaptive control in future if required. Arrangements are also made for monitoring and controlling different responses.

Each system has been designed in such a manner that it should work independently without affecting the other systems rather it should correlate properly with them. As for example, at the time of designing the mechanical system proper cognizance should have been given on the interactions between the mechanical circuit and hydraulic circuit, as well as between mechanical circuit and electrical circuit in addition to the mechanical circuit as such. The above principles can be represented by the following matrix form :

$$\begin{array}{c}
 \text{Parameters} \\
 \left[\begin{array}{ccc}
 1 & \text{Mechanical Circuit} & \text{Mechanical Circuit} \\
 \text{Hydraulic Circuit} & 1 & \text{Hydraulic Circuit} \\
 \text{Electrical Circuit} & \text{Electrical Circuit} & 1
 \end{array} \right]
 \end{array}
 \times
 \begin{array}{c}
 \text{Restrictions} \\
 \left[\begin{array}{c}
 \text{Mechanical Circuit} \\
 \text{Hydraulic Circuit} \\
 \text{Electrical Circuit}
 \end{array} \right]
 \end{array}
 =
 \begin{array}{c}
 \text{Objectives} \\
 \left[\begin{array}{c}
 \text{Mechanical System} \\
 \text{Hydraulic System} \\
 \text{Electrical System}
 \end{array} \right]
 \end{array}$$

5.2 Schematic Layout of the Machine Set-up

The machine set-up comprises of the following major units:

- Main body
- Grinding wheel mounting unit (Cathode)
- Workpiece and vice (Anode)
- Kinematic arrangement for feeding workpiece
- Hydraulic control unit
- Electrolyte supply, control and measurement unit
- D.C source
- Force recording unit (Dynamometer & accessories)

A schematic layout of all these above units has been represented as follows:

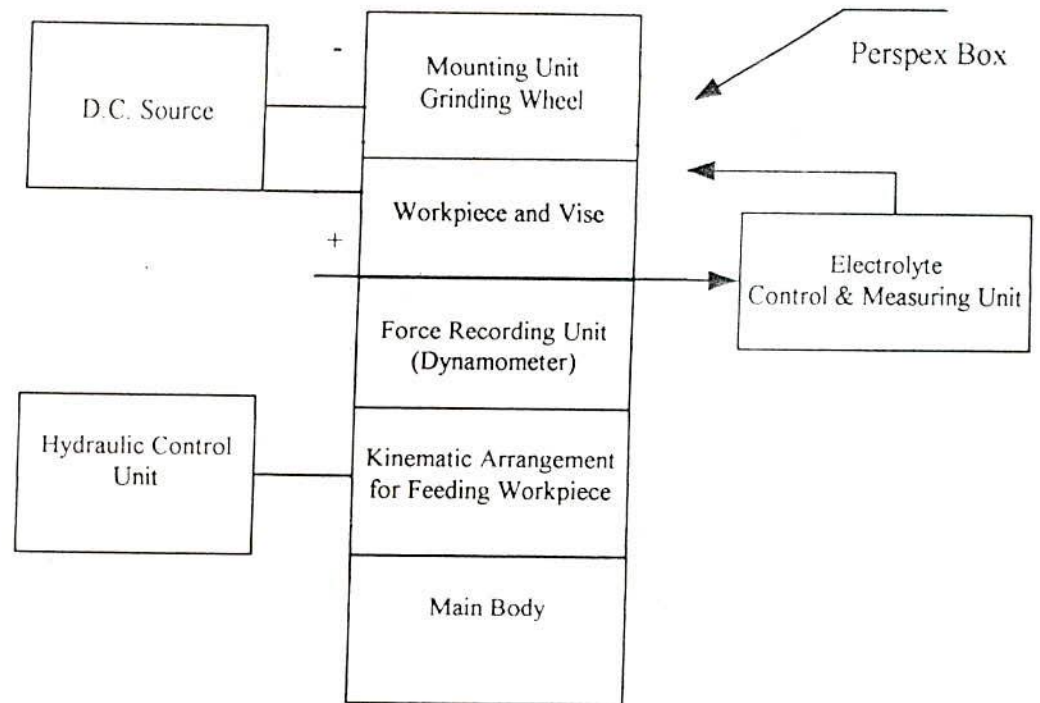


Figure 5.1 Schematic Layout of Electrochemical Grinding Machine

5.3 Principle of Operation

Principles of the electrochemical grinding process are relatively very simple and straight forward, have already been elaborated earlier. To summarise, the basic principle of metal removal by ECG is a combination of

- anodic dissolution of the anode material
- a mechanical abrasive action and
- the removal of oxide films

Since the process is based on electrochemical dissolution, the active components of the process are a cathode (wheel), electrolyte, anode (workpiece) and a DC power source. An electrolyte usually a neutral salt solution is generally directed

into the gap between the two electrodes with the help of a chemical pump set through a non-conductive nozzle. This electrolyte also serves the purpose of completing the electrical circuit. Due to the electrolysis phenomena, the workpiece material becomes soft and metal oxide or hydroxides are formed. The continuous flow of electrolyte flushes away the above unwanted materials from the machining area and prevents it from building up on the work and tool surface.

Generally a low DC voltage of 4 to 10 volts is applied and a high current density is set up in the machining area. The electrolyte causes the machining reactions to occur, and also carries the heat produced during operation. The process has been discussed at length in Chapter 4. The abrasives of the grinding wheel are insulating in nature and they are held by conductive binding material in the wheel. Metal removal will be by simultaneous electrochemical and mechanical abrasive actions.

The main components of the schematic diagram as shown in Fig. 5.2 are the wheel and workpiece, force monitor, a grinding dynamometer, electrolyte pump and flow meter, a DC power supply, reciprocating feed mechanism unit, and hydraulic control unit. The grinding wheel mounted at the end of the spindle in a closed housing, is rotated at 3000 rpm by a DC motor through a belt-pulley system. The induction motor of 3 Φ , 1.5/2 kW/hp, 1400 rpm has been employed for this purpose. For assessing the electric power, an ammeter and a voltmeter are connected to anode and anode-cathode respectively as shown in Fig. 5.2. A properly calibrated tachometer has been used for on-line monitoring the rpm of the wheel. The motor current is monitored by an ammeter.

The electrical connections have been made as shown in the schematic diagram of the set-up. Dynamometer provides an indication of force produced during cutting operation. Since the force developed during machining operation is small, an operational amplifier of high gain has been used to record the force which is described in Article 5.5.

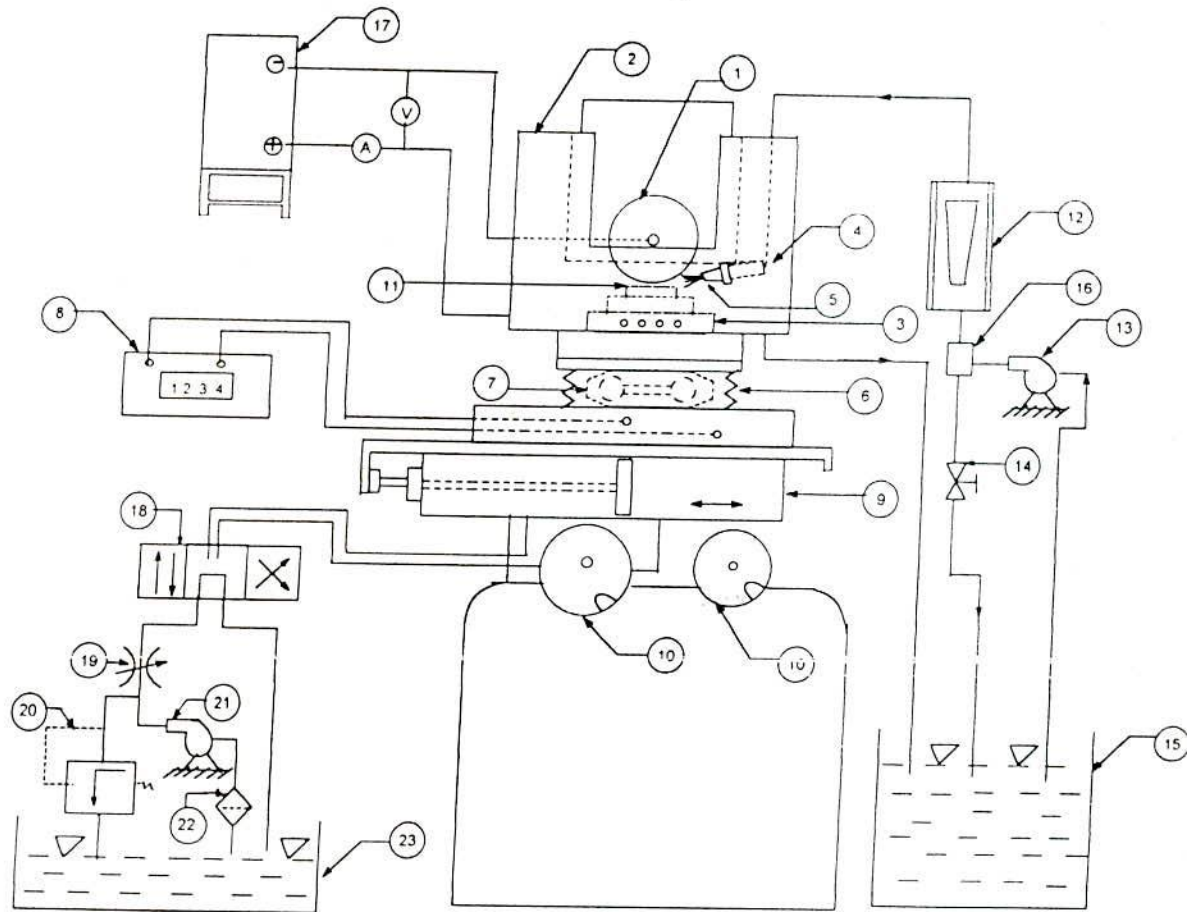


Figure 5.2 Schematic Diagram of Experimental Set-up for ECG

LEGEND

| Item | Name | Item | Name |
|------|------------------------|------|-----------------------------|
| 1 | Grinding wheel | 14 | Bypass valve |
| 2 | Perspex box | 15 | Electrolyte tank |
| 3 | Vise | 16 | T-Elbow |
| 4 | Nozzle | 17 | D.C source |
| 5 | Electrolyte | 18 | 4/3 Direction control valve |
| 6 | Bellows | 19 | Flow control valve |
| 7 | Dynamometer | 20 | Pressure relief valve |
| 8 | Force recorder | 21 | Hydraulic pump |
| 9 | Hydraulic cylinder | 22 | Filter |
| 10 | Hand wheel (graduated) | 23 | Hydraulic oil tank |
| 11 | Workpiece | V | Voltmeter |
| 12 | Rotameter | A | Ammeter |
| 13 | Electrolyte pump | | |

5.4 Development of Hydraulic and Electrolytic Circuits

5.4.1 Cylinder and Piston

For the development of experimental set-up, an obsolete grinding machine has been retrofitted with the hydraulically operated system. The criteria of determining the type and dimensions of the hydraulic cylinder are the functional requirements, space availability and accommodation feasibility. In the present arrangement, the piston and cylinder has been designed, constructed and accommodated into the space between the work table and cross slide casting. The hydraulic fluid control circuit enables to reciprocate as shown in Fig. 5.3. Since there was no available space in the existing system, the body of the machine has been suitably machined to a desired dimension to accommodate the cylinder-piston arrangement so that it can operate smoothly without any interference with other systems.

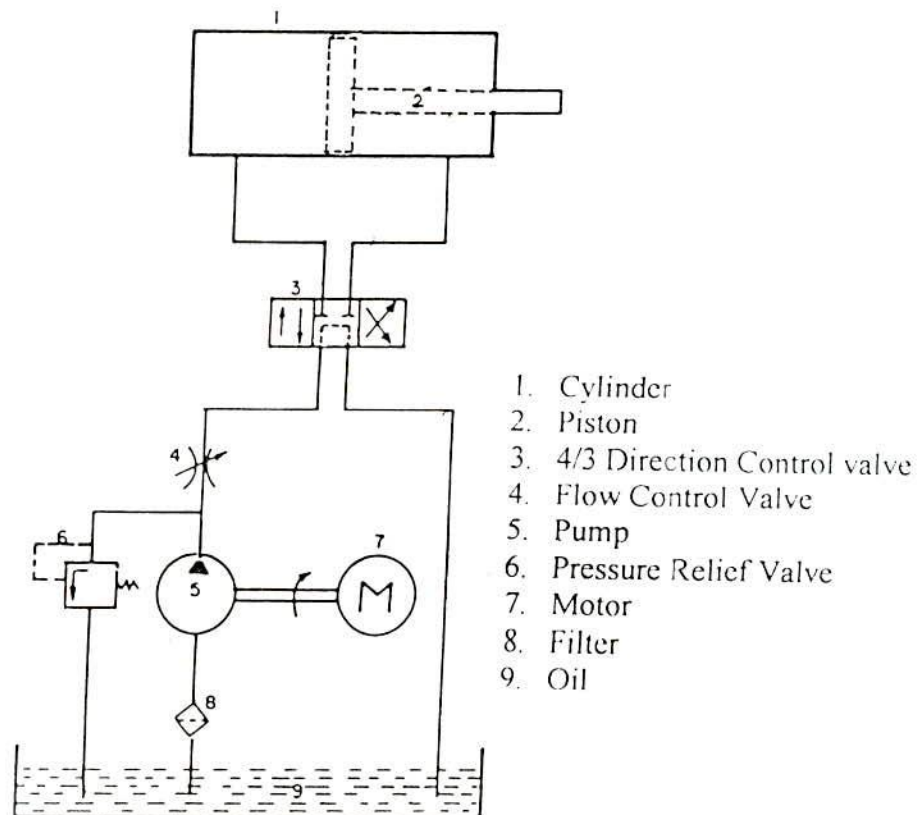


Figure 5.3 Hydraulic Circuit for Feed Control

Calculation of Load

In the existing system (after removing the pulley), the available longitudinal gap for the cylinder is 530 mm, where as, in the previous system the gap was 350 mm only. So the total length of the cylinder is considered as 525 mm. And the available space for placing the cylinder is 34 mm, that means, the maximum diameter that can accommodate is 34 mm.

For designing the cylinder and piston, the load required for the reciprocating movement of the table is 1050 N (refer A5.1 and A5.2). Keeping the above load in view, and the availability of the space, and accommodation feasibility, the following dimensions are selected and applied for the design as shown in Fig. 5.4.

5.4.2 Hydraulic Circuit

Hydraulic Fluid Flow

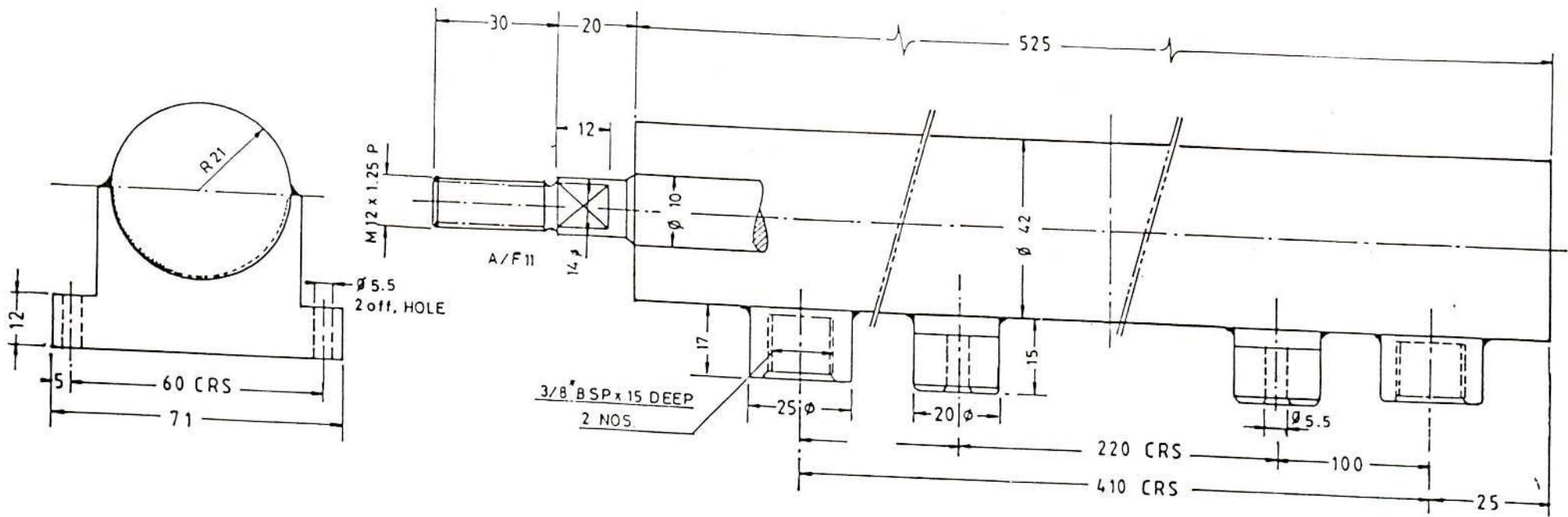
The feed velocity in ECG process is assumed to be around 80 mm/min. Acting area of the hydraulic cylinder on piston side is

$$A_p = 4.91 \text{ m}^2$$

and acting area of the hydraulic cylinder on piston rod side is

$$A_{pr} = 2.89 \text{ cm}^2$$

Hence, the required flow rate is determined as 23.18×10^{-3} lit/min.



TECHNICAL DATA

- 1. BORE - ϕ 25 mm
- 2. ROD - ϕ 16 mm
- 3. STROKE - 330 mm
- 4. W. PRESSURE - 20 BAR
- 5. TESTING PR. - 30 BAR
- 6. PORT SIZE 3/8" BSP
- 7. FOOT MOUNTING

Figure 5.4 Drawing of Hydraulic Cylinder and Piston

Pump Rating

The pump has been selected in such a way that it can develop sufficient fluid flow pressure to overcome the resistance to motion of the worktable smoothly.

Pressure required for the movement of the table =

(force of resistance)/(area on which force of resistance is acting)

So, required pressure of the fluid on piston side, P_p is:

$$P_p = (1050/4.91) = 213.8 \text{ N/cm}^2 = 2.13 \text{ N/mm}^2$$

Required pressure of the fluid on piston rod side, P_{pr} is

$$P_{pr} = (1050/2.89) = 363.3 \text{ N/cm}^2 = 3.63 \text{ N/mm}^2$$

So pump must develop fluid flow of 23.2×10^{-3} l/min at an operating pressure of 3.63 N/mm^2 . Accordingly a positive displacement pump is selected which can develop pressure to an extent of 3.63 N/mm^2 without making any appreciable noise.

5.4.3 Electrolytic Circuit

The electrolytic system is designed in such a manner that it can supply high volume of electrolyte. A nozzle is also used to ensure proper wetting action of the wheel and workpiece. The rotation of the wheel carries the electrolyte into the area of contact between wheel and workpiece ensuring that sufficient electrolyte is present to permit the process to proceed. Electrolytes are to be selected to enable faster formation of oxide films on the positively charged workpiece.

The electrolytic circuit consists of an electrolyte tank, flow meter, pump and nozzle etc. A centrifugal pump (r.p.m = 2800, voltage = 12.5V, current = 0.7A, output = 60W/ hp, single phase) is used to pump the electrolyte to supply continuously between the wheel and workpiece through the nozzle as shown in Fig. 5.2. The flow rate is controlled by two sets of valves, one for bypass line and the other for the main

supply purpose. For monitoring the flow rate, a properly calibrated flow meter (rotameter) is mounted at suitable positions.

The method of achieving the flow of electrolyte in the gap between the wheel and the workpiece is critical. The most common method of applying the electrolyte is with a suitable nozzle properly placed behind the wheel with respect to the feed direction and rotating the wheel in 'up cut' direction. The wheel rotation in this arrangement aids the flow of electrolyte into the gap.

5.4.4 Feed Mechanism

The kinematic system for very slow feeding of the workpiece radially against the grinding wheel consists of a screw nut driven slide and guide. The reciprocating movement of the table is controlled by the directional control valve, relief valve and pressure relief valve. The overall arrangement is shown in Fig. 5.3. The workpiece placed on the vice is connected to the positive terminal, which is fed by the reciprocating action of the system through the direction control valve. The workpiece is inserted into the groove of the vice mounted on the reciprocating table. The feed motion is given by the hydraulic circuit as mentioned earlier in Section 5.4.2. The machining operation is done for a pass at constant feed force so that the feed force can be varied by changing the speed of the reciprocating table.

5.5 Electronic Device for Force Measurement

A linear operational amplifier (OP Amp.) has been designed and fabricated which is used as a force measurement digital display unit, calibrated to an accuracy of 0.04 mV/N to measure directly the radial and feed force components. Fig.5.5 shows the amplifier installed in the system.

The dynamometer for the two axes viz. vertical and horizontal, has two 4 arms strain bridges. The value of each arm is 120 ohm. Bridge balancing circuits are also used. To minimise the interference each channel is powered independently. The

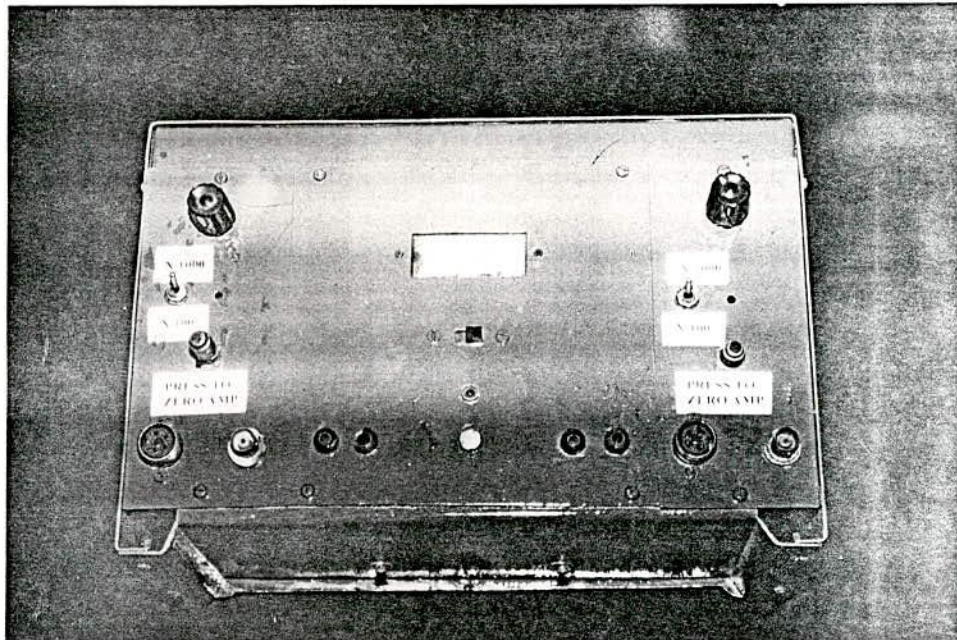


Figure 5.5 The Linear Operational Amplifier

bridge supply voltage is 6 volts, temperature compensated reference (LM 329) and low drift op- amp (OP 07E) are used. To provide reasonable high gain (in the range of 100-250) and drift free operation, AD524 instrument amplifier has been used as bridge amplifier. Offset adjustment of this amplifier is also provided. The output of each amplifier can be monitored through a DVM (LCD DISPLAY 1 volt full scale). The individual channel output is also been provided for recording purpose.

The transformer T_1 and the four diodes along with capacitor C_1 and C_2 provided ± 12 volts which are regulated by V_1 and V_2 giving ± 9 volts. U_1 provided the stable reference U_2 along with Q_1 which provides a constant voltage to power the bridge. Switch S_1 is used to adjust the offset of U_3 , whereas, switch S_2 is used to change the amplifier gain.

The following diagram (Fig.5.6) shows the operating connections of the amplifier.

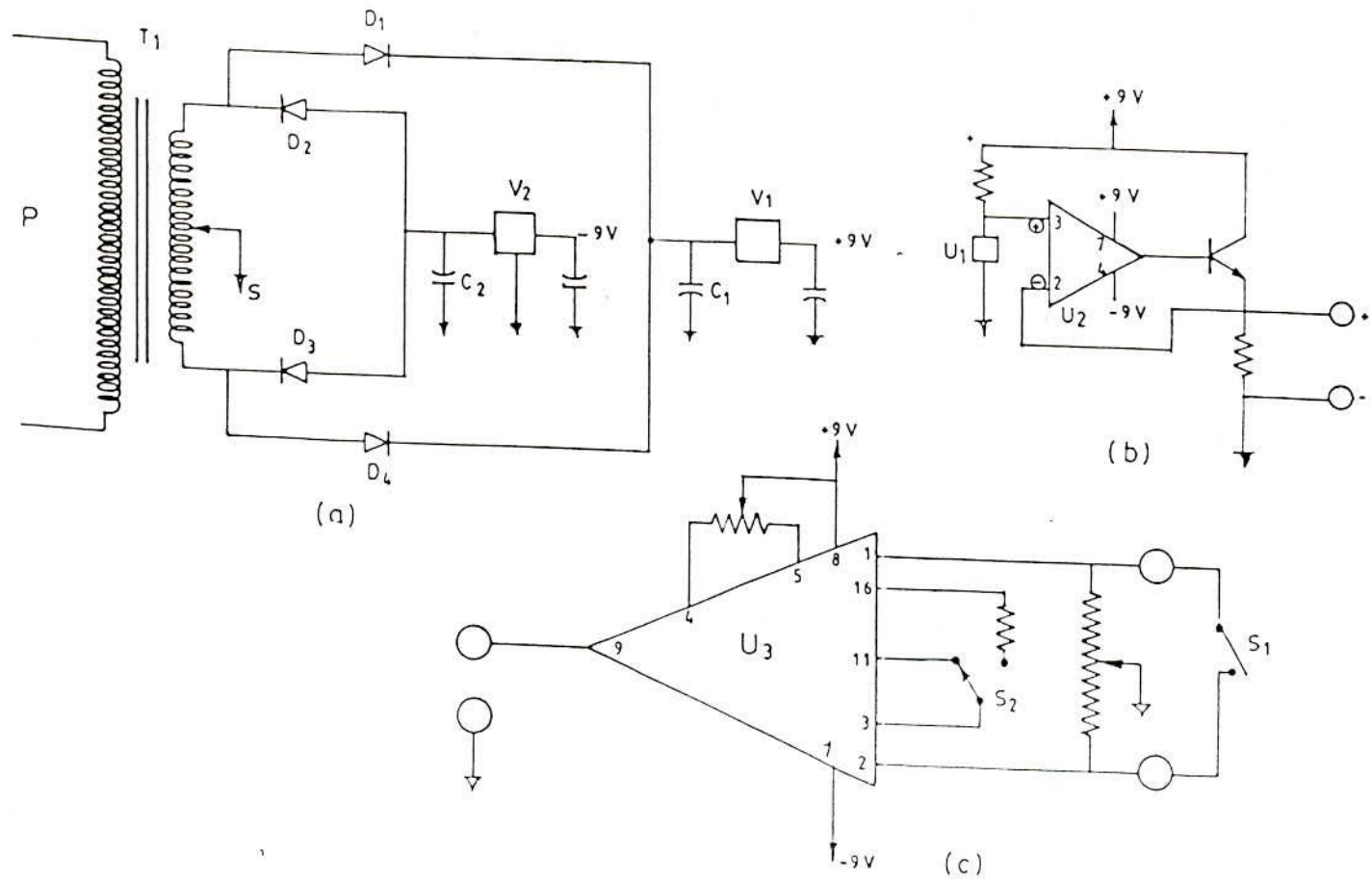


Figure 5.6 Circuit Diagram of the Amplifier

5.6 Design, Construction and Calibration of Dynamometer

5.6.1 Introduction

In case of electrochemical grinding process, different forces are acted upon the workpiece and the machine tool (grinding wheel) under a given set of cutting conditions. The measurement of cutting forces may be ascertained

- by direct power measurement
- by calorimetric methods or
- by suitable tool force dynamometers

Two components of force namely radial and feed forces are measured with the help of a grinding dynamometer developed. Normally, the dynamometer forms a link between the work and machine bed in ECG process. An octagonal extended ring type dynamometer has been designed, constructed and calibrated for measuring two components of forces. Completely circular rings are not considered because they have a tendency of rolling under the action of cutting forces. Octagonal rings are used to avoid the rolling tendencies. Keeping the essential requirements of a good dynamometer in view, stainless steel is chosen as constructional material. Besides the above, the speciality of the stainless steel is its non-corrosiveness which is very much essential for ECG process. On the surface of the dynamometer, strain gauges are cemented. The two terminals of the strain gauges are fitted to an arm of a Wheatstone bridge circuit.

5.6.2 Design Calculations

The essential requirement of the dynamometer used for ECG is its sensitivity to measure the grinding forces with sufficient accuracy. The design is based on (i) Conventional size to handle (ii) Accuracy of measurement (iii) Provision for modifications (iv) Provision for change of parameters (v) Mechanical loading (vi) Sensitivity.

Many researchers [82,101] suggested that the dynamometer should possess the following characteristics:

- i) It should be simple in design and easy to handle and vice versa.
- ii) It should be rigid enough so as not to give rise to vibrations at least within the operating range.
- iii) It should be sufficiently elastic so as to give an appreciable deformation on all bodies. Its measuring element should be sensitive and should be free from cross-effects so far as possible. That is, an applied force in the x direction should give no reading in the y or z direction.
- iv) It should be unaffected by humidity and temperature variations.

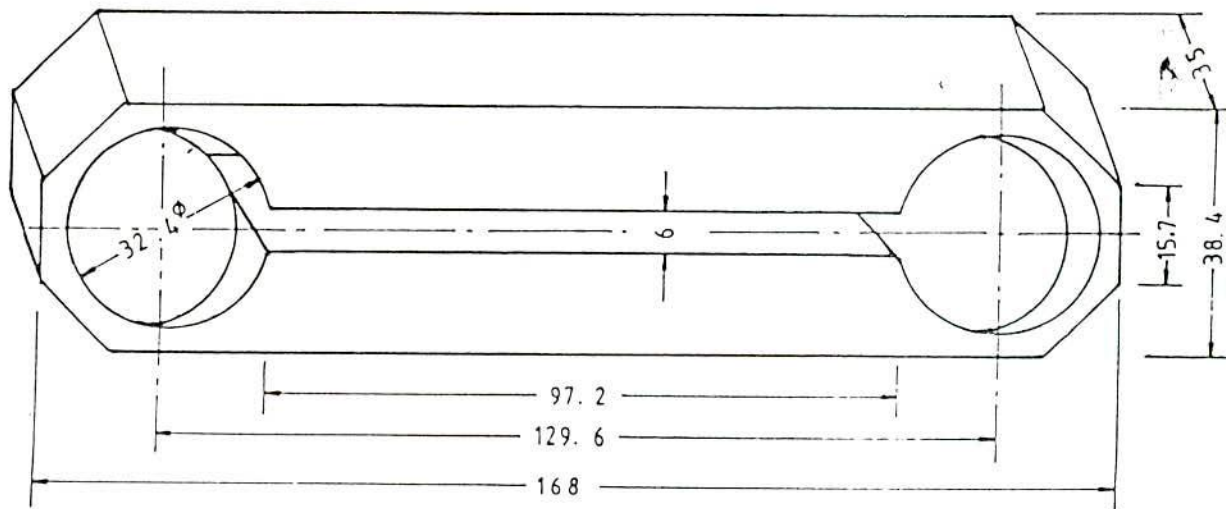
The common feature of all types of dynamometers is the measuring deflections produced during cutting operation. These deflections are proportional to the cutting forces. The major difference in the design of different types of grinding dynamometers lies in the technique employed for measuring the elastic deflection.

For designing the dynamometer, some assumptions have been considered such as, the width of dynamometer is about half of the width of the vice, the minimum load conditions neglecting the cross-sensitivity of strain gauges, and the two octagonal rings are of identical shape and size so that it can carry equal loads.

The total minimum load has been found to be 183.7 N (refer Appendix A5.3). Similarly, considering the wheel and electrolyte pressure, for maximum value, the total load would be calculated as 473.5 N. The thickness of the dynamometer and the arm length of octagonal ring edge have been determined as 3 mm and 15.7 mm respectively (refer Appendices A5.4 and A5.5).

5.6.3 Fabrication

All the fabrication works are performed in house. A rectangular stainless steel block is roughly made by a shaper for maximum stock removal, and a vertical milling machine is used to get the desired size as per drawing shown in Fig. 5.7. In making the octagonal rings, first of all two holes are drilled by radial drilling machine followed by boring operation. The stainless steel block is cut into an octagonal shape with the help of a vertical milling machine. The slit between the two horizontal members is made using a slitting saw in column and knee type horizontal milling machine. Finally, all the surfaces are ground and polished. Two blind holes are made on the dynamometer to fit with the vice by nut-bolt system.



(All dimensions are in mm)

Figure 5.7 Designed Dimension of the Dynamometer

5.6.4 Mounting of Strain Gauges

Considering the factors like environment, space availability, extent and type of deformation and the desired life of gauges, strain gauges are cemented. The scales, rust, grease or any type of contamination of the measuring surfaces are removed and

cleaned with chemical agent. The bottom surface of the gauge is cleaned by cotton wool soaked in acetone and a thin layer of cement is applied on the back of the gauge by means of soft brush. The corners are also covered with cement. The test surface is then coated with a thin adhesive layer (Bakelite adhesive) with a suitable hair brush. It is kept about 10 minutes to dry in open air. The strain gauges of Bakelite type (refer Appendix A5.7) are put on the prepared surfaces of the ring in proper direction as shown in Fig.5.8.

The blotting paper, foam, and small wooden block are put against the body and a load of about $\frac{1}{2}$ kg is applied for few hours for proper cementing. The weight and cushions are removed after drying. The resistance of the gauge is checked. When strain gauges are cemented, they are connected to lead wires to form the required bridge for measurement (Fig. 5.9) and the connections can be seen from the photograph as shown in Fig.5.10.

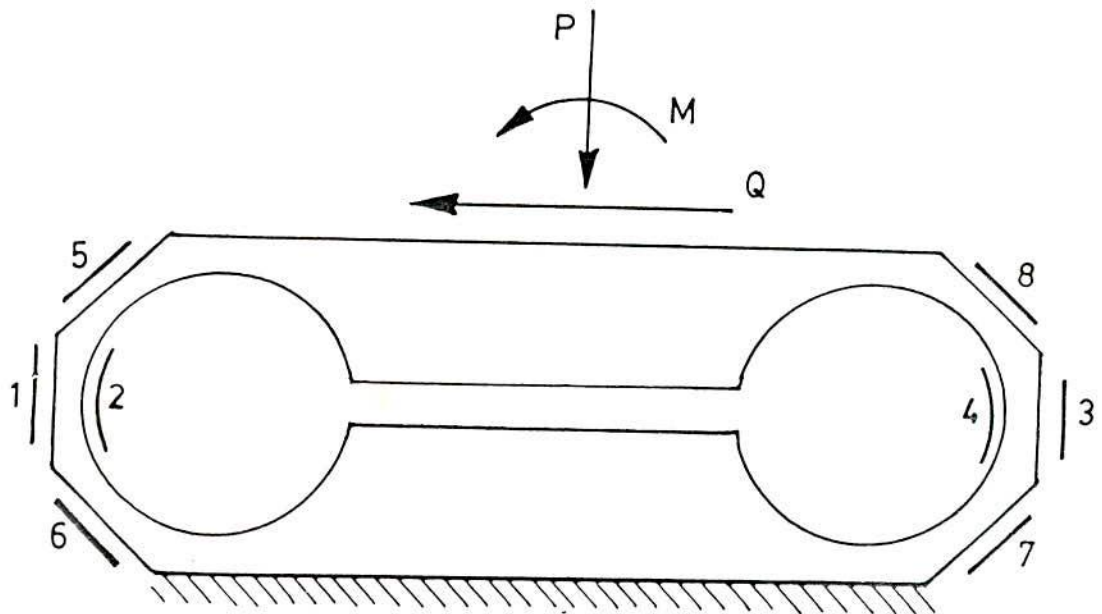
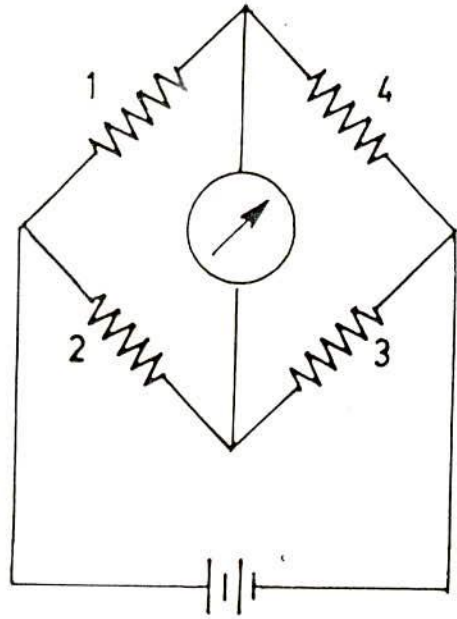
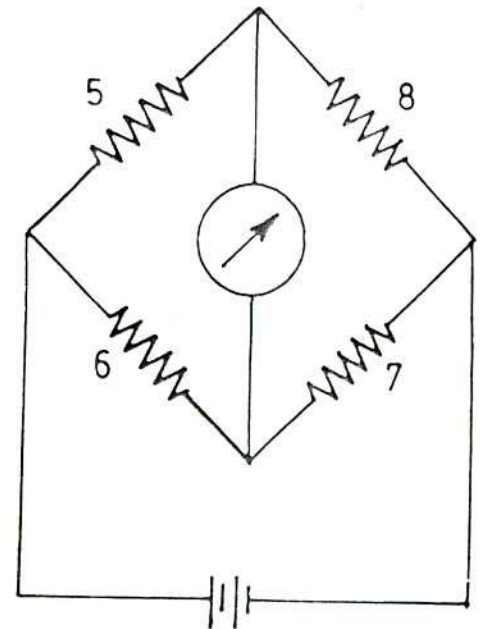


Figure 5.8 Grinding Dynamometer Showing the Position of Strain Gauges



(a) Bridge Connections for Measuring Vertical Force



(b) Bridge Connections for Measuring Horizontal Force

Figure 5.9 Bridge Connections

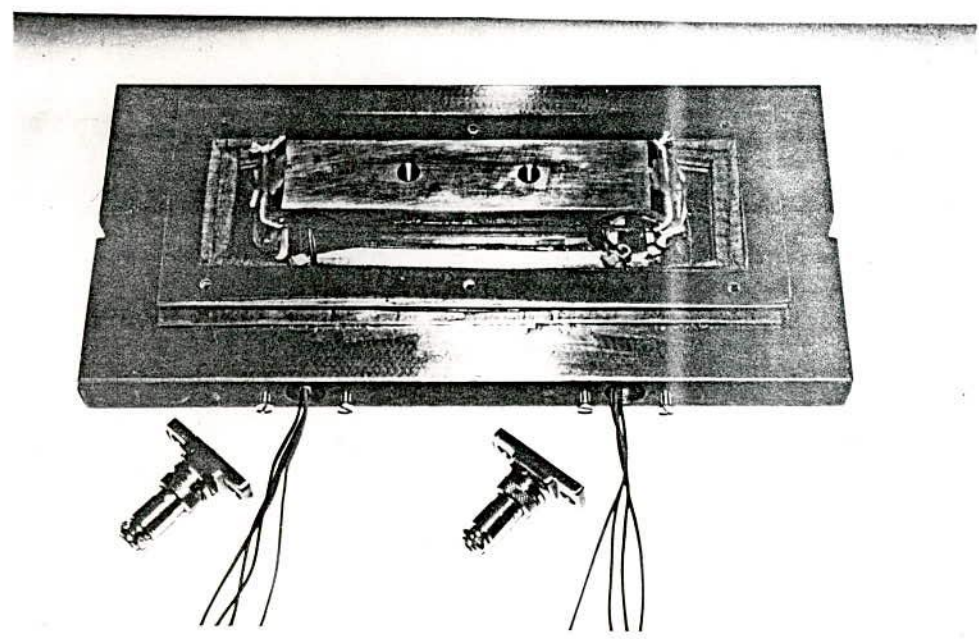


Figure 5.10 Strain Gauge Connections

5.6.5 Calibration

Generally the construction of the dynamometers are different depending on the purposes. Various equipments are used for the calibration of the dynamometers. Some precautions are to be taken to eliminate the error due to influence of temperature and other human errors. The aim of the calibration is to obtain the calibration curves. Force transducer is to be calibrated at regular interval.

The dynamometer has been calibrated by applying dead loads in vertical and horizontal directions and observing the corresponding meter readings. For the calibration of dynamometer due to vertical load, dead loads are applied from 1 to 15 kg in step of 1 kg (9.81N). The cycle of loading is done by increasing the load and then decreasing in same steps. Corresponding meter readings in milivolt are recorded. This process has been repeated for ten times. For each step loading, average of ten readings is taken to plot the calibration curves. The same method has been followed for the calibration of dynamometer for horizontal load. The curves are shown in Figs.5.11 and 5.12. The meter readings recorded for the calibration curves are provided in Tables A5.1 and A5.2.

The equations of calibration curves for horizontal and vertical loads have been determined as follows:

$$\text{Horizontal : Meter Reading} = 0.186905 \times \text{Applied Load} + 0.7271714$$

$$\text{Vertical : Meter Reading} = 0.417468 \times \text{Applied Load} + 0.880476$$

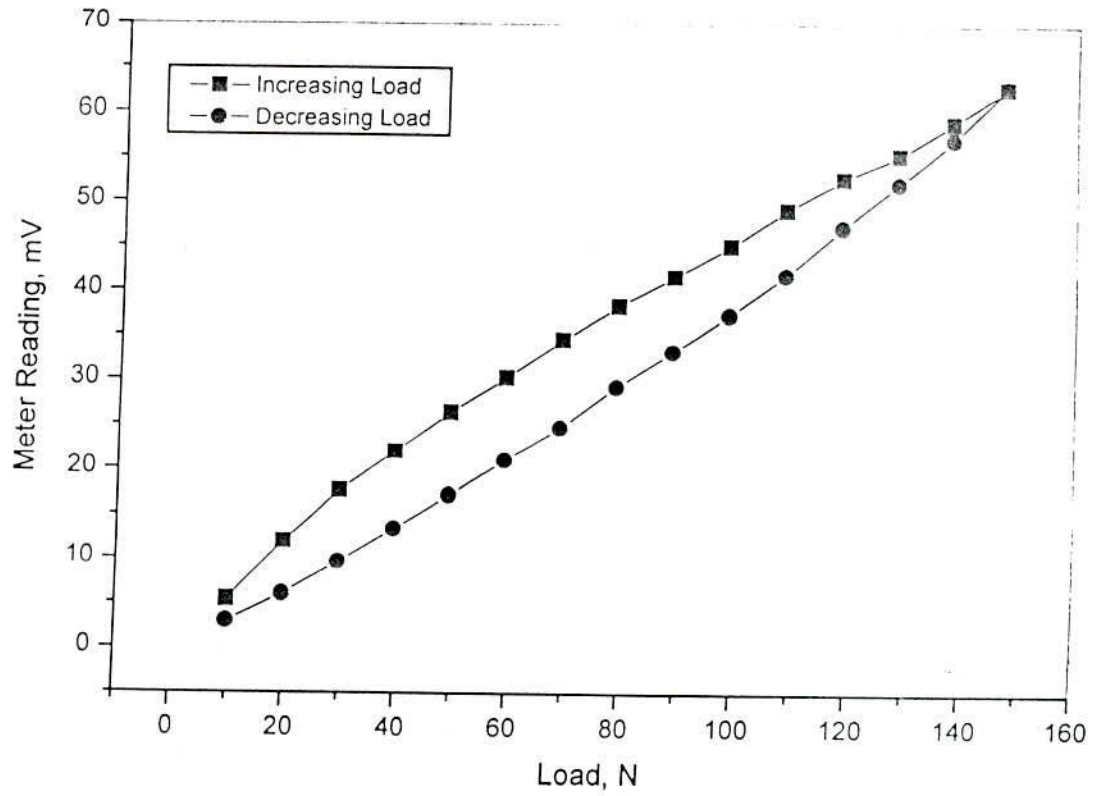


Figure 5.11 Calibration Curves for Horizontal Load

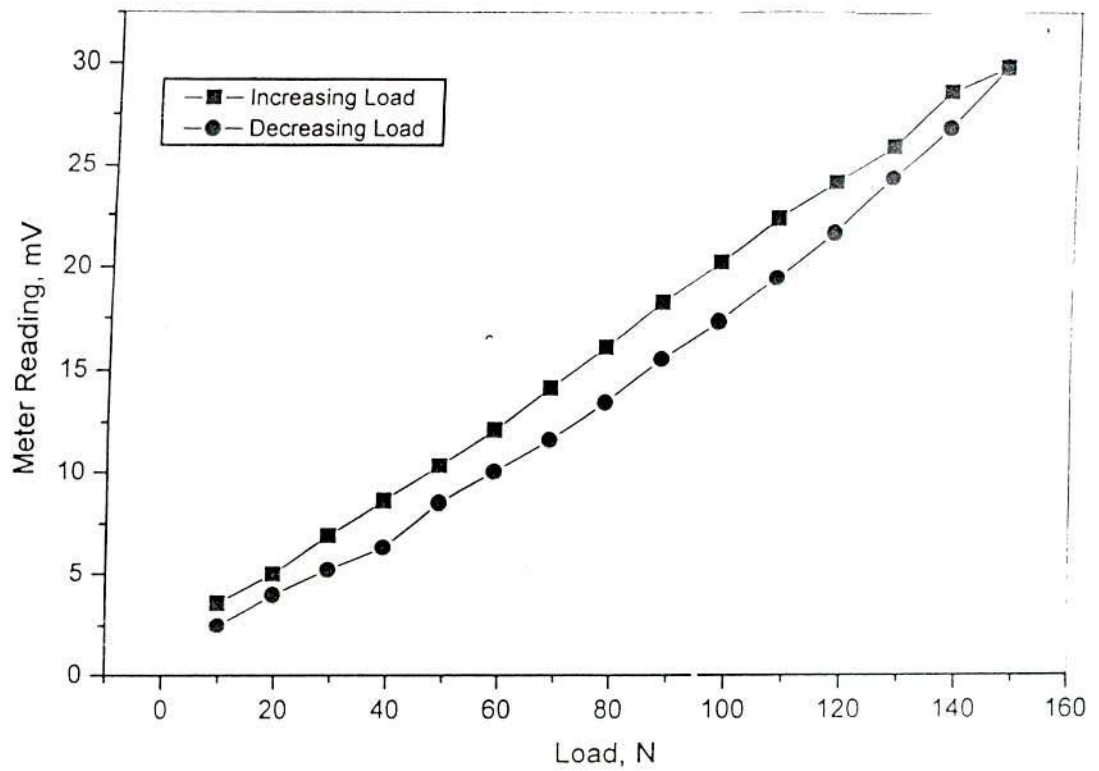


Figure 5.12 Calibration Curves for Vertical Load

5.6.6 Summary

The dynamometer, designed and fabricated, works successfully in machine set-up. From the above discussion it is found that the thickness of the dynamometer is 3.0 mm when the strain value becomes 8.7×10^{-7} . And the sensitivity of the dynamometer is found to be satisfactory. Though the deflection due to minimum load is very small, 6mm gap has been considered for the design. From the calibration and performance test of the dynamometer, it can be concluded that the dynamometer is simple, robust, and convenient for use and calibration. No noticeable cross effect is observed between the two components of the dynamometer.

The calibration curve shows that strain varies more or less linearly with both vertical and horizontal components of forces, and facilitates interpolation of intermediate ranges.

5.7 Development of the Experimental Set-up

The experimental set-up has been built up through the modification of an obsolete mechanically operated surface grinder. The table movement due to mechanical action has been modified for hydraulic control. The existing electrical connections except the motor connection have been removed. The hydraulic cylinder-piston arrangement has been fitted to the frame. For this, the upper portion of the working table has been sized so as to accommodate the cylinder-piston. The cylinder has been placed on the base of the machine and fitted by Allen bolts. The connecting rod of the piston has been fastened with the working table with the help of bracket and adjustable nuts so that the table can move along with the movement of the piston rod. The table feed has been so designed that, there is no slip-stick effect on the table or slides when motion is slow.

The PVC high pressure pipes are connected with the different operating valves (SS) of the system as shown in Fig. 5.3. Direction control valves are employed to determine the routine of fluid in the hydraulic system. These are classified by the

number of positions and ways or ports in the valve body.

A cast iron rectangular block (305x152x25mm) has been fitted with the working table base by means of T-bolts and nuts, on which the dynamometer is placed to adjust the height. The upper portion of the dynamometer was fitted to the MS plate (460x200x10 mm) by two bolts. A perspex box is fixed on that plate which acts as an electrolyte container. A job holding vice of stainless steel has been set inside the box in such a way that the centre line of the dynamometer and vice lie in one plane. Provisions for connecting wires for dynamometer to the force measuring unit are made by thorough holes (hermetically sealed) through cast iron block. The dynamometer has been rigidly mounted to the machine bed and accurately aligned to main axis. A hand made rexin bellows has been introduced in the system that covered the dynamometer to protect it from any type of outside dirt and fluid. Fig. 5.13

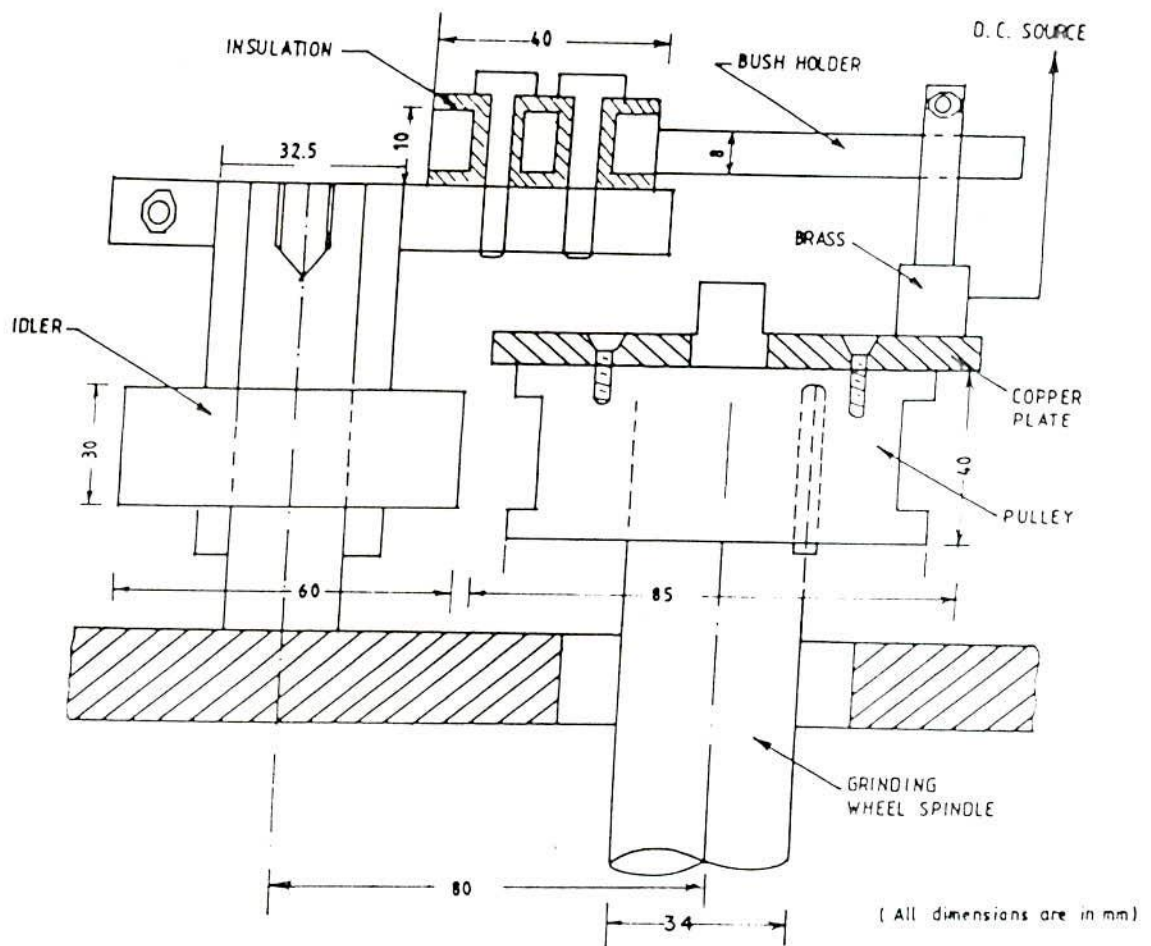


Figure 5.13 Fabricated Parts and the Connections Tapped for D.C. Source

represents the fabricated parts and the connections tapped for D.C. source. The orthographic views of different elements attached to work table of the experimental set-up are provided in Fig. 5.14. The complete experimental set-up is shown by photograph as shown in Fig. 5.15.

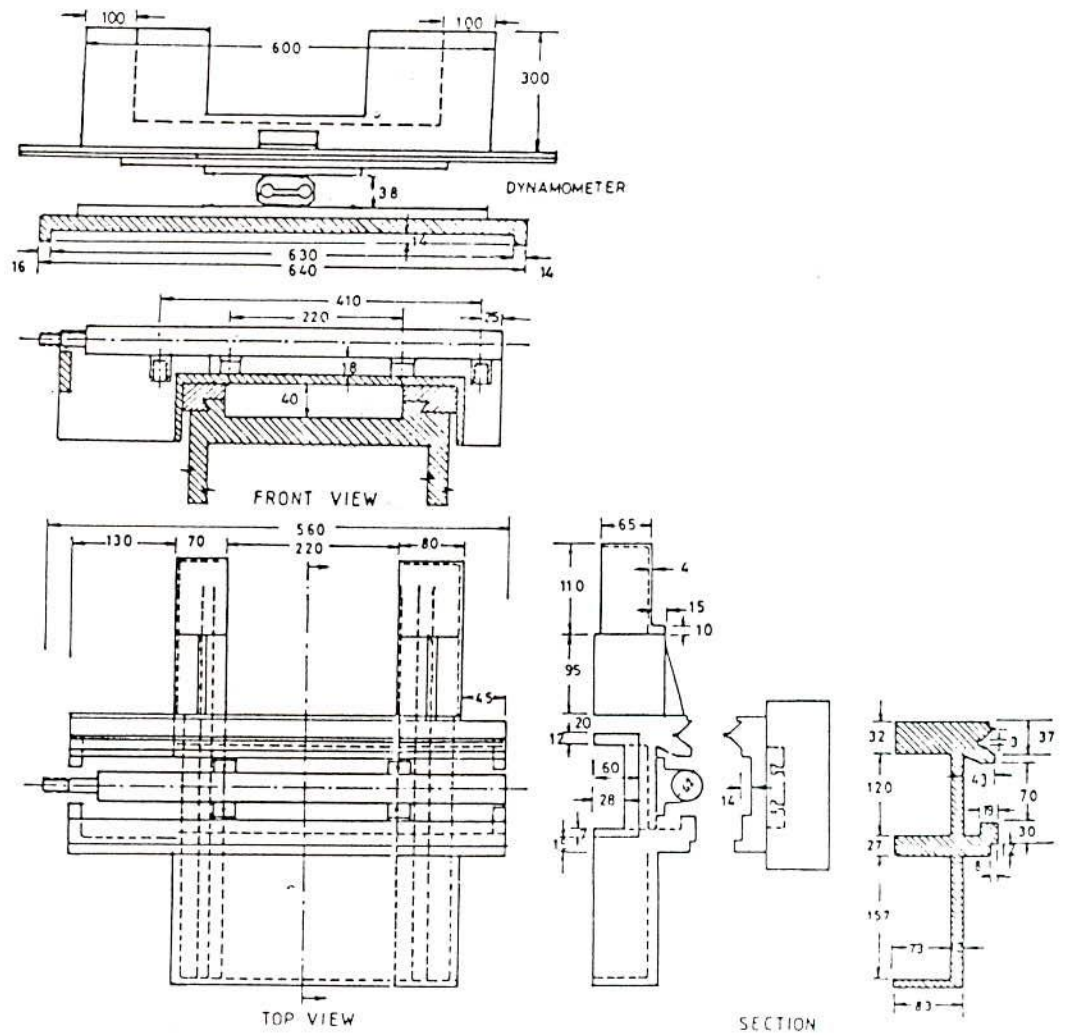


Figure 5.14 Orthographic Views of Different Elements Attached to Work Table

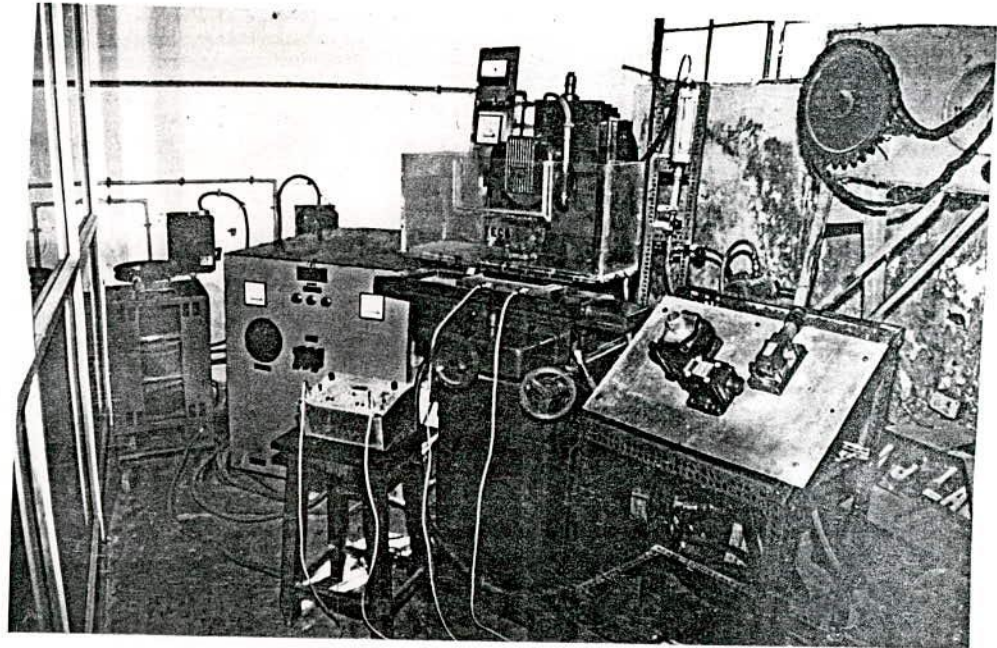


Figure 5.15 Experimental Set-up

5.8 Conclusion

All the parts and units have been assembled in such a compact manner that it occupies a very less space for its placement and its individual part can be disassembled for any modifications or maintenance if necessary. Before mounting of strain gauge the dynamometer has been annealed. A dynamometer has been designed, fabricated and calibrated for measuring radial and feed forces. The design, fabrication and calibration of the dynamometer provide force measurements. The amplifier provides the accuracy of measurements of forces. In a nutshell, the above work contributes a success in the development of an ECG machine. Regarding the working performance of the machine, it can be concluded that it works satisfactorily even under any extreme working condition. A very negligible cross-sensitivity in the strain gauge connections has been observed, may be due to the following reasons:

- i) Inaccurate positioning of the strain gauges,
- ii) Inherent transverse sensitivity of the gauges,
- iii) Slight (with tolerance) difference in G.F. and resistance of the gauges, and
- iv) Anisotropy of the material of the dynamometer

It may be commented here that the nonconventional machining techniques will never eliminate the existing methods but on the other hand, will improve the flexibility in the machining technique to meet industrial improvements.)

CHAPTER - 6
EXPERIMENTATION

CHAPTER 6

EXPERIMENTATION

6.1 Introduction

To study the performance of the electrochemical grinding machine, fabricated in-house and to determine the effect of different process parameters on material removal rate, surface finish, and feed force, different sets of experiments are carried out. A force recording device with built-in transducer and amplifier has been designed and fabricated.

Before doing the experiments, the dynamometer has been calibrated for feed and radial forces during ECG operation. The main objectives of the experimental studies are to analyze the behaviour of the electrochemical and mechanical material removal mechanisms and to corroborate analytical models developed for material removal rate. An attempt has also been made to ascertain the feed force required for the operation of the ECG process and that must be very less than that of the conventional grinding process. The comprehensive experimental studies involve the most important parameters such as electrolyte type and its concentration, DC supply voltage, electrolyte flow rate, feed rate and depth of cut. The various responses of the process parameters such as the current, radial and feed forces during operation, volumetric MRR and surface finish are studied for machining tungsten carbide and stainless steel workpiece materials, because of the increasing use of stainless steel for different types of applications, such as medical instruments, aircraft industry, and tungsten carbide for nozzle and cutting tool materials.

6.2 ECG System Components

6.2.1 Electrolyte Solution

In electrochemical grinding, a suitable electrolyte solution is used depending upon the properties of workpiece material, type of wheel and environmental

condition. Generally, any salt such as sodium nitrate, potassium nitrate, sodium or potassium carbonate etc. mixed with water are used as electrolytes. Strong electrolytes like NaCl solution are used as the main electrolytes in the process. Strong electrolyte means the electrolyte that becomes greatly dissociated for concentrations. The concentration may be varied as desired. Some additives may be added to main electrolyte to increase the material removal rate or to inhibit rust formation. The most efficient electrolyte for ferrous, nickel, and cobalt alloys is sodium chloride solution [11].

This NaCl solution is a very good electrolyte but it is highly corrosive in nature even though it is used. For the experimental work, stainless steel specimen was used and fitted to a vice within a container made of perspex. The concentration and pH value of the electrolyte can be varied by adding water or chemicals to it. Their properties are important due to the fact that they either affect the conductivity of the electrolyte and hence the electrical resistance within the machining gap or electrochemical reaction takes place at the electrode surface. The electrolyte flow distribution in the machining gap is not uniform, so the acidity level on the anode material is not constant. As a result, the electrochemical reaction rate and oxide film thickness vary on the workpiece surface. Also the temperature affects the chemical activity of the electrical resistivity of the electrolyte. Other components such as worktable, dynamometer etc. and sub-systems such as electrical and hydraulic systems etc. are described at length in Chapter 5.

6.2.2 DC Power Supply

The power supply is designed for the electrochemical grinding machine to provide the following characteristics:

- i) The supply DC voltage can be continuously varied as desired (within 0-15 volts),
- ii) When the voltage is set, the amperage can automatically vary so that current density remains constant, and

iii) The current should have a minimum of ripple.

Ripple is a residual AC component of the output voltage (the variation in the current) supplied by DC voltage generator.

A 10 KVA DC power supply (input 440 V AC 3 PH 50 Hz and output 50 V DC 200A max.) is used for the present experimentation and voltage is controlled by a variac.

6.2.3 ECG Wheels (Cathode)

For very hard materials, such as tungsten carbide, the preferred abrasives are diamond or borazon. The grinding wheels generally used at present are: i) metal bonded diamond wheels in surface grinding where high material removal rate is anticipated, ii) aluminum oxide wheels with a bond consisting of mixed of resin and copper powder, or of graphite, for form grinding, and iii) non-grit graphite wheels for both surface and form grinding [97].

The wheel produces an electrolyte pressure and creates the flow velocity in the machining gap for machining operation. If the wheel runs very slowly, the electrolyte can not reach to the machining gap, and on the other hand, if the wheel rotates with too high speed, it will through the electrolyte off the wheel before coming in contact with the wheel-workpiece interface.

In the present experiment, a diamond - impregnated metal-bond wheel, 150 mm in diameter and 9 mm in width is used. The width of the layer containing diamonds is 3mm and the abrasive grit size is 80/100. The spindle rotates at 3000 r.p.m. corresponding to a peripheral speed of 1413 m/min.

6.2.4 ECG Machine

The design and development of the machine has been discussed in Chapter 5. Voltage has been adjusted to maintain constant current. The table movement is made by hydraulic means adjustable by reciprocating motion. The electric current is supplied by power source through brushes on the wheel spindle. Table feeds are allowed so that at low speed there is no slip-stick effect on the table or slides. The grinding wheel is run through a belt pulley drive system. The electrolyte system is equipped with a pump made of teflon which runs at 2800 rpm. This teflon material is chosen for its non-corrosive action.

6.2.5 Workpiece (Anode)

The materials used for the experimental studies are tungsten carbide and stainless steel. The details of their compositions are given in Tables 6.1 and 6.2.

Table 6.1 The Composition of Stainless Steel

| Metal | Symbol | % Weight |
|-----------|--------|----------|
| Carbon | C | 0.10 |
| Chromium | Cr | 15.5 |
| Nickel | Ni | 10.15 |
| Manganese | Mn | 0.66 |
| Iron | Fe | 73.59 |

Table 6.2 The Composition of Tungsten Carbide (GT-20)

| Metal | Symbol | % Weight |
|----------|--------|----------|
| Cobalt | Co | 12 |
| Tungsten | W | 82.6 |
| Carbon | C | 5.4 |

Other features are hardness, 123-1311 HV ; and grain size, 2.42-2.8 μm



Stainless Steel : Stainless steel is the most widely used alloy for its noncorrosive action. This ability to resist corrosion is attributable to a surface chromium oxide film that forms in presence of oxygen. The film is essentially insoluble and nonporous [76]. A minimum chromium content of 12% is essential for film formation, and 18% is sufficient to resist the most severe atmospheric-corrosive environments. Other elements, such as nickel, aluminum, silicon, and molybdenum may also be present. The standard stainless steel grades are divided into three categories such as austenitic, ferritic, and martensitic.

The electrochemical equivalent weight of the workpiece material is essential so far electrochemical grinding process is concerned. In this case, carbon does not exist as ion. So it is not dissolved in the electrolyte solution. Since carbon does not dissolve anodically it should leave the anode mechanically and there is no need to include it in the calculation of electrochemical equivalent weight of the metal. Some elements have more than one valency; for example, in stainless steel. The calculation is made based on the smallest or highest valency involved with each element in the alloy. Table 6.3 presents the calculation provided for each element in its composition. The equations used are as follows:

$$q = \sum_i^z K_i \times q_i \quad \dots 6.1$$

Where,

$$q_i = \frac{\text{Atomic Wt.}}{F \times \text{Valency} \times \text{Density}} \quad \dots 6.2$$

Table 6.3 Calculation Steps for ECE Weight (Stainless Steel)

| Symbol | % Composition | At. Wt. (molar) gm | Valencies | | Density(ρ) gm/cm ³ | ECE wt. of metal removed mm ³ /amp.s | |
|--------|---------------|--------------------|-----------|---------|--------------------------------------|---|--------------|
| | | | Lowest | Highest | | Lowest Val. | Highest Val. |
| C | 0.10 | 12.011 | 2 | 4 | 3.52 | 0.0176 | 0.0088 |
| Cr | 15.5 | 51.996 | 2 | 6 | 7.20 | 0.0374 | 0.0124 |
| Ni | 10.15 | 58.70 | 2 | 3 | 8.90 | 0.0341 | 0.0227 |
| Mn | 0.66 | 54.933 | 2 | 7 | 7.30 | 0.0389 | 0.0111 |
| Fe | 73.59 | 55.847 | 2 | 3 | 7.87 | 0.0368 | 0.0245 |

With regards to the stainless steel, considering the reactions involve smallest valency for each element occurs, the electrochemical equivalent weight of the metal removed becomes $0.03661 \text{ mm}^3 / \text{amp s}$, and $0.02238 \text{ mm}^3 / \text{amp.s}$ for highest valency of each element.

Tungsten Carbide : Tungsten carbide alloys of a given cobalt content become harder, the finer the grain; That is, they are softer and tougher, the coarser the grain. They are harder as well, the lower the total carbon content; and softer and tougher, the higher the free-carbon content. That means the hardness of tungsten carbide alloys decreases with the increase of cobalt content. The changes in physical mechanical properties of WC-Co materials with increasing cobalt content are available in Table A6.1. The electrochemical equivalent weight for tungsten carbide is determined in similar way as described for stainless steel. But in this case, carbon acts as anion (negatively charged) and goes to anode. So carbon is included in calculation of ECE of the metal.

By using Eqns.(6.1) and (6.2), and considering the smallest valency for each element, the electrochemical equivalent weight of the metal removed becomes $0.04719 \text{ mm}^3 / \text{amp.s}$, and $0.02448 \text{ mm}^3 / \text{amp.s}$ for highest valency of each element as shown in Table 6.4.

Table 6.4 Calculation Steps for ECE Weight (Tungsten Carbide)

| Symbol | % Composition | At.Wt (molar) gm | Valencies | | Density gm/mm ³ | ECE Wt of metal removed, mm ³ /amp.s | |
|--------|---------------|------------------|-----------|---------|----------------------------|---|-------------|
| | | | Lowest | Highest | | Lowest Val | Highest Val |
| W | 82.6 | 183.85 | 2 | 4 | 0.01930 | 0.049357 | 0.024678 |
| C | 5.4 | 12.0115 | 2 | 4 | 0.00352 | 0.020740 | 0.010375 |
| Co | 12 | 58.938 | 2 | 3 | 0.00690 | 0.044257 | 0.029505 |

It is obvious from the above results that the element with highest valency provides lower electrochemical action and vice versa.

6.3 Planning of Experimentation.

6.3.1 Experimental Studies

Two sets of experiments have been carried out for two different workpiece materials as discussed below. In the first experimental study, the process variables considered are the type of electrolyte, electrolyte flow rate, electrolyte concentration, supply DC voltage, feed rate, and depth of cut. The discrete variables considered during the experiments are wheel speed, abrasive grit material, grit concentration, grit size. The discrete variables are those variables whose level can not be changed during experiments. The dimension of the workpiece is 75 mm × 9.23 mm. The pH value of electrolyte has been kept within the range of 7.02 to 6.94. The wheel speed 3000 rpm, length of stroke 90 mm, and length of cut 75 mm are kept constant.

For the second experimental study, tungsten carbide has been used as work material of size 85 mm. × 3.2 mm. Some of machining conditions are kept constant ; for example, wheel speed at 3000 rpm, length of cut at 85 mm, and length of stroke at 100 mm. During the experiments, current has been recorded (average value) that appears on the ammeter connected on the electrical circuit as shown in Fig.5.2. The total volumetric removal rate has been found out theoretically by using Eqn. (4.60).

The actual amount of material removed is obtained by gravimetric method using an electronic micro-balance, weighing before and after each run. More information on experimental studies is already mentioned in Chapters 4 and 5. To analyze the effects of desired different parameters on the chosen criteria, and to verify the theoretical models for material removal rate and feed force for electrochemical grinding process, the experimental scheme has been so designed as to affect the proper utilization of the ECG set-up.

The initial shape of the workpiece is maintained flat and smooth to ensure constant current machining operation. The electrolyte used for stainless steel is fresh NaCl solution with 10% concentration. It is selected because it has little or no passive

effect on the work surface. Before starting the experiment, all the connections, joints and other expected leakage points are checked and sealed properly wherever and whenever needed. The hydraulic system is checked and ensured that their connections are made quite satisfactory. After completing the extensive preliminary tests to make sure of the accuracy and repeatability of instruments, main experiments are conducted.

Different experiments are planned and grouped into the following phases for simplicity of the analysis:

Phase I: Performance test of the machine

Phase II: Influence of different variables on MRR

Phase III: Influence of different variables on feed force

Phase IV: Verification of the theoretical results

6.3.2 Process Variables

The following process variables are considered for experimental analysis:

- Feed rate
- Depth of cut
- Voltage
- Electrolyte type
- Electrolyte concentration
- Electrolyte flow

Feed Rate : The feed rate is controlled by controlling the reciprocating movement of the work table. This reciprocation is due to regulating elements (flow control valves) to control either flow or pressure. That has been shown in Fig 5.1 in Chapter 5.

Depth of Cut: Different depths of cut are provided by setting the workpiece by lowering or raising the work table by means of the graduated hand wheel located at the right front corner of the body of the machine.

Voltage: With the help of a variac, the supply voltage is varied as a result of which the flow of current varied during the operation of the process. For an ECG operation voltage is varied from 4 to 20 V.

Electrolyte type: The electrolyte used for stainless steel material is sodium chloride solution. The available sodium chloride salt has been mixed with deionized water to have different concentrations. For tungsten carbide workpiece material the electrolyte solutions used are KNO_3 , NaNO_3 , and NaNO_2 mixed with deionized (less than 10μ mho) water at different concentrations.

Electrolyte Concentration : The concentrations of the different electrolytes used are 10%, 15%, for stainless steel and 5%, 10%, 15% for GT 20, tungsten carbide.

Electrolyte Flow: The electrolyte flow is controlled by regulating the bypass valve, and exact flow rate is recorded from the rotameter provided in the electrolyte circuit. An irregular flow distribution is created due to high feed rate and high depth of cut.

6.4 Details of Experimentation

6.4.1 Performance Test of the Machine

Since the existing electrochemical grinding machine is a modified grinding machine, the performance of different sub-systems and the machine as a whole are studied elaborately. The workpiece is fitted properly with the help of a vice on the work table. Before setting the workpiece sample, the perspex enclosure, constructed for holding the vice and containing the flow of electrolyte, has been checked for loose

connections, and leakage. By allowing the flow of tap water through the nozzle to the position of workpiece on the vice, recirculation is checked thoroughly. The reciprocating movement of the table has been tested by allowing it to move with constant feed velocity. The hydraulic oil, (SAE-30) comes through the hydraulic power pack and controlled by the control station comprises of three major regulating valves such as direction control, pressure relief, and flow control valves as described in Fig.5.11. The cylinder with piston is placed properly so that a reciprocating movement is produced and tested through experiments.

The depth of cut is adjusted by raising the work table with respect to grinding wheel by means of the graduated hand wheel. The motor connections to the grinding wheel is checked and allowed to rotate at its rated speed with the help of a motor and belt pulley system. Current is adjusted with the help of a variac within the permissible limit. The electrolyte flow system is so adjusted that it can flood the workpiece material. Since the width of the workpiece is less than the width of the wheel, transverse feed is not required in these experimental works.

The machining performance has been evaluated with respect to current, metal removal rate, and surface reproduction under the following conditions :

- a) applied voltage : 4-18 V.
- b) feed rate : 2.67-6.67 mm/s.
- c) set depth of cut : 5-30 μm .

Material removal rate has been found out to give a satisfactory result and the surface produced due to electrochemical grinding. The feed and radial forces are recorded by a grinding dynamometer associated with an electronic amplifier.

6.4.2 Influence of Different Variables on MRR

Material removal rate is an important requirement of this process. It depends on the combined effect of electrochemical dissolution and mechanical action rate. For this process,

$$MRR_T = MRR_E + MRR_M$$

Where MRR_T is the total metal removal in the process, MRR_E the contribution by electrochemical removal and MRR_M the contribution by mechanical removal. The major portion of material removal is due to anodic dissolution which depends on current density, and electrochemical equivalence of the alloy

The feed rate influences MRR and cutting time. If the feed rate is high, the cutting time is low, and total volume of material removal is also lower than that of lower feed rate due to lower electrochemical action. However, due to reduction in cutting time total MRR increases. At a particular feed rate, the total MRR depends upon the total volume of metal removed which is mostly determined by the electrochemical action during the grinding operation. When feed rate is slow, electrochemical action is higher and total material removal is higher. Total volumetric MRR increases at high feed rates due to less cutting time provided with faster worktable speeds. To study the independent effect of various process parameters on MRR, the experiments are carried out in such a manner that a particular parameter is varied keeping all other parameters constant. It is also to be noted that some parameters are found to influence other parameters that ultimately influences MRR. For example, effect of flow rate on current density. The details of different process parameters that govern MRR has been illustrated in Section 4.4.

6.4.3 Influence of Variables on Feed Force

Since electrochemical process is a chemical dissolution process no feed force is required for this. Therefore, the feed force is only responsible due to the

mechanical abrasive action and viscous drag produced due to electrolyte pool. Practically no material is removed by chemical action. It is because of the electrochemical grinding reaction, where, only feed force is required to make contact with unmachined material ahead of the wheel. So there is no contribution towards feed force due to chemical action.

Current density increases with the decrease of gap width, and gap width decreases with increase of feed force. The grinding force is increased as the gap becomes smaller, and the abrasives on the wheel tend to remove the oxide layer enabling further electrochemical action. At higher grinding forces, the gap becomes too small. The electrolyte is carried out by centrifugal force and viscous drag of electrolyte present at the cavities formed by the abrasives. The current density is found to increase initially but at higher grinding forces it falls. It also indicates that at high electrolyte flow rate, the feed force does not influence the gap width significantly and hence the current density as well.

During ECG, the abrasives not only rub with the work surface but also scrub the oxide layer from the work surface. Material removal rate is found to increase with feed force and accelerated by increasing the rubbing speed. The intensity of feed force does not play any significant role unless voltage is high. The rate of increase of MRR is diminished with high feed force. From the analysis it is found that feed force is also affected by the followings:

- i) Size of grinding wheel and its speed,
- ii) Workpiece feed velocity,
- iii) Infeed rate per revolution,
- iv) Depth of cut, and
- v) Flow of electrolyte.

6.5 Results and Discussion

This section is divided into two parts. The first part discusses the experimental results with reference to the influence of various parameters affecting them. The second part discusses the theoretical results, and compares them with experimental results. Some experiments are conducted to study the effect of different process variables such as voltage, depth of cut, electrolyte flow rate on current density, MRR, surface finish, and interdependency of the process variables. The results are studied and discussed in the following sections.

The most important parameter that affects the electrochemical aspects of the ECG process is current flow between the wheel and workpiece, determines the decomposition of anode material and MRR due to electrochemical action. There are some other parameters that govern the mechanical aspects of the process. They affect the machining gap, contact area, and width of the job between two electrodes. The electrolyte exposure time depends upon feed rate of the worktable. The grinding force components (radial and feed forces) are due to that feed rate.

6.5.1 Effect of voltage on current density

With reference to the Fig. 6.1 it is obvious that the current density increases rapidly with the increase in voltage, and then increases slowly with rise of voltage up to about 12 volts. With further rise of voltage, the current density increases rapidly and this trend is also observed at different depths of cut. Greater voltage leads to some undesirable effects like sparking and arcing (a sustained arcing will result in surface damage and short circuit), heating of electrolyte and gas evolution.

Fig.6.2. shows that different electrolytes do not affect the voltage and current density relationship much. At a very high voltage i.e. beyond 12 volts, the electrolyte NaNO_2 gives maximum current density compared to other electrolytes for example, KNO_2 and NaNO_3 , and NaNO_3 shows the best.

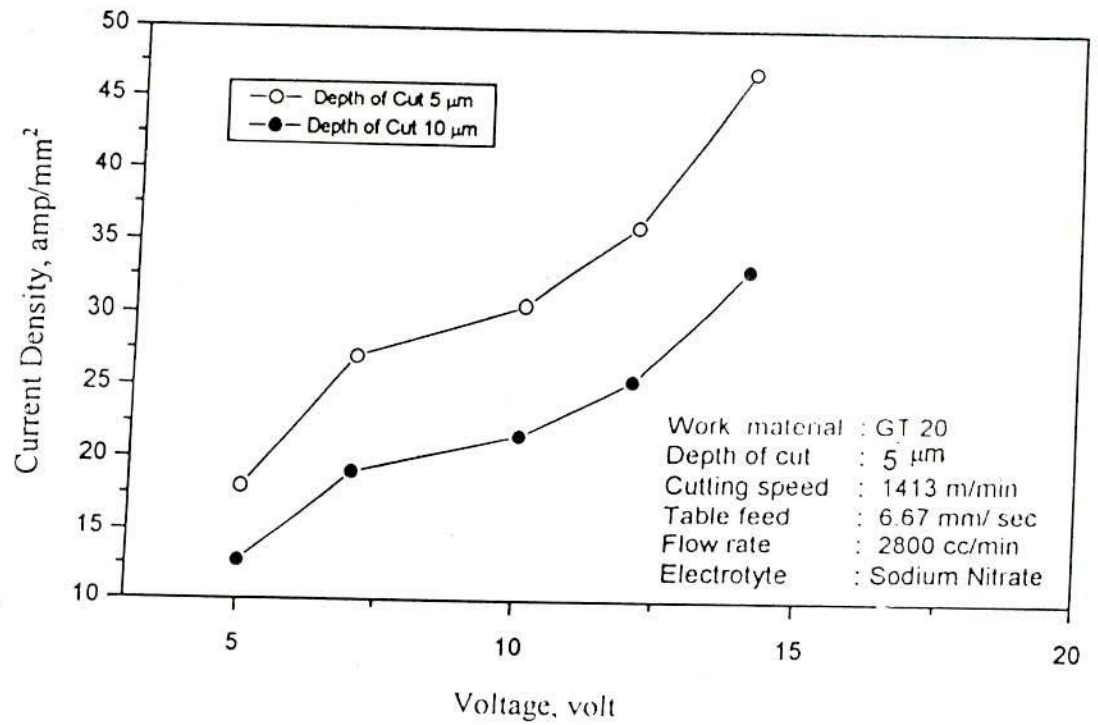


Figure 6.1 Effect of Voltage on Current Density for Different Depths of Cut

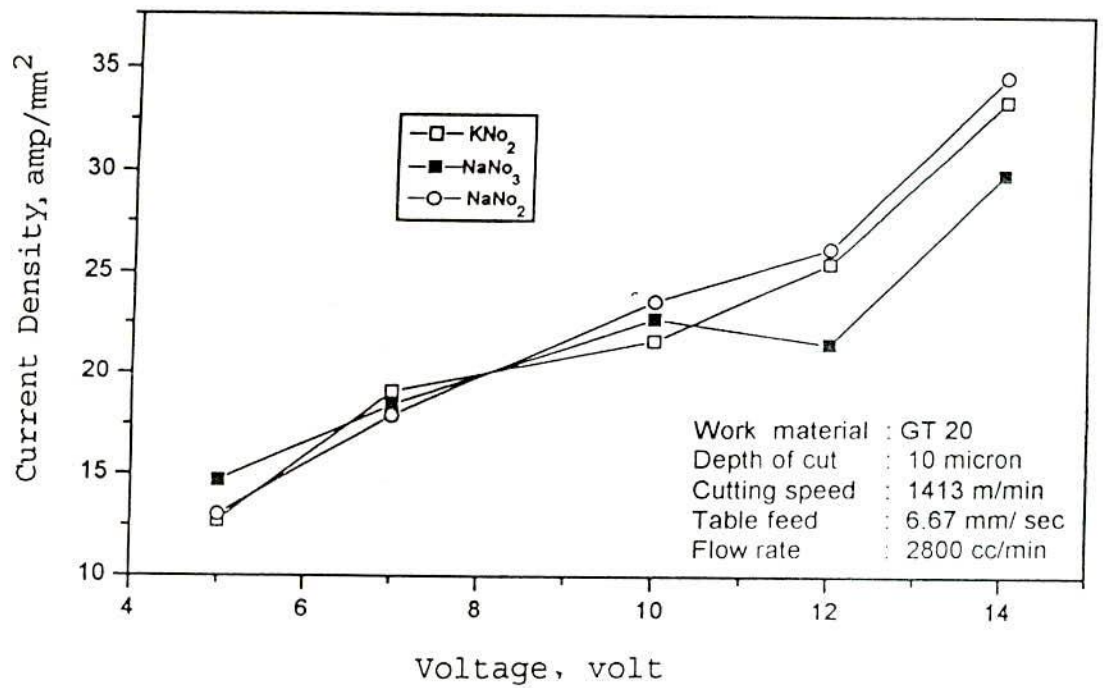


Figure 6.2 Effect of Voltage on Current Density for Different Electrolytes

It is found that the current density increases almost uniformly with the increase in voltage for all values of electrolyte concentrations as evident from Fig.6.3. It is also observed from above figure that at 10% concentration the current density becomes higher in comparison with the concentration of 5% and 15% for different voltages. At a very high concentration, the current density does not increase rather decreases, may be due to passivation. Hence the optimum concentration may be chosen to be 10% by weight.

Dilute electrolytes provide less oxidizing ions resulting in better surface finish, lower electrochemical action, and high MRR. Electrolyte concentration affects MRR (because of current density). It is noticeable that unless the voltage is raised to a certain minimum value of the order 2 to 3 volts, significant amount of current does not flow. This voltage may be considered to be the electrode drops (decomposition voltage).

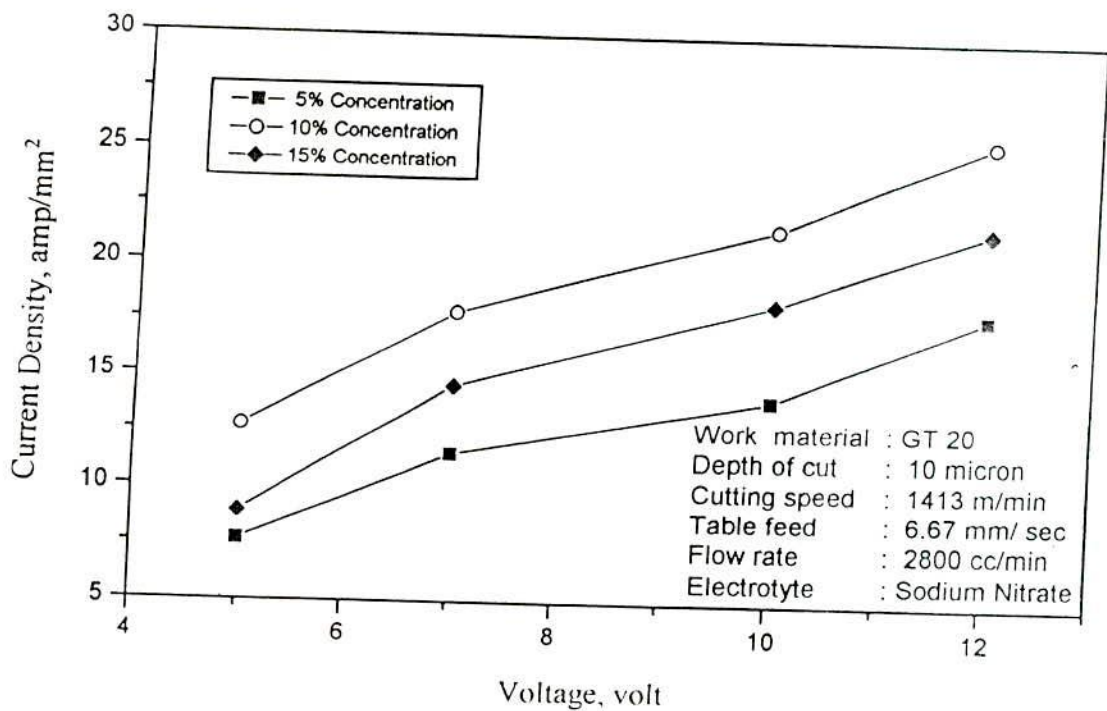


Figure 6.3 Effect of Voltage on Current Density for Different Electrolyte Concentrations

6.5.2 Effect of Current Density on MRR

The experimental values of material removal rate with different current densities are shown in Fig.6.4 for stainless steel. It is compared with the theoretical predicted values for lowest and highest valencies of the elements constituting the workpiece material. It is found that the trend in variation of MRR is more or less similar to the theoretical predicted values. But the actual MRR at different current densities are found to be even less than the lower theoretical values, may be for passivation. However, total removal rate depends mainly on electrochemical removal rate. Material removal due to mechanical action is very low compared to that due to electrochemical action.

The variation of MRR at different current densities for tungsten carbide is shown in Fig.6.5. Material removal rate is found to increase rapidly within current density of 2.1 and 3.1 amp/mm² and then at slower rate with the increase in current density.

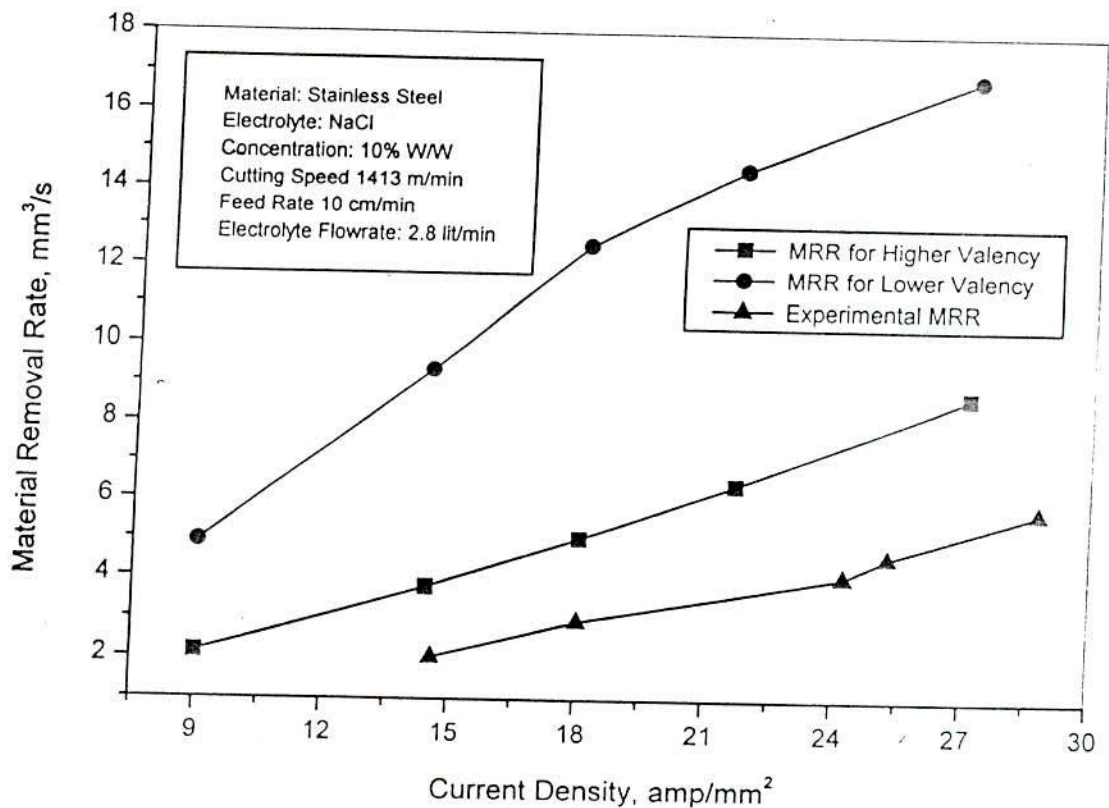


Figure 6.4 Effect of Current Density on MRR (Stainless Steel)

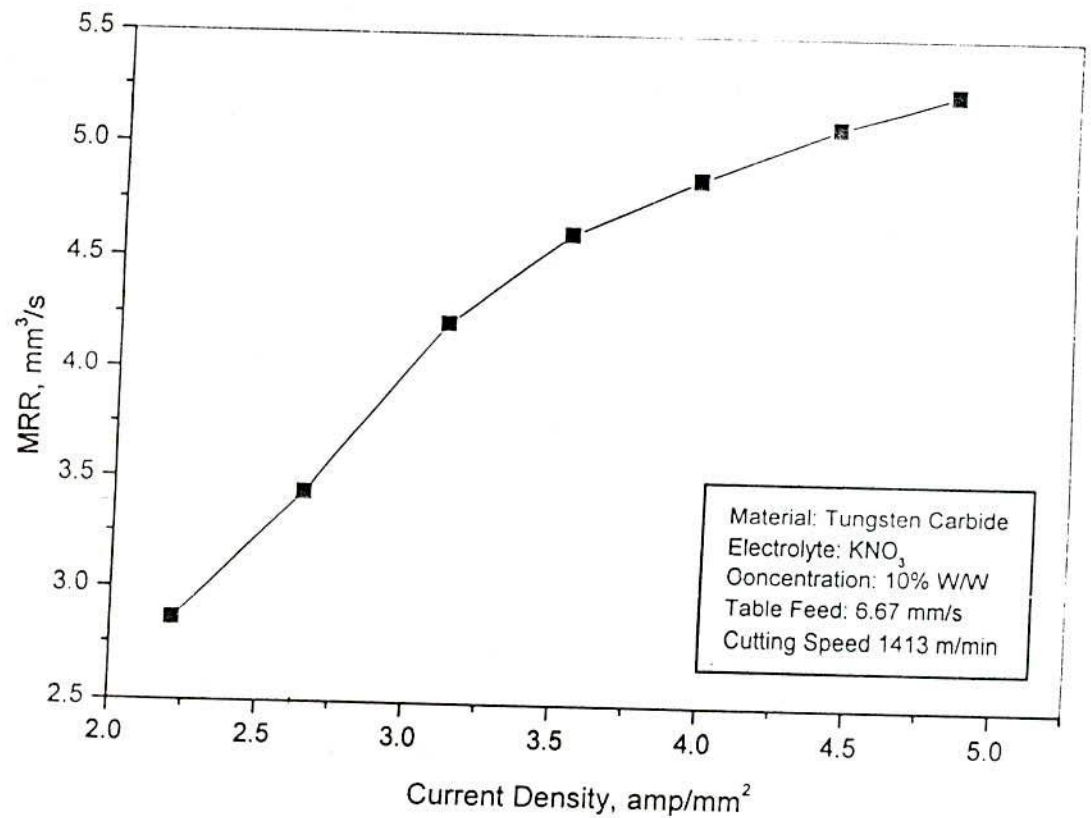


Figure 6.5 Effect of Current Density on MRR (Tungsten Carbide GT 20)

6.5.3 Effect of Voltage of Surface Finish

At different loads the surface finish is found to be more or less constant with increase in voltage as shown in Fig.6.6. It is also observed that surface finish improves slightly with lower feed force. Decreased feed force provides better surface finish.

For different depths of cut, the variation of surface roughness with increasing applied current is shown in Fig.6.7. The figure shows that the surface roughness increases with the increase in current and decreases with depths of cut. Among the three depths of cut 10, 15, and 25 micron, the depth of cut 25 μm gives the better surface finish.

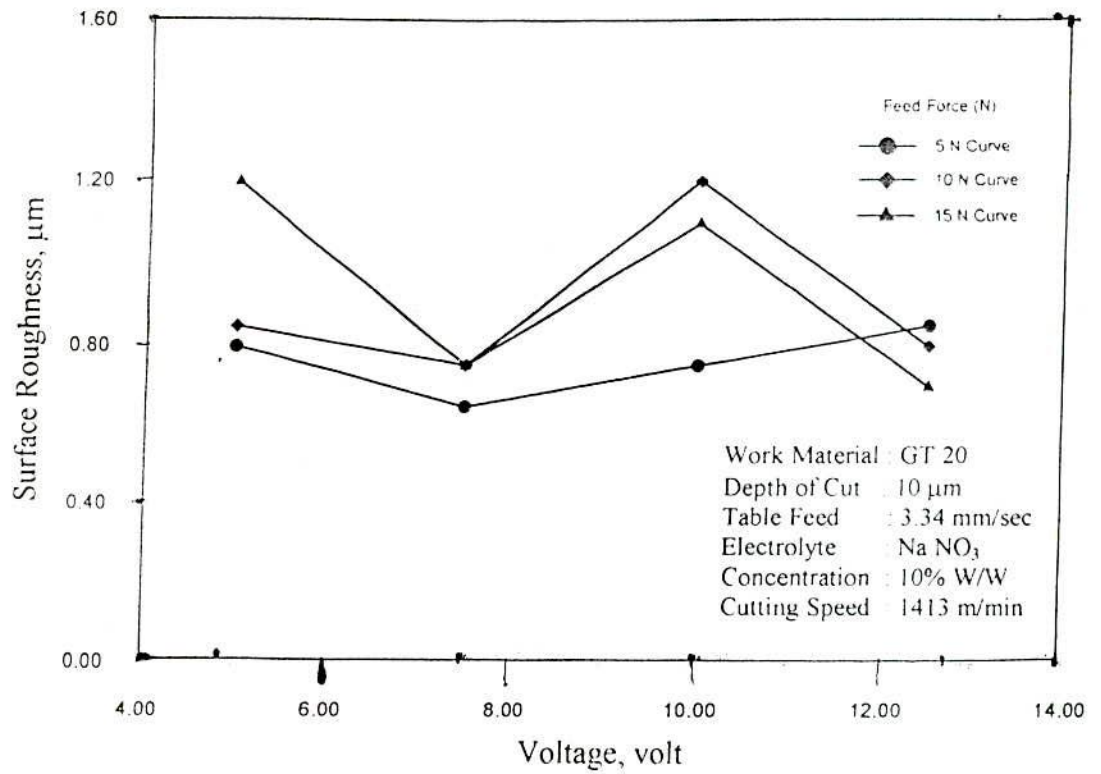


Figure 6.6 Effect of Voltage on Surface Roughness for Different Feed Forces

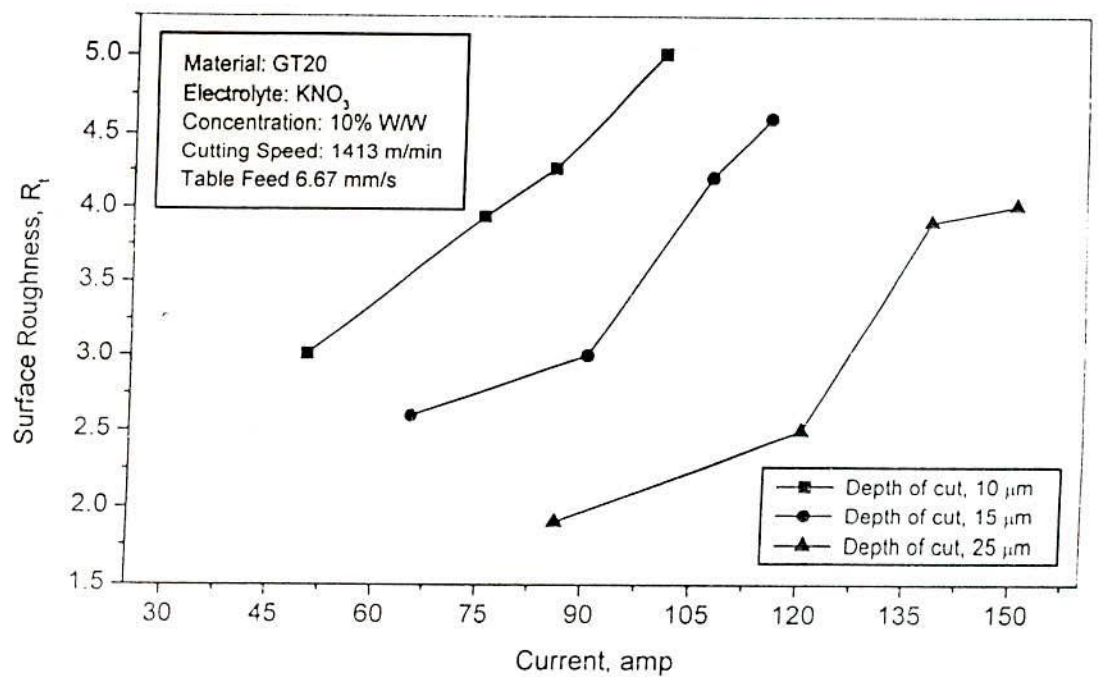


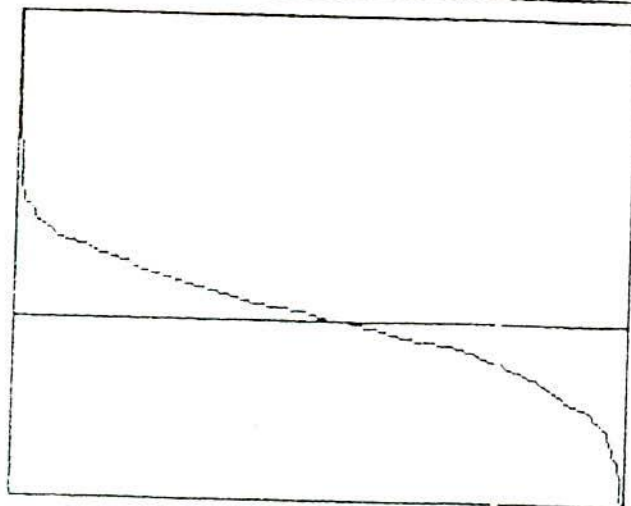
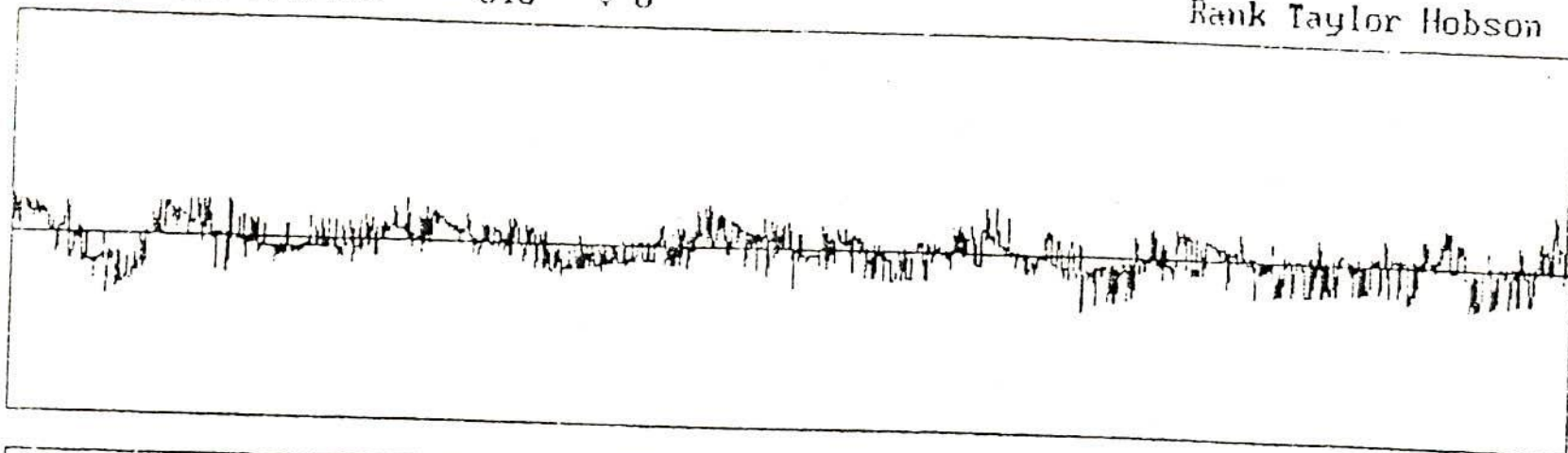
Figure 6.7 Effect of Current on Surface Roughness for Different Depths of Cut

The surface roughness is measured with the help of a Talysurf unit (Surtronic 3P). The Figs.6.8 and 6.9 represent surface texture for tungsten carbide and stainless steel respectively. It is observed that the centre line average (R_a) value for GT 20 is less than that of stainless steel. The other surface characteristic criteria such as R_q represents root-mean-square of the R_a parameters, and R_{ms} represents the mean of all maximum valley-to-peak heights of the surface profiles. Similarly, the other tribological characteristics such as amplitude density, bearing ratio are also presented in the same figure. Roughness measurements are taken at cut off value of 0.8mm and traverse length of 4.5 mm.

The surface roughness values of R_a and R_q are determined on this Talysurf analyzer. For stainless steel, it is found not to exceed the value of $0.59 \mu\text{m}$ in R_a , and have a minimum value of $0.36 \mu\text{m}$. Similarly, for tungsten carbide, the value of R_a is found within the range of 0.22 to $0.6 \mu\text{m}$.

Roughness Profile ST3 v 6

Rank Taylor Hobson

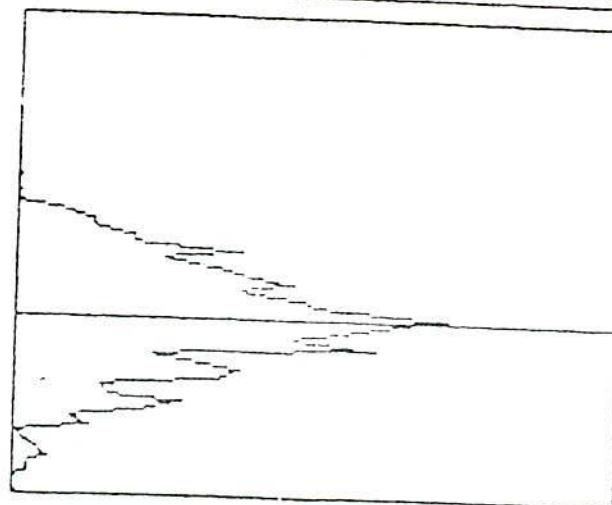


Bearing Ratio

| | |
|-------|------|
| Ra um | 0.36 |
| Rq um | 0.46 |
| Rt um | 4.0 |
| Rp um | 2.5 |

| | |
|-----------|------|
| Cutoff | 0.80 |
| Roughness | |
| ISO | |
| Metric | |

Uv 10000

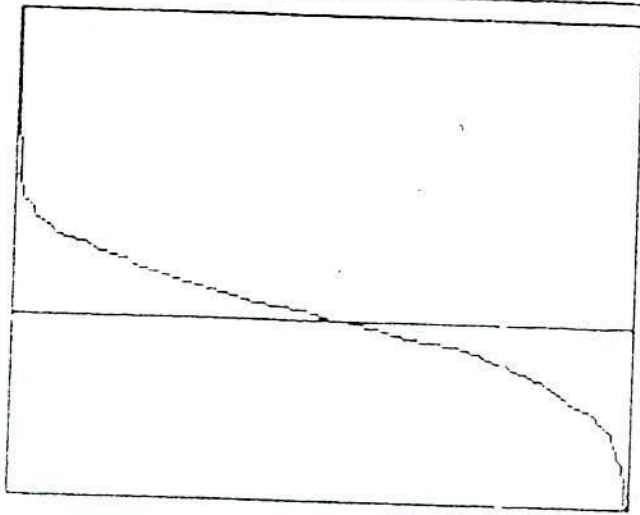
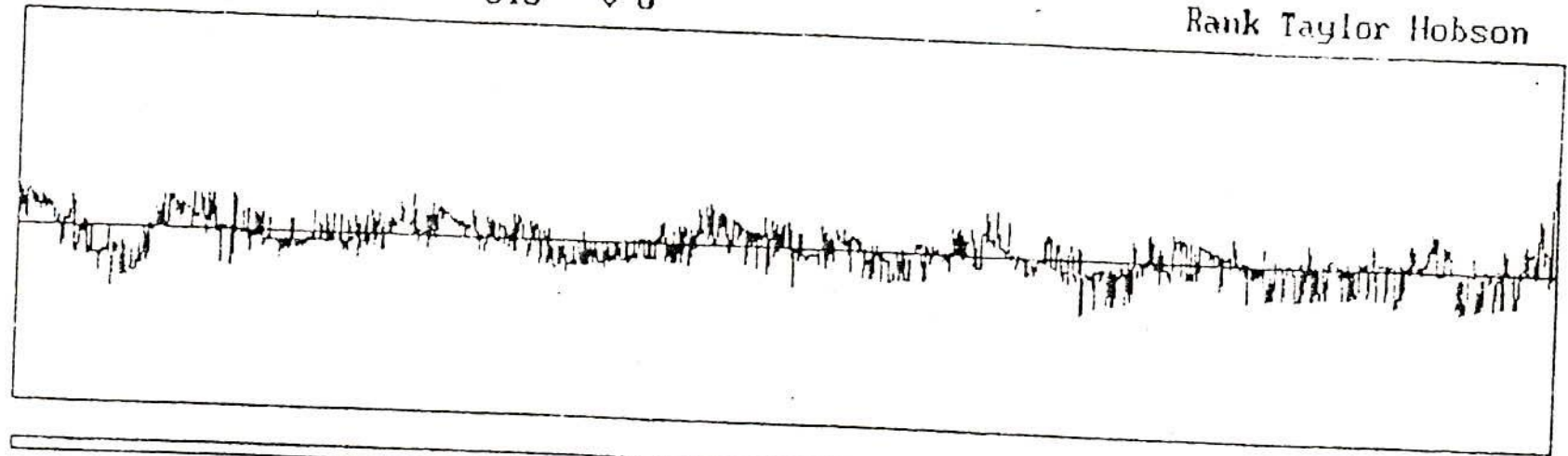


Amplitude/density

Figure 6.8 Surface Texture of Tungsten Carbide

Roughness Profile ST3 v 6

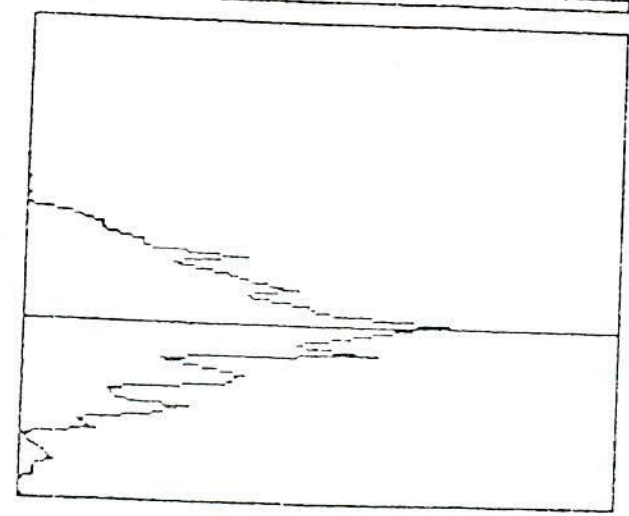
Rank Taylor Hobson



Bearing Ratio

| | |
|-----------|------|
| Ra um | 0.36 |
| Rq um | 0.46 |
| Rt um | 4.0 |
| Rp um | 2.5 |
| Cutoff | 0.80 |
| Roughness | |
| ISO | |
| Metric | |

Vv 10000



Amplitude/density

Figure 6.9 Surface Texture of Stainless Steel

145

6.5.4 Effect of Voltage on Spindle Load

Spindle load is measured as percentage of the total power that is required to drive the mechanical elements under idle or cutting conditions and is directly affected by mechanical action. Fig. 6.10 provides the effect of current on spindle load for different feed rate conditions. Higher mechanical action and higher spindle loads are found at higher feed rates. The electrochemical action increases linearly with the increase of current. Lower spindle load is found to increase with higher current.

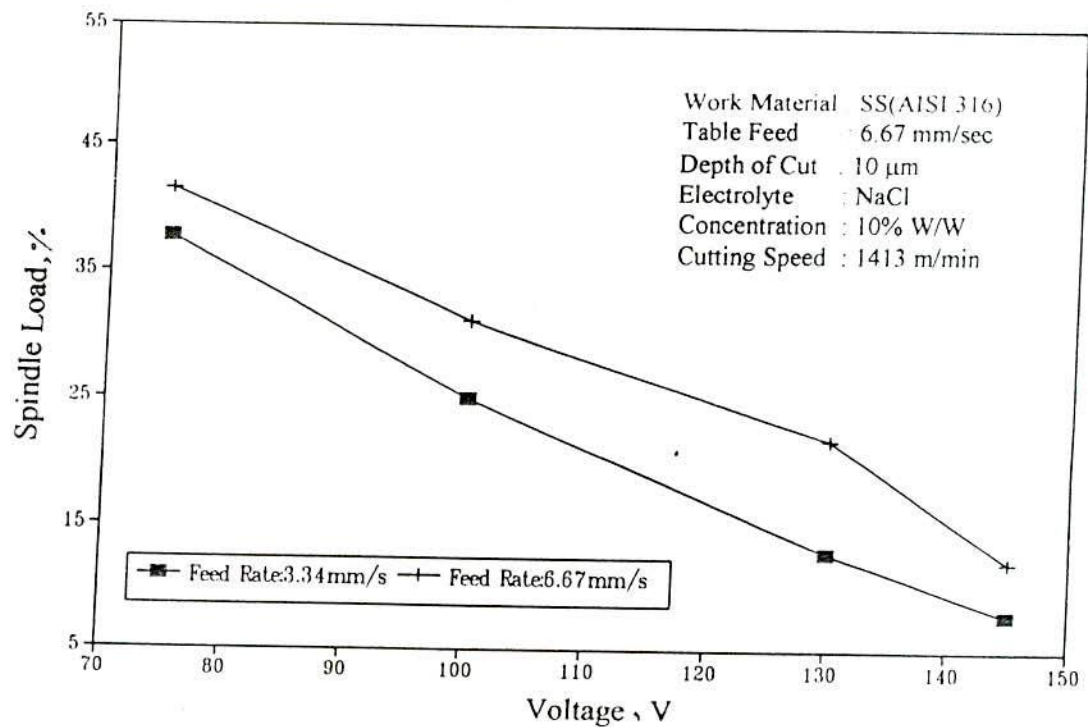


Figure 6.10 Effect of Voltage on Spindle Load for Different Feed Rates

6.5.5 Effect of Electrolyte Flow Rate on Current Density

All experimental runs are made at an electrolyte flowrate monitored through a rotameter. Fig.6.11 shows that current density increases rapidly with the increase in electrolyte flow rate up to 2.6 lit/min and then increases very slowly for same operating conditions, the current density is found higher for NaCl electrolyte solution than KNO_3 . At too high flowrate the current density does not increase with the flowrate. This is mainly because at high flowrate major portion of electrolyte bypass

the machining gap resulting in misuse. This may also due to constant surface area of the wheel and workpiece, and perfectly saturation with the incipient ions. Small change in electrolyte flow rate has negligible effect on current density.

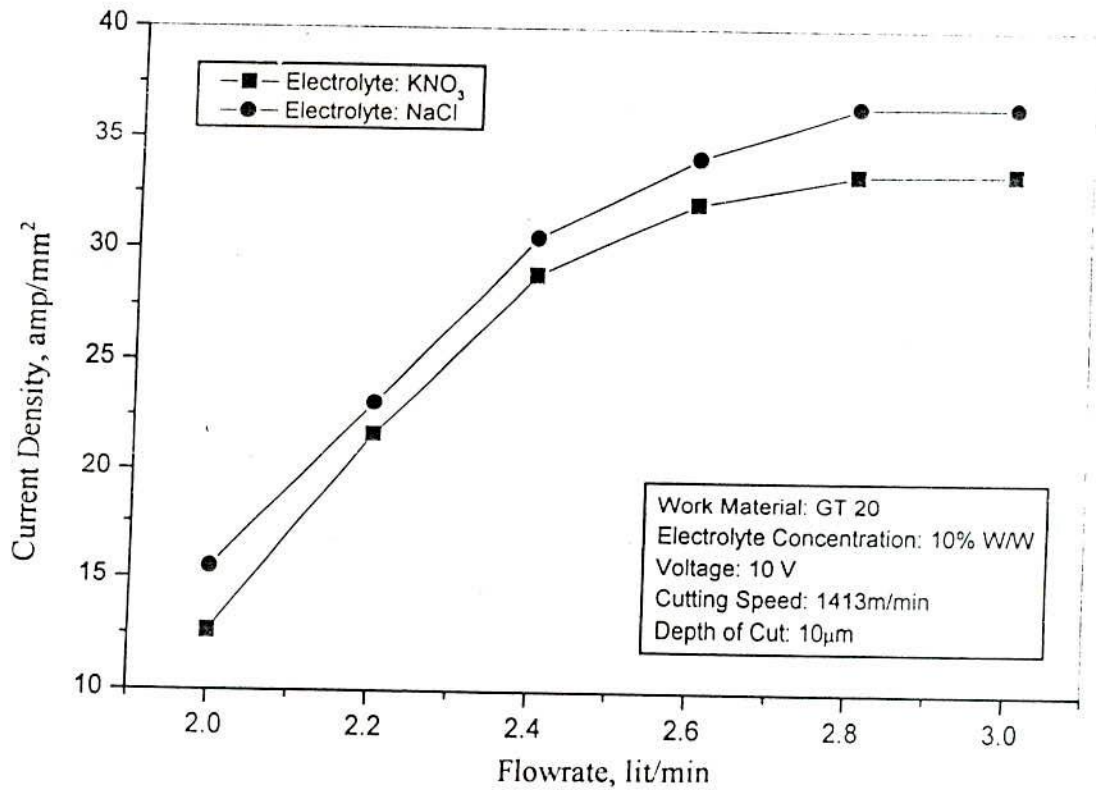


Figure 6.11 Effect of Electrolyte Flow Rate on Current Density

The grinding force comprises of two forces namely radial and feed forces. The variation of the feed force for different electrolytes at different current densities is shown in Fig.6.12. The feed force is found to decrease with the increase of current density for the both the electrolytes. The higher the current density, higher would be the electrochemical action and hence less would be the mechanical action resulting in less feed force as evident in the figure. Feed force is found very less for KNO₃ compared to NaCl solution.

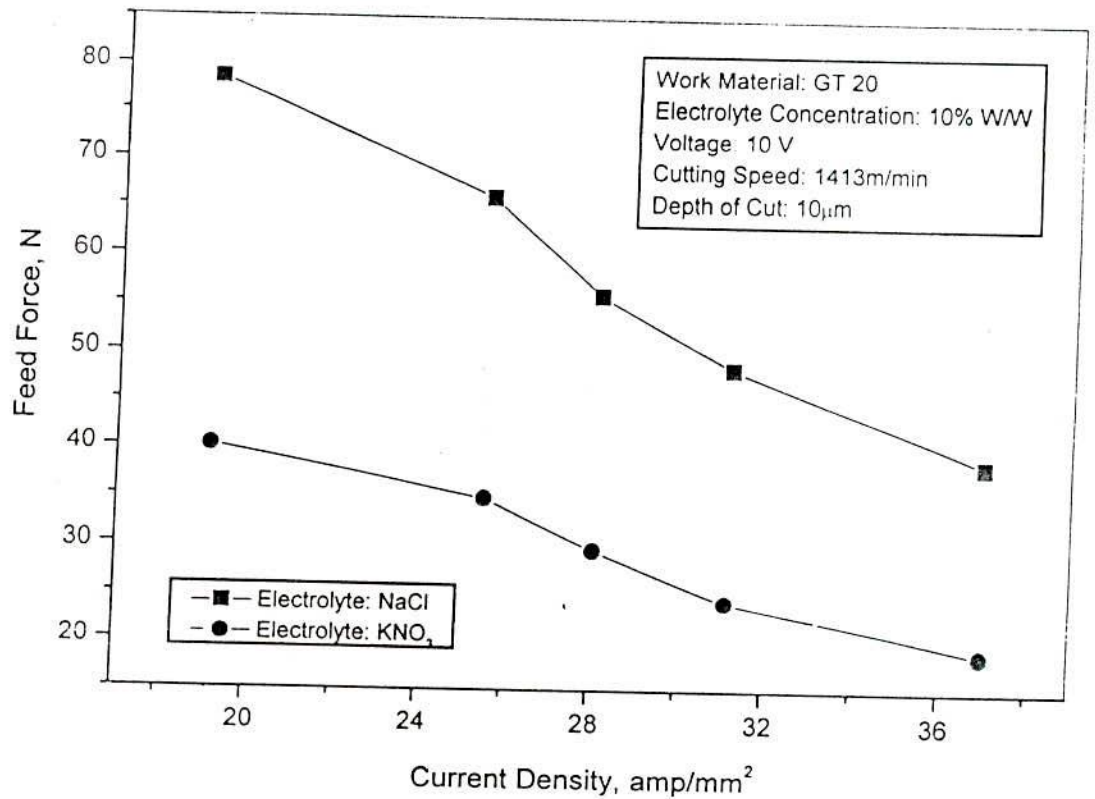


Figure 6.12 Effect of Current Density on Feed Force

Similarly, the variation of the feed force for stainless steel at different current densities is shown in Fig.6.13. It is seen that up to about 3.1 amp/mm², the grinding force components decrease rapidly followed by a slow decrease in feed force with further increase in current density. The radial force is found much higher than the feed force produced during electrochemical grinding process. Literature review indicates that radial force component may be greater in ECG than in conventional grinding with larger current densities and higher feed rates [24].

6.5.6 Effect of Depth of Cut on MRR

With increase in depth of cut, MRR increases slowly as shown in Fig.6.14 because of the fact that the MRR due to mechanical action is very less compared to electrochemical action. The experimental value of MRR is also compared to the theoretical predicted MRR value for lower (2) and higher (1) valencies of the

elements of anode material. It is found that experimental values are slightly less than theoretically predicted value for higher valency.

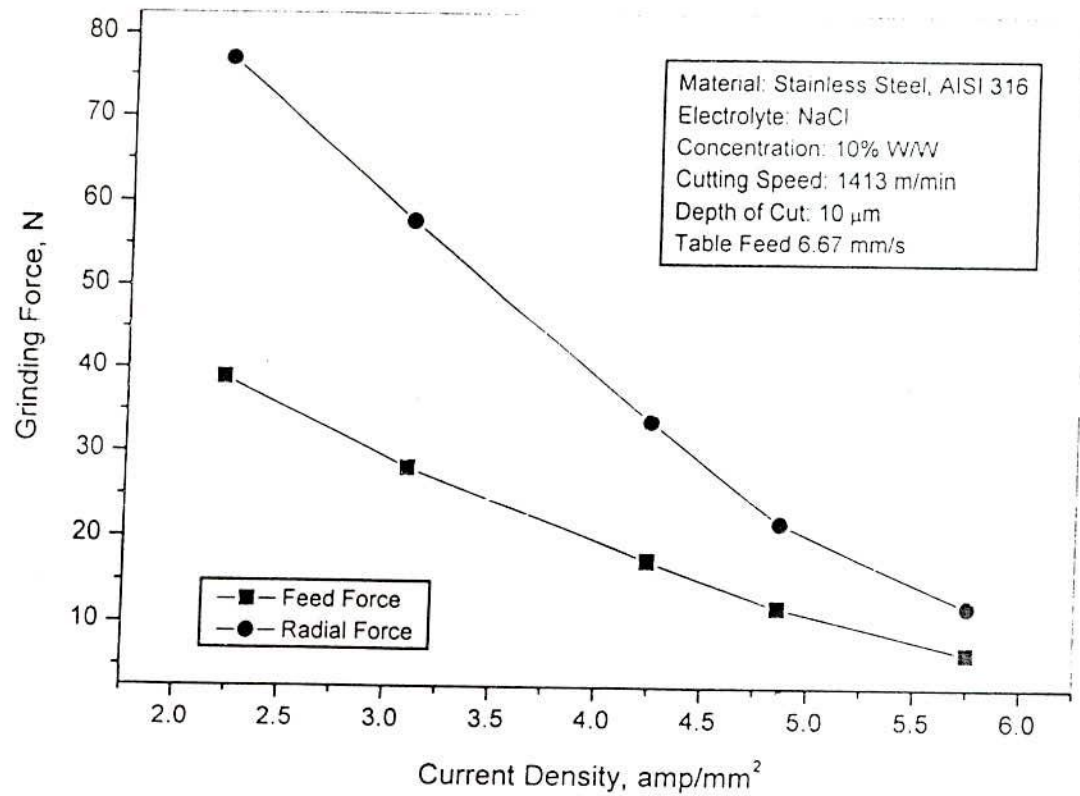


Figure 6.13 Effect of Current Density on Radial and Feed Forces

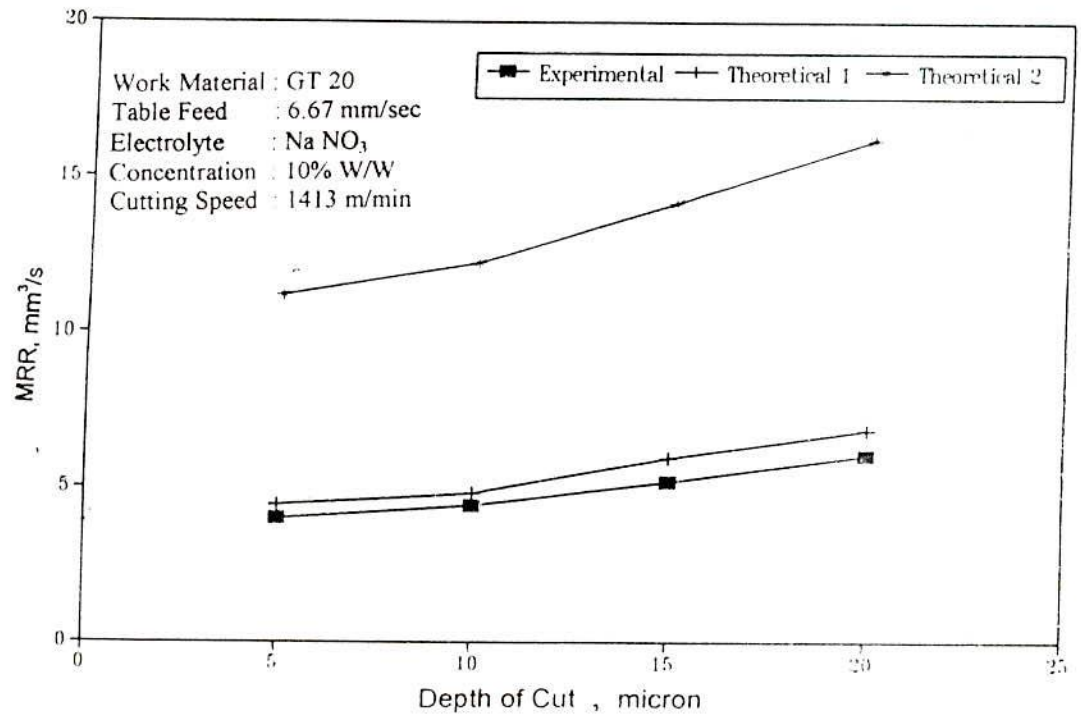


Figure 6.14 Effect of Depth of Cut on Material Removal Rate(MRR)

6.5.7 Effect of Current Density and Feed Force on Process Efficiency

Process efficiency with regards to the ECG process is defined as the ratio of electrolytic metal removal to the total removal. With increase in current density the electrochemical action becomes predominant and hence process efficiency also increases as shown in Fig.6.15. But with the increase in feed force since mechanical action predominates, process efficiency is found to decrease as shown in Fig.6.16.

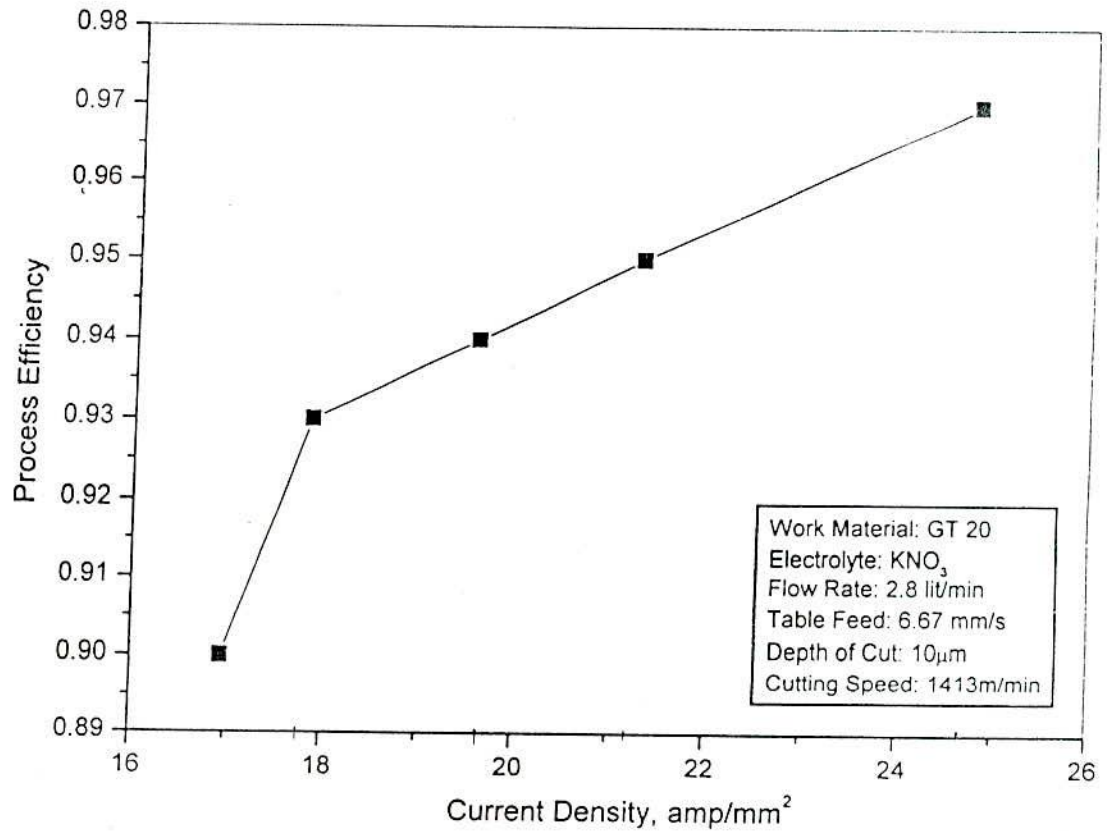


Figure 6.15 Effect of Current Density on Process Efficiency

6.5.7 Effect of Current Density and Feed Force on Process Efficiency

Process efficiency with regards to the ECG process is defined as the ratio of electrolytic metal removal to the total removal. With increase in current density the electrochemical action becomes predominant and hence process efficiency also increases as shown in Fig.6.15. But with the increase in feed force since mechanical action predominates, process efficiency is found to decrease as shown in Fig.6.16.

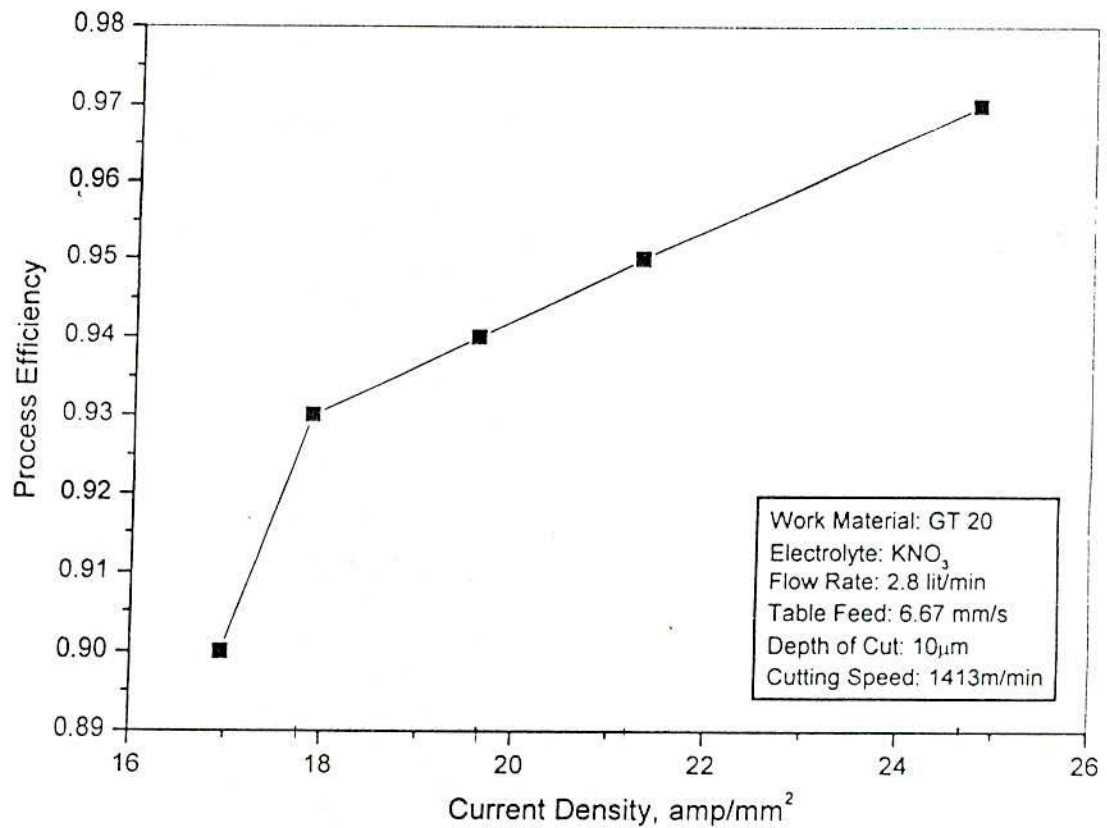


Figure 6.15 Effect of Current Density on Process Efficiency

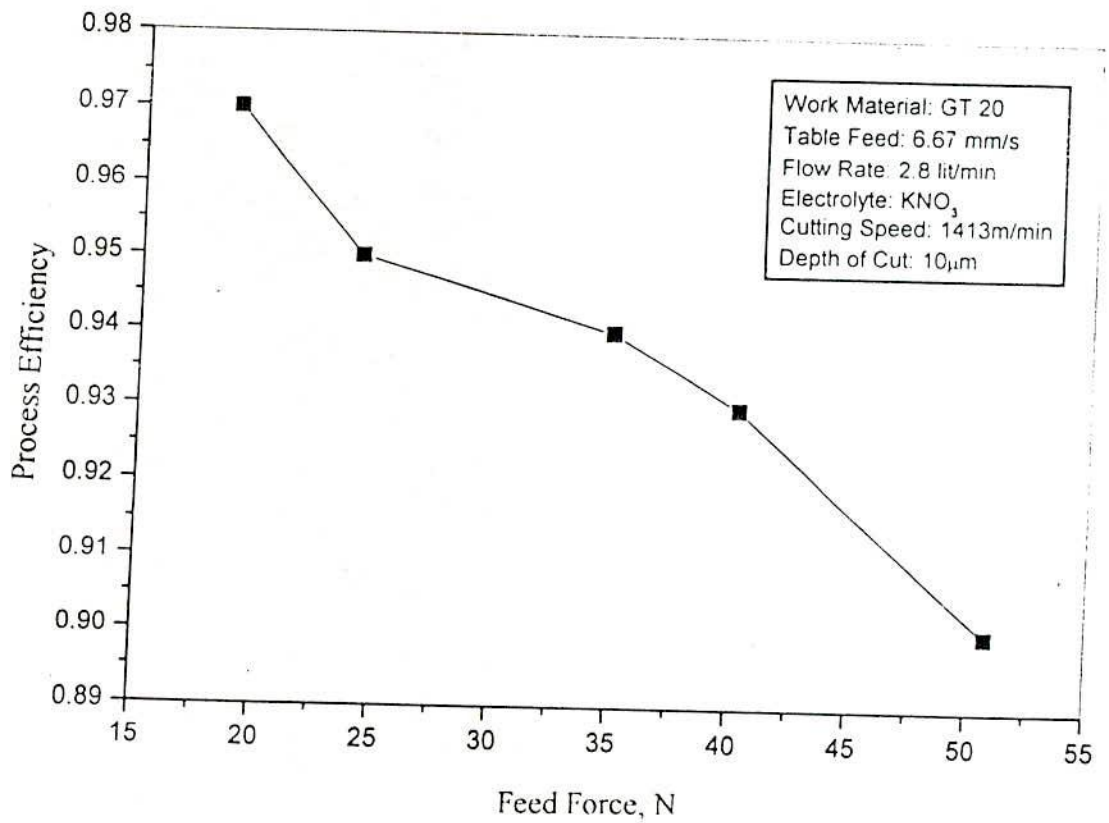


Figure 6.16 Effect of Feed Force on Process Efficiency

6.5.8 Effect of Feed Rate on Grinding Force

When feed rate is high, mechanical action is more and electrochemical action is less. With increase in feed rate, the feed force increases slowly and more or less linearly. The radial force also increases slowly up to about feed rate of 5.8 mm/sec and then increases at a faster rate as shown in Fig.6.17. The feed force is found about half of the radial force.

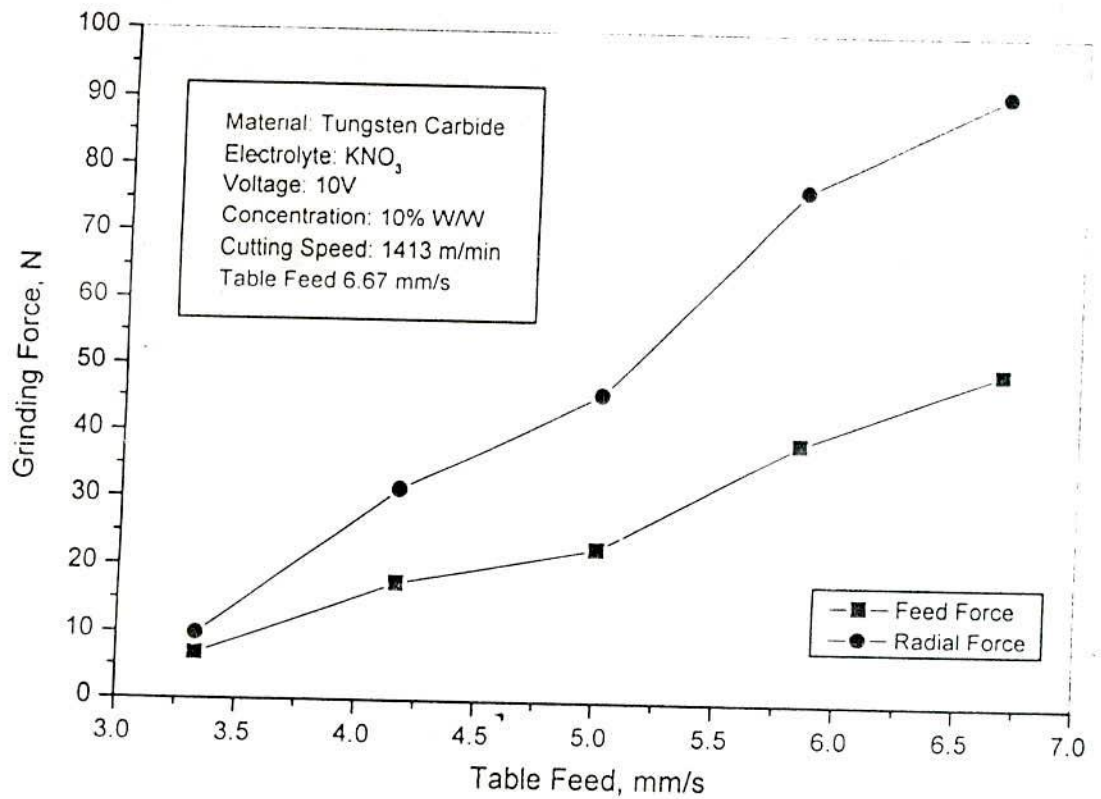


Figure 6.17 Effect of Feed Force on Radial and Feed Forces

6.5.9 Effect of Current on Feed Force

The relationship between current and feed force in electrochemical grinding is shown in Fig.6.18. This shows that as current increases feed force decreases keeping all other conditions unchanged which means that ECM activity predominates over mechanical grinding. The variation is almost hyperbolic in nature. It also indicates that for a depth of cut $10\mu m$ and table feed rate of 6.67 mm/sec at 80 amperes of current, feed force is very low probably what is required to remove the passive layer.

Slower feed rate results in more exposure time of electrolyte on the work material, and consequently, a tremendous electrochemical action is acted in the machining zone. The material removal in this case is mostly due to electrochemical action. The total amount of metal removed is found to be higher with increased

electrolyte flow rate. When the electrolyte flow is low, higher mechanical action prevails compared to higher flow of electrolyte.

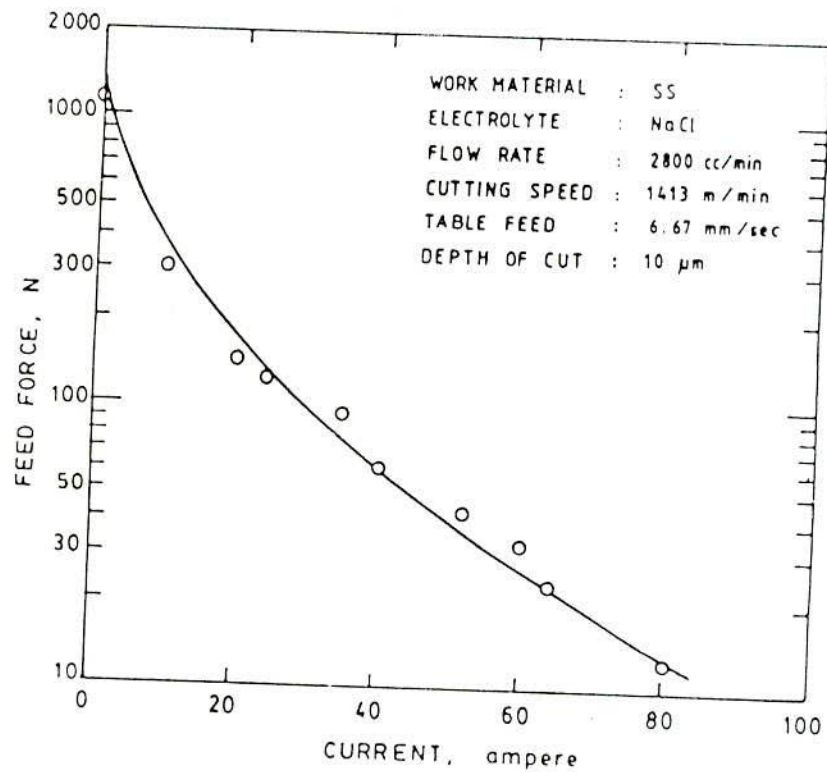


Figure 6.18 Relationship between Feed Force and Current in ECG

6.6 Verification of the Theoretical Results

6.6.1 Material Removal Rate

Experiments are conducted to corroborate the theoretical analysis developed for MRR for machining tungsten carbide specimen. The analyses are made separately for MRR due to mechanical action and that of due to electrochemical action. For instance, at 20 μ m depth of cut and 21.28 amp/mm² current density it is found that the theoretical MRR due to mechanical action is 0.43 mm³/sec and that of for electrochemical action is 6.45 mm³/sec. Under similar conditions experimental investigations are also conducted. The electrolyte used is KNO₃ for GT 20, and NaCl solution for stainless steel. After each run the specimen is weighed with an electronic balance, that gives material removed due to combined action. A sample calculation

for both theoretical and experimental MRR is given in Appendix (A4.4). At 20 μm depth of cut, Fig. 6.19 shows that material removal rate is 6.02 mm^3/sec which is lower than that of theoretical values. The theoretical and experimental results are also shown in this figure. The operating conditions are depths of cut and current densities.

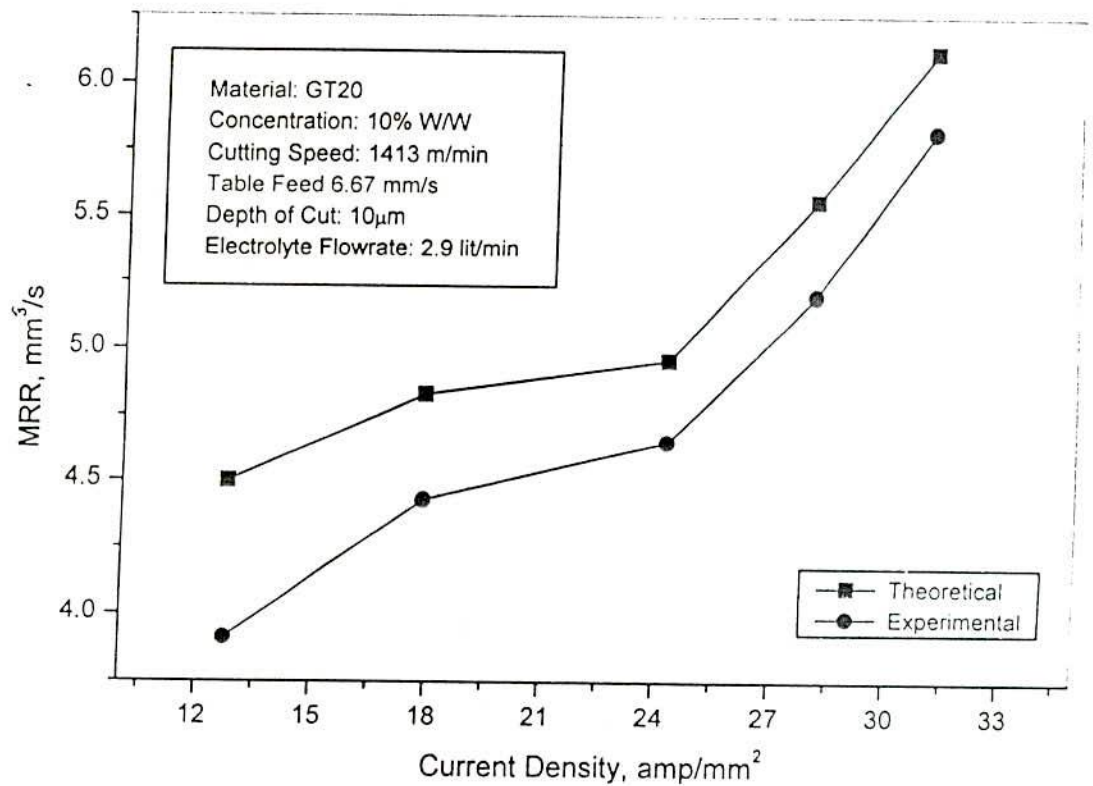


Figure 6.19 Comparison of Theoretical and Experimental MRR

It is observed that the theoretical predicted values for MRR are close to the experimental results indicating a good agreement between the two. The maximum variation between experimental and theoretical results is about 15% (corresponding to 3rd set of readings).

Table 6.5 shows the comparison of theoretical and experimental values. Similarly it is tested for stainless steel and shown in Fig.6.4. Theoretically, the MRR value for the lowest valency differs from that of the highest valency of the elements of the alloy. For higher valencies the variation is less. The same figure also shows that the MRR predicted value for higher valency is lower than that of for lower valency.

Fig.6.4 shows that the experimental results are closer to the theoretical results when higher valency states of elements are considered

Table 6.5 Comparison of Theoretically and Experimentally Obtained MRR

| Depth of Cut μm | Current Density amp/mm^2 | Theoretical MRR | | | Experimental MRR | |
|-------------------------------|---|---------------------------------|---|---------------------------------|---------------------------------|---------------------------------|
| | | Mech. mm^3/s | Electrochemical mm^3/s | Total mm^3/s | Mech. mm^3/s | Total mm^3/s |
| 5 | 16.95 | 0.11 | 4.34 | 4.45 | 0.51 | 4.02 |
| 10 | 17.86 | 0.21 | 4.62 | 4.83 | 0.68 | 4.43 |
| 15 | 19.58 | 0.32 | 5.66 | 5.98 | 0.72 | 5.20 |
| 20 | 21.28 | 0.43 | 6.45 | 6.88 | 0.82 | 6.02 |

6.6.2 Feed Force

With the use of same experimental set-up, the feed forces are measured by the strain gauge dynamometer. Eight strain gauges are mounted on the tail centre forming two bridges, and connected to a digital amplifier. For a particular dept of cut, 10 μm and table feed rate of 6.67 mm/s at 80 amperes of current, the feed force is found very less as compared to conventional machining under similar conditions as shown in Fig.6.18.

In developing the theoretical feed force model, expressions for radial and feed forces are established in terms of some coefficients. The values of those constants are taken into account from other investigator's experimental result [15]. Using Eqn. 4.41, the feed force is calculated and found to be very less. This feed force is responsible only for mechanical action but major portion of total removal takes place for electrochemical action.

The last part of the feed force equation i.e. feed force due to viscous effect of electrolyte is found to be negligible compared to the other force components. The calculation for a particular set of operation given in Table A6.6.1 and Table A6.6.2 in Appendix, shows that feed force is 23.8 N. Experimentally, it is found to be 28.21 N results in the variation of less than 17%. The comparison between the experimentally obtained value and the theoretically predicted value shows that experimental feed force is higher than that of theoretical value. It is to be noted also that there is a discrepancy which may be due to the assumptions considered, and the coefficient values taken from other investigator's results for the simplicity of the analysis.

6.7 Summary

Although not many of the investigators studied the analysis of the electrochemical grinding process, yet, it is well-known that material removal rate due to electrochemical and mechanical actions can not be separately found out. Most of the researchers expressed in one way or another the importance of being able to predict, control or reduce this phenomenon.

The effect of process parameters in electrochemical grinding process may be summarized as follows. The high feed rate, low electrolyte flow rate provide increased mechanical action. Current density is the most influencing parameter for material removal rate. It is observed that short circuiting may be caused due to certain machining conditions. Mechanical sparkout is observed at low voltage and high feed rate. Poor flow of electrolyte tends to produce passivity. The small electrode gap fails to produce dissolution at the anode with the rate of anode advance. In this unstable condition, the electrodes touch causing short circuiting. At too high voltage, severe electrical sparking is observed and the temperature becomes so high that boiling of electrolyte results gas pressure which in turn throws the electrolyte off. The electrochemical action is greatly influenced by anodic passivity. Passivity conditions reduce the electrochemical action and increases mechanical action. Higher MRR is observed at a high feed rate and a less volume of metal removed by electrochemical action. High electrochemical action increases overcut, whereas, mechanical action

reduces this. Surface finish is greatly influenced by feed rate. The ECG process uses the least amount of energy and the operation would be performed economically and more efficiently.

CHAPTER - 7

EPILOGUE

CHAPTER 7

EPILOGUE

7.1 General Remarks

This section outlines important conclusion and recommendation for the design, development, and analysis based on the results of different aspects studied in the thesis. Conclusions are drawn on the results of theoretical and practical analyses. The main features of the present dissertation are concerned with the mechanical and electrochemical aspects of electrochemical grinding process. This has been organized into seven chapters including the present one which is devoted to state succinctly conclusions drawn out of the studies embodied in the thesis. The scope of future research and some of the probable modifications which may be done have also been included in the forthcoming sections. The results are summarized and the salient conclusions of this investigation may be recalled from the Chapters 3 to 6.

7.2 Conclusion

The conclusion to electrochemical grinding has not yet been reached. Its development is progressing day by day. Based on the studies undertaken during different phases of present investigation, the following conclusions are drawn.)

The present work aimed at developing an ECG experimental set-up embracing all the essential facilities to corroborate experimental results with the theoretical models. That has been done by retrofitting an obsolete conventional surface grinder. Besides the above work, an attempt has also been made for the design, construction and calibration of a grinding dynamometer. The theoretical analysis for material removal rate and feed force have been done in most generalized form applicable to all situations. However, the performance of reciprocating table at a very slow speed is not quite satisfactory. The embedded dynamometer is to provide adaptive control of the entire system in future if required.

The parameters that affect only the electrochemical aspects of the process are not constant throughout the process and follow a pattern effecting on the flow of current between the wheel and workpiece. They determine the work material decomposition and material removal rate due to electrochemical action. On the contrary, the process parameters that govern the mechanical aspects of the process affect the machining gap, contact area, and the width between the wheel and workpiece. In ECG, mechanical abrasive action of the wheel could significantly alter the machining characteristics:

- i) by effectively removing any developed passive oxide film, and
- ii) by affecting some material removal by abrasive action of the grains.

The operating parameters, viz. supplied voltage, feed rate and set depth of cut etc. can easily be varied over a wide range in order to meet needs such as material removal and form accuracy.

The electrolyte exposure time on the workpiece depends on the feed rate. For different feed rates, the radial and feed forces vary. High feed rate results high feed force on workpiece and vice versa. Total volumetric removal rate increases at higher feed rates. The selection of electrolyte is very important in controlling passivity.

The performance of the machine has been tested through experiments and found to run satisfactorily. This procedure of development of such systems for obsolete conventional grinding machine would help industries. The theoretical results have been experimentally verified and found them within the closure range of acceptance for industrial exploitation. Some of the observations and results are highlighted as concluding remarks:

- More uniform current flow provides better surface finish
- Surface roughness increases with increasing supply voltage and decreasing feed rate under electrolytic conditions.

- Mechanical removal rate is less than 10% of the total material removal rate under normal operating conditions

Though the above statements are very common but these are essential for the evaluation of performance of such a modified set up, to determine the operating conditions.

- Total volumetric material removal increases with higher voltage, high electrolyte flow rate and its concentration, and increase feed rate. But MRR due to mechanical action only increases with high feed rate and low electrolyte flow. The theoretical evaluation of the process is not the exact, because of the facts, that the valency states of the ions produced are not exactly known, especially for the divalence elements of the workpiece, for instance, Fe in stainless steel. As a result, the theoretical predicted values possess two results. The results show that for the lower valency during electrochemical action, the MRR is high and vice versa. At the anode, dissolution is not the only reaction phenomenon.
- Current density increases with increase in voltage unless the supply voltage is too high to cause intensive gas evolution due to boiling of electrolyte and severe sparking. In this regard it may be mentioned that the magnitude of feed force does not play significant role. On the other hand, until the supply voltage reaches a magnitude of 2 to 3 volts, electrolysis phenomena does not occur. This minimum voltage may be assumed to be the decomposition voltage. Current density increases proportionately with the electrolyte concentration so long as concentration is 10 to 15% by weight.
- Process efficiency in electrochemical grinding of tungsten carbide by metal bonded diamond wheel using KNO_3 electrolyte reaches upto 90 to 97%, and slowly decreases with the increase of feed. Anodic dissolution rate tends to fall when the process efficiency gradually decreases. In that condition the contribution of mechanical action becomes significant. With grinding speed the mechanical material removal rate increases faster than that of electrochemical rate and hence process efficiency decreases with the increase of speed. The depth of cut for combined action increases as electrochemical action increases.
- The failure to achieve constant current flow is the major cause of poor surface finish and dimensional control problems. Based on these preliminary tests, it is a fact that

higher gains in the efficiency and applicability of ECG are the most likely to be achieved through the steady current flow and specialized wheels.

- The metal removal rate and surface finish obtained are within satisfactory range. Their orders are $1.6 \times 10^3 \text{ mm}^3/\text{min}$. and $0.1 \text{ }\mu\text{m}$ respectively.
- Surface integrity is mainly governed by the differential electrochemical activity of the microstructural constituents involved in the process, voltage and by the amount of mechanical contribution to the process.

The present trends in the design of aerospace components indicate the use of materials of high tensile strength, for example, titanium and its alloys. They have high strength to weight ratios, corrosion and fatigue resistance, and more important, retain their mechanical properties at elevated temperature. Studies have shown that whilst conventionally grinding titanium, serious reductions in fatigue strength can occur without any visible evidence showing on the affected surface. Further, titanium can crack when ground under production conditions similar to these used for steels. The nature of the grinding process is such that the surface mechanical properties of titanium may be affected to an unusual extent compared with other metals. Unlike the cases, ECG is one of the best solutions for grinding of such stringent materials.

The thesis enumerates the scope of future work needed on this topic, presents appendices as a supplement to the theoretical and experimental investigations, and finally concludes giving a list of references consulted during the course of the work.

7.3 Scope of Further Work

Research has no end. Directions of thoughts vary from person to person. The various directions in which future work on electrochemical grinding can be taken up are as follows.

Since the present work mostly deals with the theoretical analysis for design and development of the ECG machine, it creates a knowledge for any theoretical analysis in such machining process, develops a creative idea to build such a machine.

As per the present and future need is concerned, this machine is quite useful. There is also scope for future modification in the existing system, such as:

- i) Variation of wheel speed by changing the pulley drive system,
- ii) Arrangement for spindle power measurement,
- iii) Installation of a precision feed rate meter,
- iv) Use of adaptive control to regulate feed rate automatically to maintain a constant feed force. According to the requirements for the cutting operation the mechanical cutting point can be found out and any modification can be made by adjusting set parameters like supply voltage, wheel speed, feed rate etc.
- v) Design and development of a vibrator for introducing stirring effect in the electrolyte solution with varying frequency and amplitude in the process.
- vi) Proper filtration for sludges removal.
- vii) An optimization approach can be achieved from the models developed for material removal rate and feed force, which in turn will lead to a developed system that will control the process. Ultimately this will minimize wheel wear and maximize MRR.
- viii) To accommodate for variations in wheel and work materials, the present methodology may be needful to combine with any expert system to achieve consistent results.
- ix) Spark detection and protection circuit to be incorporated to the power supply.

The experimental work can be extended to various other materials as well. The efficiency and applicability of electrochemical grinding can be improved through the development of special wheels.

REFERENCES

REFERENCES

1. Bhattacharyya, A., *New Technology*, Institution of Engineers, India, 1973.
2. Benedict, G. F., *Nontraditional Manufacturing Processes*. Marcel Dekker Inc., New York, 1987.
3. *Machining Data Handbook*, Machinability Data Centre, Cincinnati, Ohio, 1980.
4. Pandey, P. C., and Shan H. S., *Modern Machining Processes*, McGraw-Hill Co. Ltd., New Delhi, 1980.
5. Dr. Geddam A., "Electrochemical Grinding", *Proceedings of the 6th All India MTDR Conference*, 1973, pp. 514-521.
6. Thompson, J. R., "Operating Parameters in Electrochemical Grinding with Aluminum Oxide Wheels", *New Developments in Grinding*, International Grinding Conference, Edited by M. C. Shaw. Pittsburgh, Pennsylvania, Camegie Press, April 1972, pp. 793-812.
7. Geddam, A. and Noble, C. F., "An Assessment of the Influence of Some Wheel Variables in Peripheral Electrochemical Grinding", *Int. J. of MTDR*, Vol. 11, 1971, pp. 1-12.
8. Chalkley, J. R., "The Mechanical Contribution to Electrolytic Grinding", *Industrial Diamond Review*, No. 29, 1969, pp. 188-195.
9. Brandi, R. R., "Basics of Electrochemical Grinding", *American Machinist*, April 1974, pp. 45-50.
10. Phillips, R. E., "ECG: Combining Electrochemical Attack and Abrasion", *Manuf. Engg.*, December 1986, pp. 46-48.
11. *Tool and Manufacturing Handbook*, Vol. 1, 4th Edition, SME, Michigan. 1983.
12. McMillen, J., "Electrochemical Grinding, What's Fact-What's Fiction", *The Carbide and Tool Journal*, Jv-14, Sept.-Oct. 1982, pp. 20-21.
13. Phillips, R. E., "Electrochemical Grinding", *Metals Handbook*, 9th Edition, Vol. 16, 1989, pp. 542-547.

14. Krar, S. F., *Technology of Machine Tools*. McGraw Hill, New York, 1977.
15. Younis, M., Sadek, M. M. and El-Wardani, T., "A New Approach to Development of a Grinding Force Model", *Transaction of the ASME, J. of Engg. for Industry*, vol. 109, November 1987, pp. 306-313.
16. De Barr, A. E., *Electrochemical Machining*, Macdonald Pb., London, 1968.
17. Roy, A. Lindberg, "Processes and Materials of Manufacture", University of Wisconsin, Prentice Hall of India, New Delhi, 1982, pp. 592-597.
18. Weller, E. J., *Nontraditional Manufacturing Processes*, Society of Manufacturing Engineers, Dearborn, Michigan, 1983.
19. Coleman, J. R., "Electrochemical Grinding of Carbide Tooling", *Tooling and Production*, May 1980, pp. 90-92.
20. Ilhan, R. E., Sathyanarayanan, G. and Adams, J. W., "Influence of Variables on Overcut in Electrochemical Surface Grinding", 17th NAMRC Proc., *Transactions of NAMRI*, May 1989, pp. 193-200.
21. Atkinson, J. and Noble, C. F., "The Surface Finish Resulting from Peripheral Electrochemical Grinding", 22nd MTDR, 1981, pp. 371-378.
22. Cole, R. R., "An Experimental Investigation of the Electrolytic Grinding Process", *Journal of Engineering for Industry*, ASME, Vol. 83, May 1961, pp. 194-201.
23. Colwell, L. V., "Automatic Adaptive Control for Electrochemical Grinding", *Annals of CIRP*, Vol. XVIII, 1970, pp. 577-584.
24. Levinger, R. and Malkin, S., "Electrochemical Grinding of WC-Co Cemented Carbides", *Journal of Engineering for Industry*, Vol. 101, Aug. 1979, pp. 285-294.
25. Malkin, S. and Levinger, R., "Quantitative Characterisation of Surface Damage to WC-Cobalt Composites by Electrochemical Grinding", *Wear*, Vol. 51, 1978, pp. 157-167.
26. Zelwer, O. and Malkin, S., "Grinding of the WC-Co Cemented Carbides-Part 2", *Industrial Diamond Review*, May 1980, pp. 173-176.

27. Zelwer, O. and Malkin, S., "Grinding of WC-Co Cemented Carbides", *Industrial Diamond Review*, April 1980, pp. 135-139.
28. Hasegawa, Y., Hanasaki, S., Touge, M. and Yamamoto, T., "Electromechanical Grinding at High Work Feed Rate", *Precision Engg.*, Vol. 10, No. 2, April 1988, pp. 71-79.
29. Noble, C. F., "Electro-Mechanical Action in Peripheral Electrochemical Grinding", *Annals of CIRP*, Vol. 32, No.1, 1983, pp. 123-127.
30. Kaczmarek, J. and Zachwieja, T., "Investigations on the Material Removal Rate by Electrochemical Grinding of Cutting Tool Materials in Dependence on the Properties of the Grinding Wheel", *Int. J. MTDR*, Vol. 6, March 1966, pp. 1-13.
31. Shan, H. S., "A Theoretical Analysis of Electrolytic Grinding Process", *Microtecnic*, Vol. XXV, 1971, pp. 472-474.
32. Kaldos, E. "The Application of Electrochemical Grinding in Toolmaking", *Periodica Polytechnica, Mechanical Engineering*, Vol. 20, 1976, pp. 271-281.
33. Okhten, V. D., "Effect of Wheel / Workpiece Contact Area on Electrolytic Diamond Grinding", *Machines and Tooling*, Vol. XLI, No.11, 1971, pp. 26-29.
34. Breev, Yu. M., "Role of Electrochemical Dissolution in Electrolytic Diamond Grinding", *Sverkhtverdye Materialy*, Vol. 6, No.4, 1984, pp. 51-54.
35. Kaldos, E., "A Study on Electrochemical Grinding of Small Diamond Specimens Made of Tungsten Carbide", *Periodica Polytechnica, Mechanical Engineering*, 1974, pp. 21-32.
36. Kuppuswamy, G., "Wheel Variables in Electrolytic Grinding", *Tribology International*, Feb. 1976, pp. 29-32.
37. Kuppuswamy, G. and Venkatesh, V. C., "Magnetic Field on Electrolytic Grinding", *Proceedings of the 8th AIMTDR Conf.*, IIT, Bombay, 1978, pp. 546-549.
38. Sfantsikopoulos, M. M. and Noble, C. F., "Vertical Spindle Electrochemical Surface Grinding", *Proc. 12th Int. MTDR Conf.*, Sept. 1971, pp. 265-270.

39. Sfantsikopoulos, M. M. and Noble, C. F., "Dynamic and Geometric Aspects of Vertical Spindle ECG", 13th MTDR, 1972, pp. 323-329.
40. Geva, M., Lenz, E. and Nadiv, S., "Peripheral Electrochemical Grinding of Sintered Carbides - Effect on Surface Finish", *Wear*, Vol. 38, 1976, pp. 325-339.
41. Balashov, Y. A., "Electrolytic Grinding", *Machines and Tooling*, Vol. XXXVII, No. 3, 1966, pp. 31-34.
42. Jones, W. F., "Electrochemical Grinding", *SME Tech. Paper No. 84-266*, 1984, pp. 1-19.
43. Phillips, R. E., "What is Electrochemical Grinding and How does it Work", *Nontraditional Machining*, American Society for Metals, 1986, 65-70.
44. Ilhan, R. E., Sathyanarayanan, G., Storer, R. H. and Phillips, R. E., "A Study of Wheel Wear in Electrochemical Surface Grinding", *Transactions of the ASME*, Vol. 82, No. 114, February 1992, pp. 82-93.
45. Grigorev, V. A. and Menitskii, I. D., "Machines for Electrolytic Grinding", *Machines and Tooling*, Vol. XLIII, No. 4, 1972, pp. 43-45.
46. Geddam, A. and Noble C. F., "An Assessment of the Influence of Some Wheel Variables in Peripheral Electrochemical Grinding", *Int. J. MTDR*, Vol. 11, 1971, pp. 1-12.
47. Banerjee, S. and Chattopadhyay, A. B., "On Improvement of Performance Efficiency of Electrochemical Grinding", *Proceedings of the 2nd Int. Symposium on Industrial and Oriented Basic Electrochemistry*, SAEST, India, pp. 4.2.1 - 4.2.7.
48. Gavrilov, V. N. and Burochkin, Yu. P., "Effect of Wheel Bond on Electrochemical Diamond Grinding", *Machines and Tooling*, Vol. XL, No. 2, 1969, pp. 43-44.
49. Kita, Y., Ido, M., Kuno, M. and Miguchi, A., "Electrochemical Creep Feed Grinding with Ni-Coated WA Wheel", 23rd Int. MTDR, 1982, pp. 265-272.

50. Ilhan, R. E. and Sathyanarayana, G., "Modelling of Electrochemical Grinding Process for Minimum Overcut", SME 4th Int. Grinding Conference, Technical Paper No. ME.90-537, Vol. 2, Dearborn, Michigan, Oct. 1990, pp. 1-18.
51. Sorkhel, S. and Sur, B., "Mechanism of Electrochemical Grinding", J. of Institution of Engineers (India), Vol. 53, pt. ME-1, Sept. 1972, pp. 45-48.
52. Hughes, F. and Notter, A., "Evaluation of the Electrolytic Grinding Process", De Beers Diamond Research Laboratory, Part-4, No. 26, 1966, pp. 231-233.
53. Hanasaki, S. and Touge, M., "Study of Electrolytic Grinding Mechanism Using a Single Diamond Cutting Tool with a Wear Flat Area", Wear, V. 139, No. 2, Aug. 1990, pp. 285-301.
54. Lavrinenko, V.I., Zakharenko, I. P. and Solod, V. Y., "Electrochemical Grinding of Tungsten-free Hard Alloys Using SHM Wheels", Sverkhterdye Materialy, Vol. 8, No. 3, 1986, pp. 61-64.
55. Nankov, M. M., Popov Z. D. and Nedelchev D. N., "Investigation of the Process of External Cylindrical Electrochemical Grinding with the Face of a Cup Wheel Made of Synthetic Superhard Materials", Proc. of 7th Int. Sym. on Electrochemistry, U.K., 1983, pp. 321-337.
56. Haberstich, M., "Electrochemical Grinding as Applied to Jet Engine Overhaul", SAE Paper No. 680662, 1968, pp. 2630-2640.
57. Antipov, E. L., et al "Research on the Suitability of Electrolytic Grinding for the Machining of Creep-resistant Alloys". Stanki i Instrument, Vol. 46, Issue-10, 1975, pp. 34-35.
58. Kubota, M., "Electrochemical Discharge Mechanical Grinding with a Graphite Inserted Abrasive Wheel", Proc. 7th Int. Sym. on Electrochemistry, Birmingham, U.K., April 1983, pp. 277-284.
59. Lenz, E. and Levy, G. N., "An Approach to Optimization of Electrochemical Grinding", SME Technical Paper No. MR 72-238, 1972, pp. 1-46.
60. Pearlstein, F., "Test Results on Electrolytic Grinding", Metal Working Production, March 1958, pp. 418-420.

61. Ranganathan, V., "Electrochemical Grinding of Titanium", Proceedings 7th AIMTDR Conference, PSG College of Technology, Coimbatore 641004, June 1976, pp. 365-367.
62. Colwell, L. V., "A Physical Model of the Electrochemical Grinding Process". Proceedings of CIRP, Sept. 1967, pp. 365-381.
63. Frisch, J. and Cole, R. R., "Surface Effects and Residual Stresses in Electrolytically Ground Steel", J. of Engg. for Industry, Nov. 1962, pp. 483-489.
64. Amrhein, H. G., "Electrolytic Grinding - One Method for the Optimum Solution of Machining Jobs", Industrial Diamond Review, February 1970, pp. 64-69.
65. McGeough, J.A., Principles of Electrochemical Machining, Chapman and Hall Ltd., London, 1974.
66. Colwell, L. V., "Why Adaptive Control of Electro-chemical Grinding?", Society of Manufacturing Engrs., Dearborn, Michigan 48128, MS 70-560, 1970, pp. 1-11.
67. Kuppuswamy, G., "Magnetic Field Affects Electrochemical Grinding", Tribology International, Vol. 10, No. 3, June 1977, pp. 184-188.
68. Kuppuswamy, G. and Venkatesh, V. C., "Wheel Parameters and Effect on Magnetic Field on Electrolytic Grinding", J. of Inst. of Engrs., India, July 1979, pp. 17-20.
69. Kuppuswamy, G. and Venkatesh, V. C., "Electrochemical Grinding with Magnetic Field", Annals of CIRP, Vol.27, 1978, pp. 107-111.
70. Kuppuswamy, G. and Venkatesh, V. C., "Study of Some Process Variables in Electrolytic Grinding", Proceedings of the Seminar on Application of New Technology in India, The Inst. of Engineers, Nov 1976, pp. 26-33.
71. Banerjee, S. and Chattopadhyay, A. B., "On Performance Characteristics of Electrochemical Grindings", Seminar Oct. 5, 1983. Organized by Indian Institution of Plant Engineers, West Bengal Chapter, pp. 1-10.

72. Kuppuswamy, G. and Venkatesh, V. C., "Effect of a Magnetic Field on Electrolytic Grinding", IIT Madras, Proc. of Int. Conf. ICPE, New Delhi, Vol. 2, 1977, pp. (viii) 52-59.
73. Shpitalni, M., Koren, Y. and Lenz, E., "Adaptive Control System for Optimizing the ECG Process Under the Overcut Constraint", Annals of the CIRP, Vol. 31, No. 1, 1982, pp. 97-123.
74. Mikoshiba, T., Suzuki, Y. and Kawafune, K., "Electrochemical Formed Grinding with Graphite Wheel", Proceedings of the International Conf. in Production Engg., Tokyo, 1971, pp. 73-77.
75. Kuppuswamy, G., "Electrochemical Grinding : An Investigation of the Metal Removal Rate", Proceedings of 7th AIMTDR Conference, PSG College of Technology, Coimbatore 1004, June 1976, pp. 337-340.
76. Brady, G. S., Materials Handbook, McGraw-Hill, Inc., New York, 1977.
77. Ranganathan, V., "Grinding Including Electrolytic Grinding of Titanium", Int. Conf. Proceedings on Production Engg., Vol. 2, No. VIII, New Delhi, 1977, pp. 106-115.
78. Gaddam, A. and Noble, C. F., "Peripheral Electrochemical Grinding with a Formed Wheel", 13th MTDR, 1972, pp. 315-321.
79. Knight, T. W., Barrow, R. B., Williams III, L. W. and Wells, C. H., "Electrochemical Grinding of Cylindrical Test Specimens", Transactions of the ASME, Nov. 1971, pp. 1090-1092.
80. Atkinson, J. and Noble, C. F., "Residual Stresses in Workpieces after Peripheral Electrochemical Grinding", Proceedings of 19th MTDR Conf., Manchester, Sept. 1978, pp. 525-532.
81. Tsofin, E. E., "Electrolytic Grinding Machine for Tools and Cutters", Machines and Tooling, Vol. XXXVIII, No. 9, 1967, pp. 47-49.
82. Ponkshe, G.R. "Design Construction and Calibration of a Two-component Heavy Duty Lathe Dynamometer", U.D.C. 531.78 : 621.941, pp. 142-150, 1966.
83. Shaw, M. C., Metal Cutting Principles, Clarendon Press, Oxford, 1984.

84. Micheletti, G. F., et al, "Recommendation on Calibration and Operation of Machine-Tool-Dynamometers" CIRP Annals, Vol. 23, No. 2, 1974.
85. Schwarzkopf, P. and Kieffer, R., Cemented Carbides, The McMillen Company, New York, 1960.
86. Lange, N. A., Lange's Handbook of Chemistry, McGraw-Hill, Inc., New York, 1979.
87. Bhowmick, T. P. and Mishra, P. K., "Modelling of Feed Force for Electrochemical Grinding Process", Proc. of 18th AIMTDR Conf., IIT, Kharagpur, December 1998, pp. 379-383.
88. Bockris, J. O. M. and Reddy, A. K. N., Modern Electrochemistry, Vol. 1, New York, 1970, pp. 1-44.
89. Malkin, S., Grinding Technology, Theory and Applications of Machining with Abrasives, Ellis Horwood Ltd., England, 1989.
90. Diggle, J. W., "Dissolution of Oxide Phases", Oxides and Oxide Films, Vol.2, Marcel Dekker Inc., 1976, pp. 281-277.
91. Brach, K., Pai, D.M., Ratterman, E. and Shaw, M. C., "Grinding Forces and Energy", Journal of Engineering for Industry, Vol. 110, 1988, pp. 25-31.
92. Maksoud, T. M. A. and Brooks, A. J., "Electrochemical Grinding of Ceramic Form Tooling", Journal of Materials Processing Technology, Vol. 55, U.K., 1995, pp. 70-75.
93. Gutt, S. and Gutt, G., "Contribution to the Mass and Energetic Balance in Electrochemical Grinding", Revista De Chemic, Vol. 44, : 11, Nov. 1993, pp. 912-977.
94. Dabrowski, L., Mapciniak, M. and Rajurkar, K. P., "Kinematics of Nonconventional Grinding", Journal of Materials Processing Technology, Vol. 28, 1991, pp. 179-187.
95. Kubota, M., "Mechanical Cutting Ability of Electrochemical Grinding Wheels", International Symposium for Electromachining, ISEM-6, ECM 4, pp. 365-367.

96. Antipov, E. L. and Kiryukhin, V. A., "Efficiency of Electrolytic Grinding", *Stanki i Instrument*, Vol. 45, Issue 9, 1974, pp. 31-32.
97. Opitz, H. and Heitmann, H., "The Influence of the Working Parameters on the Result in Electrochemical Machining (ECM, ECG)", *Proc. Int. Conf. on Manufacturing Technology*, ASTME, University of Michigan, 1967, pp. 397-416.
98. Bhowmick, T. P. and Mishra, P. K., "An Analysis for Material Removal Rate in Electrochemical Grinding Process", 17th AIMTDR Conf., REC, Warangal, January 1997, pp. 323-327.
99. Sfantsikopoulos, M. M. and Noble, C. F., "Electrochemical Surface Grinding", *The Production Engineer*, May 1976, pp. 245-249.
100. Agasaryan, A. R. and Airapetyan, E. S., "Electrochemical Band Grinding", *Machines and Tooling*, Vol. XLIII, No. 9, 1972, pp. 53-54.
101. Veromen, V. Y., "Electrolytic Diamond Grinding of Cemented Carbides", *Machines and Tooling*, Vol. XXXIV, 1963, pp. 29-32.
102. Sfantsikopoulos, M. M. and Noble, C. F., "The Conic Wheel for Electrochemical Surface Grinding", 14th International MTDR Conference Proceedings, 1974, pp. 365-372.
103. Shlykov, Yu. A. and Osipov, V. S., "Electrochemical Deep Diamond Grinding of Internal Surfaces" *Stanki i Instrument*, Vol. 58, Issue 5, 1987, pp. 29-30.
104. Hausfater, H. and Weber, I., "Electrochemical Grinding of Screw Threads", *The Tool and Manufacturing Engg.*, 1969, pp. 110-113.
105. Wilson, J. F., *Practice and Theory of Electrochemical Machining*, John & Son, New York, 1971.
106. Strauss, H. J., *Handbook of Technical Technicians*, McGraw-Hill, Inc., New York, 1976.
107. Bhattacharyya, A., *Metal Cutting Theory and Practice*, Books and Allied Private Ltd., India, 1984.

108. Sfantsikopoulos, M. M. and Noble, C. F., "Conditioning a Diamond Grit Cup-wheel for Electro-chemical Grinding", Proc. 15th Int. MTDR Conf., Sept. 1974, pp. 365-372.
109. The Institute of Metals, A working Party Report on Practical Corrosion Principles, European Federation of Corrosion, 1989.
110. Ito, S., Sakai, S. and Ishikawa, M., "A Study on a Two Dimensional Dynamometer for Surface Grinding", Bull. Japan Soc. of Prec. Engg., Vol. 14, No. 1, 1980, pp. 25-30.

APPENDICES

APPENDICES

A 4.1 Derivation of Equation of Contact Length

Referring to Fig.4.3, the length of underformed chip i.e. the arc length BC or to a good approximation to the chord length BC (Since θ is small) may be written as

$$l = BC = \sqrt{CF^2 + d^2} \quad \dots A4.1$$

From ΔOCF ,

$$\cos \theta = \frac{OF}{OC} = \frac{D/2 - d}{D/2}$$

$$\therefore d = D/2 (1 - \cos \theta) \quad \dots A4.2$$

$$\text{And, } \sin \theta = \frac{CF}{D/2}$$

$$\text{which gives, } CF = D/2 \sin \theta \quad \dots A4.3$$

Putting the value of d and CF from Eqns.(A4.2) and (A4.3) in Eqn.(A4.1) undeformed chip length becomes,

$$\begin{aligned} l &= \sqrt{\frac{D^2}{4} \sin^2 \theta + \frac{D^2}{4} + \frac{D^2}{4} \cos^2 \theta - \frac{2D^2}{4} \cos \theta} \\ &= \sqrt{\frac{2D^2}{4} - \frac{2D^2}{4} \cos \theta} \\ &= \sqrt{D \cdot \frac{D}{2} (1 - \cos \theta)} \\ &= \sqrt{D \cdot d} \quad \dots A4.4 \end{aligned}$$

A 4.2 Determination of Chip Thickness

Referring to the Fig. 4.3, chip thickness has been calculated as follows:

$$h = EG = CE \sin \theta = CE \left(\frac{CF}{D/2} \right) \quad \dots A4.5$$

and

$$CF = \sqrt{l^2 \cdot d^2} \quad \dots A4.6$$

Substituting the value of 'l' from Eqn.(A4.4) in Eqn.(A4.6) we get,

$$CF = (D \cdot d - d^2)^{1/2}$$

$$\text{Thus, } h = \frac{2CE}{D} \sqrt{Dd - d^2} = CE \sqrt{d/D - (d/D)^2}$$

Since $d/D \ll 1$, $(d/D)^2$ is neglected.

CE is the distance the table advances during the time it takes the wheel to make $1/N_t$ revolutions (where N_t is the number of teeth) and can be expressed as

$$CE = \frac{v}{N_t \cdot N_w} \quad \dots A4.7$$

Putting the value of CE and CF in Eqn.(A4.5)

$$h = \frac{2v}{N_t \cdot N_w} \sqrt{d/D}$$

But, the number of grains lined up one behind the other around the circumference of the wheel is

$$N_t = (\pi D b) C \quad \dots A4.8$$

Where,

C = grains cutting per mm^2

b = width of each cut, mm

Hence, for surface grinding

$$h = \frac{2v}{\pi D \cdot b \cdot C \cdot N_w} \sqrt{d/D} \quad \dots A4.9$$

Assuming a chip of constant width throughout its length and that a taper section yields the average depth of cut, $r = \frac{b}{h/2}$

Thus, 'h' becomes

$$h = \left[\frac{4v}{\pi D N_w C_r} \sqrt{d/D} \right]^{1/2} \quad \dots A4.10$$

When $h_m \ll l_c$, the volume of undeformed chip can be approximated analogous to that of a triangular pyramid, as $1/3$ times the product of maximum cross sectional area ($\frac{rh^2}{2}$) and length l_c , the volume of chip ' V_c ' can be expressed as

$$V_c = \frac{rh^2}{6}$$

Using this expression in the equation of volumetric removal rate

$$d V_w \cdot b = (C \cdot b \cdot V_s) V_c, \text{ and } l_c = \sqrt{D \cdot d}$$

Which implies,

$$h = \left[\frac{6v}{\pi D N_w C_r} \sqrt{d/D} \right]^{1/2} \quad \dots A4.11$$

A.4.3 Derivation of Area A_1 , A_2 , and A_3

Referring to the Fig. 4.13, the rectangular area, $A_1 = X_1 (\text{max}) \times d$

Where,

$$X_1 (\text{max}) = \sqrt{\frac{2d}{a}} \left(a + \frac{V_f}{\omega} \right)$$

$$A_1 = \sqrt{\frac{2d}{a}} \left(a + \frac{V_f}{\omega} \right) d$$

$$\text{Area } A_2 = \int y_1 dx_1$$

Where,

$$x_1 = a \sin \omega t \text{ (with respect to point D)}$$

$$\text{or } dx_1 = a \omega \cdot \cos \omega t \cdot dt$$

$$\begin{aligned}
\therefore A_2 &= \int a(1 - \cos \omega t) a \omega \cos \omega t dt \\
&= a^2 \omega \int (\cos \omega t - \cos^2 \omega t) dt \\
&= a^2 \int_0^\alpha (\cos \theta - \cos^2 \theta) d\theta \\
&= a^2 \left\{ \sin \alpha - \int_0^\alpha \left(\frac{1 + \cos 2\theta}{2} \right) d\theta \right\} \\
&= a^2 \left(\sin \alpha - \frac{\alpha}{2} - \frac{\sin 2\alpha}{4} \right)
\end{aligned}$$

Which may also be written in the form

$$\begin{aligned}
A_2 &= a^2 \left(\sqrt{\frac{2d}{a}} - \frac{1}{2} \sqrt{\frac{2d}{a}} - \frac{1}{4} \cdot 2 \sin \alpha \cos \alpha \right) \\
&= a^2 \left(\sqrt{\frac{2d}{a}} - \frac{1}{2} \sqrt{\frac{2d}{a}} - \frac{1}{2} \sqrt{\frac{2d}{a}} \cdot \frac{a-d}{a} \right) \\
&= a^2 \sqrt{\frac{2d}{a}} \left(1 - \frac{1}{2} - \frac{1}{2} \left(\frac{a-d}{a} \right) \right) \\
&= \frac{ad}{a} \sqrt{\frac{2d}{a}}
\end{aligned}$$

and,

$$\begin{aligned}
A_3 &= \text{Circle sector OAHEO} - \Delta \text{OAF} \\
&= \frac{1}{2} a^2 \sqrt{\frac{2d}{a}} - \frac{1}{2} a(a-d) \sqrt{\frac{2d}{a}} \\
&= \frac{1}{2} \sqrt{\frac{2d}{a}} (a^2 - a^2 + ad) \\
&= \frac{1}{2} \sqrt{\frac{2d}{a}} \cdot a d
\end{aligned}$$

A 4.4 A Sample Calculation for Theoretical and Experimental MRR

To determine the material removal rate due to mechanical and electrochemical actions both theoretically and experimentally, the following procedure is followed.

The parameters considered are :

$D = 150$ mm, $b = 3.2$ mm, $d = 20$ mm, length of job = 85 mm, $V_g = 413$ m/min, $i = 21.28$ amp / mm², electrolyte flowrate = 2.8×10^6 mm³/min.

A 4.4.1 Theoretical MRR due to Mechanical and Electrochemical Actions

Referring to the Eqn. (4.59), the theoretical MRR due to mechanical action is given by

$$\begin{aligned} \text{MRR}_M &= V_f \cdot d \cdot b = 6.67 \times 20 \times 10^{-3} \times 3.2 \\ &= 0.43 \text{ mm}^3/\text{sec} \end{aligned}$$

Referring to the Eqn. (4.51), MRR due to electrochemical action can be found out as :

$$\begin{aligned} \text{MRR}_E &= 2 b R^2 (a/2R)^{1/2} \left\{ (d_1/R)^{1/2} - 2/3 \right\} \\ &= 2 b R^2 (a/2R)^{1/2} \left\{ \left(\frac{d+R}{R} \right)^{1/2} - 2/3 \right\} \\ &= 2 (3.2) (0.62)^2 \left(\frac{75}{2 \times 61} \right)^{1/2} \left\{ \left(\frac{0.02+0.62}{0.61} \right)^{1/2} - 0.67 \right\} \end{aligned}$$

(Considering the higher valency of each element, the value of R is found out from the Eqn.(4.44) as 0.61 mm / sec)

$$\text{MRR}_E = 6.45 \text{ mm}^3/\text{s}$$

Hence, the percentage of theoretical MRR due to mechanical and electrochemical actions can be calculated as :

$$\eta_M = \frac{MRR_M}{MRR_T} = \frac{0.43}{(0.43+6.45)} = 6.25\%$$

$$\eta_M = (100-6.25)\% = 93.75\%$$

A 4. 4. 2 Experimental MRR due to the Mechanical and Electrochemical Actions

The experimental MRR due to only mechanical action can be found out keeping the different process parameters constant such as depth of cut, feed rate etc. and allowing no current to flow across the electrolyte. The amount of metal removed is found out by weighing the specimen before and after the run. It is 0.14781 gm for the above parameters. Since density of the workplace is 0.0142 gm/mm³ [refer Table A 6.1] and time taken for the single pass is 12.7 seconds experimental MRR is

$$MRR_M = \frac{0.14781}{0.0142 \times 12.7} = 0.82 \text{ mm}^3/\text{sec.}$$

Keeping the same parameters constant and allowing the current to flow across the electrodes, the total metal removed is found out by weight measurement as 1.08564 gm. So, the total material removal rate can be expressed as

$$MRR_T = \frac{1.085646}{12.7 \times 0.0142} = 6.02 \text{ mm}^3/\text{s.}$$

Hence the MRR due to electrochemical action is given by.

$$\begin{aligned} MRR_E &= MRR_T - MRR_M \\ &= 6.02 - 0.82 = 5.20 \text{ mm}^3/\text{s} \end{aligned}$$

Therefore, the percentage of experimental MRR due to mechanical and electrochemical actions can be calculated as :

$$\eta_M = \frac{MRR_M}{MRR_T} = \frac{0.82}{6.02} = 13.62\%$$

$$\eta_E = (100 - 13.62)\% = 86.38\%$$

A5.1 Resistance Load for the Movement of the Table

Dead weight of the workpiece holding table = 400 N

Average cutting force in grinding operation = 300 N

Total normal load = 700 N

Design load is assumed as 1.5 times the total average load.

Design load = $1.5 \times 700 = 1050$ N

Coefficient of friction, μ is assumed to be unity, because at static condition coefficient of friction would be maximum of value 1.

\therefore Resistance load for the movement of table = 1050 N

A 5.2 Specifications of the Hydraulic Cylinder

The specification of the hydraulic cylinder is given below :

| | | |
|---|---|--|
| Type | : | Double acting cylinder |
| Bore diameter (Φ) | : | 25 mm |
| Distance between port centres | : | 410 mm |
| Distance between free-end and port centre | : | 25 mm |
| Cylinder body length | : | 525 mm |
| Stroke length | : | 330 mm |
| Mounting type | : | Foot mounting |
| Piston rod diameter | : | 16 mm with M12 \times 1.25 mm thread for fastening to the work table |
| Port size | : | 3/8 " BSP. |

A 5.3 Calculation for Minimum Load for Dynamometer

The total minimum load acting upon the dynamometer has been determined from the followings:

$$\text{Wheel pressure} = 0.3-1.4 \text{ MPa}[2]$$

$$\text{Electrolyte pressure} = 14-70 \text{ KPa}[3]$$

$$\text{Maximum depth of cut, } d = 2.5 \text{ mm}[2]$$

$$\text{Wheel diameter, } D = 150 \text{ mm}$$

$$\text{Wheel width, } b = 12.7 \text{ mm}$$

$$\text{Width of dynamometer} = 35 \text{ mm (conventionally assumed)}$$

Using Eqn.(4.5), total area of cut can be found as:

$$\begin{aligned} \text{Total area of cut} &= \text{Arc length} \times \text{width of wheel} [83] \\ &\cong (D.d)^{\frac{1}{2}} \times 12.7 = (150 \times 2.5)^{\frac{1}{2}} \times 12.7 \\ &= 245.94 \text{ mm}^2 \end{aligned}$$

Then the minimum load due to minimum wheel pressure of 0.3 M Pa

$$= 0.3 \times 10^6 \times 245.84 \times 10^{-6} = 73.78 \text{ N}$$

Similarly, the minimum load due to electrolyte pressure of 14 K Pa

$$= (14 \times 10^3 \times 245.94 \times 10^{-6}) = 3.44 \text{ N}$$

And the dead load of vice, perspex box and the base plate

$$= 106.4 \text{ N (weighed)}$$

$$\therefore \text{Total minimum load} = (73.78 + 3.44 + 106.5) = 183.7 \text{ N}$$

A 5.4 Thickness of the Ring of the Dynamometer

Thickness of the dynamometer is calculated from the following formulae, considering the order of strain as 40×10^{-6} . The radius of the octagonal ring 'r' has been assumed to be 16 mm so that the length 'L' becomes 64 mm according to the relation $L/r = 4$. [107] refer Fig. A5.1.

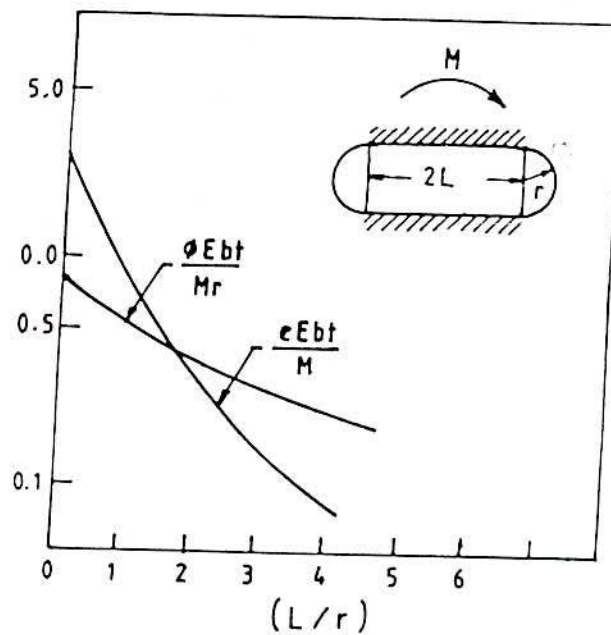


Figure A5.1 Rotational Sensitivity and Stiffness of an Extended Octagonal Ring

According to Shaw [83], the strain is expressed as

$$e = \frac{1.09 \times F_r \times r}{E \times b \times t} \quad \text{A5.1}$$

$$\therefore 40 \times 10^{-6} = \frac{1.09 \times 183.7 \times 16}{21000 \times 35 \times t^2}$$

Which implies, $t = 3.3 \text{ mm}$

For this design, the thickness is assumed to be 3.00 mm where strain for minimum total load of 183.7 N becomes (from Eqn.. A5.1)

$$e = \frac{1.09 \times 183.7 \times 16}{21000 \times 35 \times 3^2} = 48 \times 10^{-6}$$

It is found that the strain value does not change appreciable for change of the thickness from 3.2mm to 3 mm. So the strain value per unit deflection considered will be in reasonable value.

The sensitivity can be calculated as follows:

$$\begin{aligned} \text{Sensitivity} &= \frac{e}{F_r \times t} = \frac{48 \times 10^{-6}}{183.7 \times 3} \\ &= 81.6 \times 10^{-6} / \text{N} / \text{mm}. \end{aligned}$$

Radial deflection for minimum load, is expressed as :

$$\begin{aligned} \frac{F_r}{\delta_r} &= \frac{E b x t}{1.8 x r^3} \\ \delta_r &= \frac{1.8 \times r^3 \times F_r}{E \times b \times t^3} = \frac{1.8 \times 16^3 \times 183.7}{21000 \times 35 \times 3^3} = 6.6 \mu\text{m} \end{aligned}$$

And the ratio

$$\frac{t}{r} = \frac{3}{16} = 0.187$$

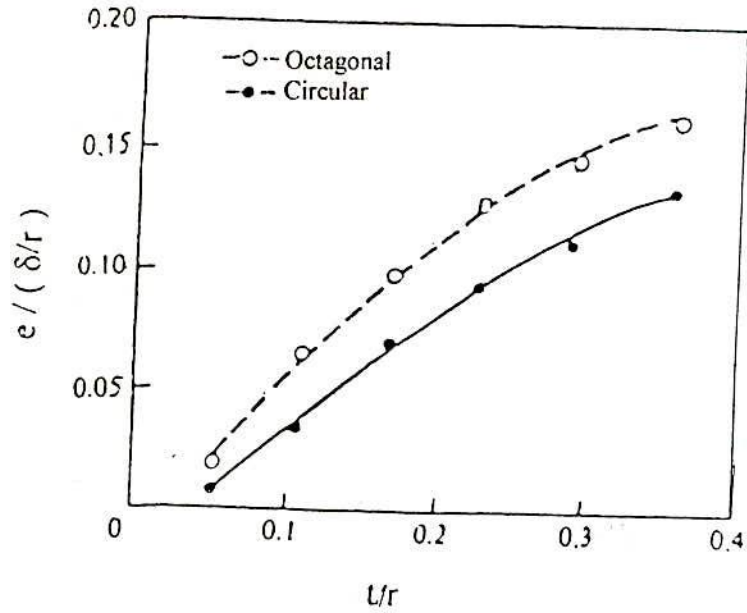


Figure A5.2 Relation Between t/r and Strain Output for Different Rings

Referring to the Fig. A5.2, strain per unit deflection with respect to $t/r=0.187$ is 0.12 and hence, the calculated value for strain per unit deflection is

$$0.61 \times \frac{t}{r} = 0.114 \quad \text{or, } t/r = 0.87$$

Which means that this value of t/r may be considered for the design purpose.

A 5.5 Arm Length of the Ring of Dynamometer

With reference to the Figs.A 5.3 (a) and A5.3 (b), geometrically it can be found that

$$\text{Each arm} = AC = 2AB$$

$$\therefore OB/AB = (r + t) / AB = \tan 67.5$$

Where,

t = thickness of the octagonal ring

$$\therefore AB = (r + t) / \tan 67.5$$

$$\therefore AC = 2(r + t) / \tan 67.5 = 2(16+3) / \tan 67.5 = 15.7 \text{ mm}$$

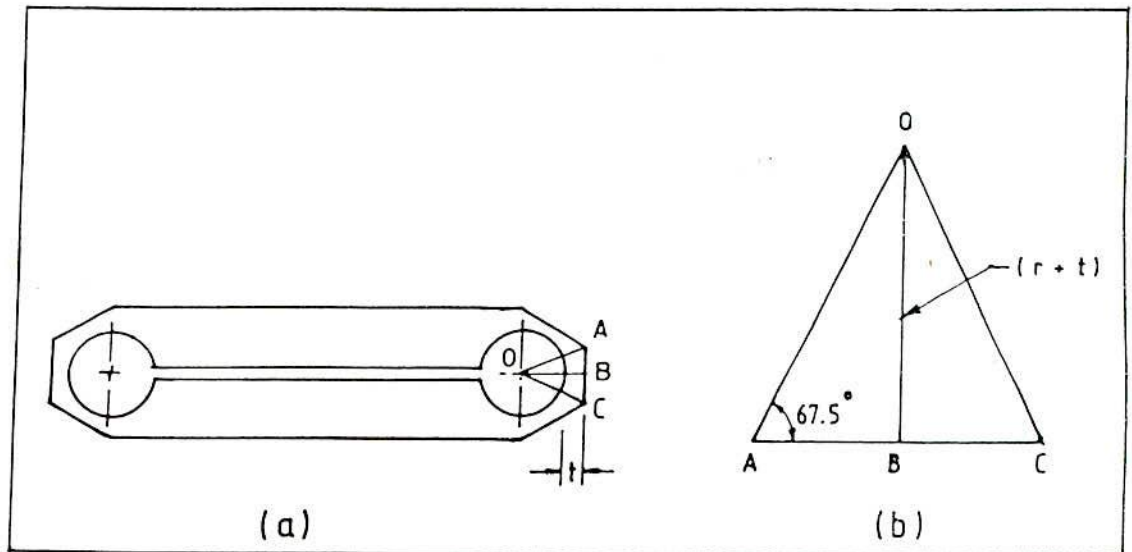


Figure A 5.3 Geometry of Dynamometer

A 5.6 Gap Between Horizontal Members

The slit of the horizontal member depends upon the deflection of the top member due to the application of load. For design purpose, this gap should be more than the actual deformation of the top member.

For simplicity of calculation, the top member is considered as simple supported beam and acting at the centre a concentrated load, the deflection of the beam can be written as:

$$\delta = \frac{w \times l^3}{48 \times E \times I} = \frac{47.35 \times 153^3 \times 12}{48 \times 21000 \times 35 \times 19^3} = 8.4 \times 10^{-3} \text{ mm}$$

Where,

w = Total concentrated load

l = Length

E = Modulus of elasticity

That value is very small compared to different dimensions of the dynamometer. So 6mm gap between the two horizontal members is considered considering the convenience of making the slit.

A.5.7 Strain Gauge Specifications

| | |
|--------------------|-------------------|
| Type | : BKSAR - 5 |
| Resistance in ohms | : 119.7 ± 0.2 |
| Gauge factor | : $2.06 \pm 2\%$ |
| Gauge length | : 5 mm |
| Gauge width | : 2.5 mm |
| Shape | : Helical grid |

Table A5.1 Data for Calibration of Dynamometer (Horizontal Load)

| Load (N) | Meter Reading in mV | | | | | | | | | | | |
|-------------|---------------------|-----------|---------|-----------|---------|-----------|---------|-----------|---------|-----------|---------|-----------|
| | Cycle 1 | | Cycle 2 | | Cycle 3 | | Cycle 4 | | Cycle 5 | | Cycle 6 | |
| | Loading | Unloading | Loading | Unloading | Loading | Unloading | Loading | Unloading | Loading | Unloading | Loading | Unloading |
| 9.81 | 4 | 3 | 4 | 3 | 4 | 3 | 4 | 3 | 4 | 3 | 4 | 2 |
| 19.62 | 7 | 5 | 6 | 5 | 6 | 5 | 6 | 5 | 6 | 5 | 6 | 3 |
| 29.43 | 9 | 5 | 8 | 6 | 8 | 7 | 8 | 7 | 7 | 4 | 5 | 5 |
| 39.24 | 11 | 7 | 9 | 7 | 9 | 9 | 10 | 8 | 9 | 5 | 8 | 6 |
| 49.05 | 12 | 10 | 11 | 8 | 11 | 11 | 12 | 10 | 10 | 7 | 10 | 8 |
| 58.86 | 14 | 11 | 13 | 9 | 12 | 12 | 14 | 12 | 12 | 9 | 12 | 10 |
| 68.67 | 16 | 13 | 15 | 11 | 14 | 13 | 16 | 13 | 14 | 11 | 14 | 11 |
| 78.48 | 18 | 16 | 17 | 13 | 16 | 15 | 18 | 15 | 16 | 12 | 16 | 13 |
| 88.29 | 21 | 18 | 19 | 15 | 18 | 17 | 20 | 17 | 18 | 15 | 18 | 14 |
| 98.10 | 23 | 20 | 21 | 17 | 20 | 18 | 22 | 19 | 20 | 17 | 20 | 16 |
| 107.91 | 26 | 23 | 23 | 20 | 22 | 20 | 24 | 20 | 22 | 18 | 22 | 18 |
| 117.72 | 29 | 24 | 24 | 22 | 23 | 22 | 26 | 22 | 24 | 21 | 23 | 21 |
| 127.53 | 30 | 27 | 26 | 25 | 25 | 24 | 27 | 25 | 25 | 24 | 25 | 24 |
| 137.34 | 31 | 30 | 31 | 30 | 28 | 28 | 29 | 27 | 28 | 26 | 28 | 26 |
| 147.15 | 33 | 33 | 32 | 32 | 30 | 30 | 30 | 30 | 30 | 30 | 29 | 29 |

| Load (N) | Cycle 7 | | Cycle 8 | | Cycle 9 | | Cycle 10 | | Average | |
|-------------|---------|-----------|---------|-----------|---------|-----------|----------|-----------|---------|-----------|
| | Loading | Unloading | Loading | Unloading | Loading | Unloading | Loading | Unloading | Loading | Unloading |
| 9.81 | 4 | 3 | 2 | 2 | 2 | 2 | 2 | 2 | 3.6 | 2.4 |
| 19.62 | 6 | 5 | 4 | 3 | 3 | 2 | 3 | 3 | 5.0 | 4.0 |
| 29.43 | 8 | 6 | 5 | 4 | 6 | 5 | 5 | 3 | 6.9 | 5.2 |
| 39.24 | 10 | 8 | 6 | 5 | 7 | 5 | 7 | 4 | 8.6 | 6.3 |
| 49.05 | 11 | 10 | 8 | 8 | 9 | 7 | 9 | 6 | 10.3 | 8.5 |
| 58.86 | 12 | 11 | 10 | 9 | 11 | 9 | 11 | 8 | 12.1 | 10 |
| 68.67 | 14 | 13 | 12 | 11 | 14 | 10 | 12 | 10 | 14.1 | 11.6 |
| 78.48 | 16 | 14 | 14 | 13 | 16 | 12 | 14 | 11 | 16.1 | 13.4 |
| 88.29 | 17 | 16 | 16 | 16 | 18 | 14 | 17 | 13 | 18.2 | 15.5 |
| 98.10 | 19 | 18 | 18 | 17 | 20 | 16 | 19 | 15 | 20.2 | 17.3 |
| 107.91 | 21 | 20 | 20 | 19 | 22 | 19 | 21 | 17 | 22.3 | 19.4 |
| 117.72 | 23 | 22 | 22 | 21 | 24 | 21 | 23 | 20 | 24.1 | 21.6 |
| 127.53 | 25 | 24 | 25 | 24 | 26 | 24 | 25 | 22 | 25.9 | 24.3 |
| 137.34 | 28 | 26 | 27 | 26 | 27 | 25 | 27 | 24 | 28.6 | 26.8 |
| 147.15 | 29 | 29 | 29 | 29 | 28 | 28 | 28 | 28 | 29.8 | 29.8 |

Table A6.1 Some Properties of WC-Co Materials

| Composition, % WC Co | Density, g/cm ³ | Rockwell hardness, R _A | Vickers hardness, kg/mm ² | Transverse rupture strength, psi | Compressive strength, psi | Modulus of elasticity, ^c 10 ⁶ psi |
|------------------------------|-------------------------------|---|--|-------------------------------------|------------------------------|---|
| 100 ----- | 15.7 | 92-94 | 1800-2000 | 43,000- 71,000 | 426,000 | 102.5 |
| 97 3 | 15.1-15.2 | 90-93 | 1600-1700 | 142,000-170,400 | 838,000 | 95 |
| 95.5 4.5 | 15.0-15.1 | 90-92 | 1550-1650 | 170,000-199,000 | 824,000 | 91 |
| 94-94.5 ^a 5.5-6 | 14.8-15.0 | 90-91 | 1500-1600 | 227,000-256,000 | 710,000 | 88 |
| 94-94.5 ^b 5.5-6 | 14.8-15.0 | 91-92 | 1600-1700 | 199,000-227,000 | 781,000 | 89.5 |
| 91 9 | 14.5-14.7 | 89-91 | 1400-1500 | 213,000-270,000 | 682,000 | 84 |
| 90 10 | 14.3-14.5 | 88.5-90.5 | 1350-1450 | 220,000-277,000 | 667,000 | 83 |
| 89 11 | 14.0-14.3 | 88-90 | 1300-1400 | 227,000-284,000 | 653,000 | 82 |
| 87 13 | 14.0-14.2 | 87-89 | 1250-1350 | 241,000-298,000 | 639,000 | 79 |
| 85 15 | 13.8-14.0 | 86-88 | 1150-1250 | 256,000-312,000 | 554,000 | 78 |
| 80 20 | 13.1-13.3 | 83-86 | 1050-1150 | 284,000-369,000 | 483,000 | 71 |
| 75 25 | 12.8-13.0 | 82.84 | 900-1000 | 256,000-384,000 | 454,000 | 66.5 |
| 70 30 | 12.3-12.5 | 80.82 | 850-950 | ----- | ----- | ----- |
| ---- 100 | 8.9 | ----- | 125 | ----- | ----- | 25.5 |

^a Coarse-grained WC phase.

^b Fine-grained WC phase.

^c Average values



Table A 6.2 Values of Different Parameters for Feed Force

| <u>Symbol</u> | <u>Value</u> |
|----------------|--|
| m | 12 |
| p | 110.5 N/mm ² |
| A | 2.27 x 10 ⁻⁸ mm ² |
| l _c | 1.22 mm |
| k ₁ | 0.8 |
| a ₁ | 0.4 |
| k ₁ | 6.1 N/mm/% of loaded area. |
| n | 2 |
| A | 0.5 mm |
| r | 0.085 mm |
| w | 9.23 mm |
| H | 0.01 mm |
| h | 0.02 mm |
| α ₁ | 1.0 N/mm ² |
| α ₂ | 0.5 N/mm ² |
| λ | 0.34 |
| τ | 0.102 rad |
| μ _r | 0.5 |
| μ ₁ | 1.36 x 10 ⁻³ N.sec/m ² |

Table A6.3 Grinding conditions for Feed Force

| | |
|-----------------|------------------------------------|
| Grinder | : Horizontal surface grinder |
| Grinding manner | : Surface grinding |
| Grinding wheel | : Diamond impregnated metal bonded |
| | Diameter = 150 mm |
| | Width = 9 mm |
| | Concentration = 75 |
| | Grit size = 80 / 100 |
| Workpiece | : Stainless steel |
| Depth of Cut | : 10 μ m |
| Work speed | : 6.67 mm/sec |
| Wheel speed | : 1413 m/min |
| Applied voltage | : 4 -10 V |
| Current | : 25-100 amps. |
| Electrolyte | |
| ingredient | : NaCl |
| concentration | : 10% w/w aqueous solution |
| flow rate | : 2.9 l.p.m. |
| temperature | : 26°C |